

Tori sequences as remnants of multiple accreting periods of Kerr SMBHs

D. Pugliese*, Z. Stuchlík

*Institute of Physics, and Research Centre of Theoretical Physics and Astrophysics,
Faculty of Philosophy & Science, Silesian University in Opava,
Bezručovo náměstí 13, CZ-74601 Opava, Czech Republic*

Abstract

Super-massive black holes (SMBHs) hosted in active galactic nuclei (AGNs) can be characterized by multi-accreting periods as the attractors interact with the environment during their life-time. These multi-accretion episodes should leave traces in the matter orbiting the attractor. Counterrotating and even misaligned structures orbiting around the SMBHs would be consequences of these episodes. Our task in this work is to consider situations where such accretions occur and to trace their remnants represented by several toroidal accreting fluids, corotating or counterrotating relative to the central Kerr attractor, and created in various regimes during the evolution of matter configurations around SMBHs. We focus particularly on the emergence of matter instabilities, i.e., tori collisions, accretion onto the central Kerr black hole, or creation of jet-like structures (proto-jets). Each orbiting configuration is governed by the general relativistic hydrodynamic Boyer condition of equilibrium configurations of rotating perfect fluid. We prove that sequences of configurations and hot points, where an instability occurs, characterize the Kerr SMBHs, depending mainly on their spin-mass ratios. The occurrence of tori accretion or collision are strongly constrained by the fluid rotation with respect to the central black hole and the relative rotation with respect to each other. Our investigation provides characteristic of attractors where traces of multi-accreting episodes can be found and observed.

Keywords: Accretion disks, accretion, jets, black hole physics, hydrodynamics
2010 MSC: 00-01, 99-00

1. Introduction

Galactic cores and active galactic nuclei (AGNs) provide a rich scenario to observe super-massive black holes (SMBHs) interacting with their galactic environments. There are several observational evidences supporting the existence of such objects in AGNs. To cite two of most recent studies on SMBHs in their host galaxies, we point out the analysis in Tadhunter et al. (2017) exploring the link between galaxy collisions and super-massive black hole feeding, while in Regan et al. (2017) the link between galaxy collapse and rapid SMBHs formation is faced. Both these studies show the existence of an intense and strong relation between the galaxy dynamics and its super-massive guest, especially in the accretion processes characterizing the strong attractors. It can be expected that, during their life-time, SMBHs would be influenced by the galaxy dynamics due to a series of multi-accreting episodes as a consequence of interaction with the galactic environment made up by stars and dusts. These activities may leave traces in the form of matter remnants orbiting the central attractor.

Chaotical, discontinuous accretion episodes can produce sequences of orbiting toroidal structures with strongly different features as, for example, different rotation orientations with re-

spect to the central Kerr BH where corotating and counterrotating accretion stages can be mixed (Dyda et al., 2015; Alig et al., 2013; Carmona-Loaiza et al., 2015; Lovelace&Chou, 1996; Gafton et al., 2015), or disks strongly misaligned with respect to the central SMBH spin may appear (Nixon et al., 2013; Dogan et al., 2015; Bonnerot et al., 2016; Aly et al., 2015). Eventually, the scenario envisaged by these studies raises a series of issues and indications about the different stages of the attractor accretion periods binding it on its intrinsic rotation. Motivated by these facts, in this work we investigate structured toroidal disks, so called ringed accretion disks (RAD), which may be formed during several accretion regimes occurred in the lifetime of non-isolated Kerr BHs. These configurations were first introduced in Pugliese&Montani (2015) and then detailed in Pugliese&Stuchlík (2015, 2016a). They feature a system made up by several axis-symmetrical matter configurations orbiting in the equatorial plane of a single central Kerr BH. Evidences of these special configurations are expected to be found in the associated X-ray spectra emission in AGNs.

The phenomenology associated with these toroidal complex structures may be indeed very wide. This new complex scenario enables to re-interpret the phenomena analyzed so far in the single-torus framework. Observational evidence is expected by the spectral features of AGNs X-ray emission shape, due to X-ray obscuration and absorption by one of the tori, providing therefore a fingerprint of the tori as a radially stratified emission profile (Karas&Sochora, 2010; Sochora et al.,

*Corresponding author

Email addresses: d.pugliese.physics@gmail.com (D. Pugliese*), zdenek.stuchlik@physics.cz (Z. Stuchlík)

2011; Schee&Stuchlik, 2009). Relatively indistinct excesses of the relativistically broadened emission-line components were predicted in different works, arising in a well-confined radial distance in the accretion structure originating by a series of episodic accretion events. Furthermore, the radially oscillating tori can be related to the high-frequency quasi periodic oscillations (QPOs) observed in non-thermal X-ray emission from compact objects. More generally, instabilities of such configurations, we expect, may reveal crucial significance for the high energy astrophysics related especially to accretion onto **BH**, and the extremely energetic phenomena occurring in quasars and **AGNs** that could be observable by the planned X-ray observatory ATHENA¹.

The investigation of these **RAD** configurations, however, is influenced by significant methodological issues. The question of how to treat this scenario, and how to model the dynamics of toroidal sequences, is undoubtedly challenging. A major methodological challenge comes from the need to study different evolutive periods of the **BH** in its environment. Conveniently, we may consider following three periods of ringed accretion disk life: (i) formation of tori, (ii) the accretion periods onto the central Kerr attractor and (iii) the tori interaction (emergence of tori collisions). In the current analysis of dynamical one-torus system of both general relativistic hydrodynamic (GR-HD) and general relativistic magnetohydrodynamic (GR-MHD) set-ups, the geometrically thick disks considered in this work are often adopted as initial configurations for the analysis– (Igumenshchev, 2000; Fragile et al., 2007; De Villiers&Hawley, 2002; Port et al., 2016). We can therefore adopt an analogue approach for the investigation of the case of a central Kerr **BH** and several tori orbiting in its equatorial plane. However, in a dynamical process the timing problem of how to depict the different periods is definitely challenging, and requires a certain number of assumptions on the history of the **BH** in interaction with the environment. Therefore, fixing a minimum model set-up inevitably will focus the analysis on a single, very special situation. It would be necessary to fix: 1. the attractor through its dimensionless spin, 2. the accretion era we are willing to describe, and eventually, 3. number of tori, 4. fluid rotation law, 5. relative tori location, 6. location of the inner torus with respect to the attractor. The immediate approach would be to let the chance in the choice of a specific scenario which even in a rich variant of the model will provide necessarily only a partially focused description of one hypothetical model. The problem remains of how to fix, in such objectively complex scenario, the initial conditions of multi-tori orbiting a spinning **BH**.

In fact, recent results presented by Pugliese&Stuchlík (2017b,a) show that it is not even immediate to choose the spin class for the central Kerr **BH**: the dimensionless spin of the Kerr black hole strongly constrains the possible couple of orbiting tori in number of orbiting tori, in location and relative range of variation for fluid specific angular momentum. In other words, to fix the initial data for a restricted dynamical scenario, one

needs to have in advance the answer to the very question one firstly wants to address within the simulation.

In this respect, our analysis stands also as a guideline to this choice providing a detailed answer to these questions. Results found here will be the guide for the set-up of any more complex dynamical system. Moreover, we are able to trace some evolutive lines for an initial configuration of a system composed by an attractor and general n fluid configurations, corotating or counterrotating relative to the attractor, at any time of the system evolution, from the formation to the occurrence of accretion. Fixing an initial set up, and distinguishing a very restricted number of classes of configurations and attractors, we discuss the final state of a dynamical evolution from an initial configuration. There are few evolutive lines with different final states; the occurrence of these paths however will be finally established by a dynamical analysis. The set-up for the ringed accretion disk model was drawn in Pugliese&Stuchlík (2015), while first proposal of these configurations was in Pugliese&Montani (2015). In Pugliese&Stuchlík (2015), constraints and discussion on perturbations were provided. Then in Pugliese&Stuchlík (2016a) sequences of unstable configurations were discussed, the investigation was focused on the unstable phases of multi accreting toroidal structures. The paper Pugliese&Stuchlík (2017b) focused on the case of two tori as “seed” for larger configurations, and paper Pugliese&Stuchlík (2017a) explicitly addressed collisions and energy release in colliding tori. In this article, we discuss the situation where several equilibrium and accreting or proto-jet (open critical) configurations are formed around a Kerr-SMBH in AGN environments. Here we take full advantage of the symmetry of the Kerr geometry, considering a stationary and axisymmetric, full general relativity (GR) model for a single thick accretion disk with a toroidal shape. Each torus is featured as an opaque (large optical depth) and super-Eddington (high matter accretion rates) disk model a radiation pressure supported accretion disk cooled by advection with low viscosity– (Paczynski, 1980; Igumenshchev, 2000; Fragile et al., 2007; De Villiers&Hawley, 2002; Port et al., 2016). More precisely, the individual toroidal (thick disk) configurations are barotropic models where the effects of strong gravitational fields are dominant with respect to the dissipative ones and predominant to determine the unstable phases of the systems (Font&Daigne, 2002b; Igumenshchev, 2000; Abramowicz&Fragile, 2013; Pugliese&Montani, 2015; Paczynski, 1980; Kovar et al., 2016). As a consequence of this, during the evolution of dynamical processes, the functional form of the angular momentum and entropy distribution depends on the initial conditions of the system and on the details of the dissipative processes. The tori are governed by “Boyer’s condition” of the analytic theory of equilibrium configurations of rotating perfect fluids (Boyer, 1965). The toroidal structures of orbiting barotropic perfect fluid are determined by an *effective potential* reflecting the spacetime geometry and the centrifugal force through the distribution of the specific angular momentum $\ell(r)$ of the orbiting fluid (Abramowicz et al., 1983; Abramowicz&Fragile, 2013; Abramowicz et al., 2010, 1978; Stuchlík et al., 2005; Abramowicz et al., 1996; Lei et al., 2008). The equipressure surfaces, $K = \text{constant}$, could be closed, de-

¹<http://the-athena-x-ray-observatory.eu/>

termining equilibrium configurations, or open (related to proto-jets configurations (Pugliese&Stuchlík, 2016a)). The special case of cusped or critical equipotential surfaces allows for the accretion onto the central black hole (Paczynski, 1980). The outflow of matter through the cusp occurs due to an instability in the balance of the gravitational and inertial forces and the pressure gradients in the fluid, i.e., by the so called Paczynski mechanism of violation of mechanical equilibrium of the tori (Paczynski, 1980).

The plan of this article is as follows: Sec. (2) introduces the ringed accretion disk model: we discuss the main features of geometrically thick accretion disk orbiting a central Kerr BH, and we then proceed to consider the case of several tori orbiting in the equatorial plane of the central attractor. Concepts and notation used throughout this work are also introduced. The introduction of new model also requires the use of an extended notation; for easy of reference we have summarized main notation in Sec. (2) and we will make reference also to Table (1) listing main Kerr BHs spins used in this work. In Sec. (3) we consider the case when all the configurations around the attractor rotate with the same orientation, i.e., all are corotating or counterrotating with respect to the central Kerr BH (*l*corotating). In fact, many of the results and constraints on orbiting tori depend mainly on the fluids relative rotation as well as on each torus rotation with respect to the central Kerr attractor. The limiting case of Schwarzschild BH is also considered. In static spacetimes, all tori may be considered as corotating, regardless of the fluids relative rotation. In general, any configuration may be in one of three possible states: non-accreting or equilibrium (C), accretion (A) or proto-jet (J). Accordingly, we developed our analysis as follows: in Sec. (3.1) we consider the proto-jets sequences (J – J). Sequences (A – J), formed by at least a configuration in accretion and a proto-jet, are studied in Sec. (3.2), for the case where the open topology is the outer one (farthest from the attractor). In Sec. (3.3), the case in which the inner configuration of the couple has proto-jet topology is investigated. Section (3.4) describes sequences formed by a non-accreting torus and a proto-jet. In Section (3.5), we focus on the case where the proto-jet is the closest to the attractor. In Sec. (3.6), some remarks on the sequences with (C – A) configurations are addressed. Analogously, Section (4) deals with the *l*counterrotating couples (tori having different relative orientation of rotation). This case turns far more articulated than the *l*corotating one, and we address the analysis by considering the proto-jet-proto-jet (J – J) systems in Sec. (4.1), in Sec. (4.2) proto-jet-accretion (J – A) systems are discussed, and in Sec. (4.3) we address the accretion-accretion (A – A) systems, with a special case where two *l*counterrotating tori are accreting onto the central BH. The case where there is an equilibrium disk and an accreting torus (C – A) is investigated in Sec. (4.4). This section ends with the study of the equilibrium disk-proto-jet (C – J) systems in Sec. (4.5). Section (5) provides indications on possible observational evidences for the Ringed Accretion Disks (RADs), discussing the phenomenology expected to be associated with these macrostructures.

Our analysis required a certain number of sideline results, fixing the location of the accretion disk edges in the spacetime

regions confined by marginally bounded, marginally stable and marginally circular (photon) orbits. It is clear that the problem to assess the location of the inner edge of a single torus is in fact a very relevant issue of the accretion disk theory—see (Krolik&Hawley, 2002; Bromley et al., 1998; Abramowicz et al., 2010; Agol&Krolik, 2000; Paczynski, 2000; Slaný&Stuchlík, 2005). Acknowledging the importance of this issue, we report in the Appendix A the direct procedure provided for this part of our analysis, with comments on the results. We note that it was necessary to consider both the triplets of radii (marginal orbits) for both corotating and counterrotating matter, consequently, we separated our discussion in two parts in Appendix A.1 and Appendix A.2. In the investigation of Sections (3) and (4), we make direct reference to the results and quantities of Appendix A. Finally, some of these results have also been used in Pugliese&Stuchlík (2016a); here we propose proof of those results. This article closes in Sec. (6) where comments and future perspectives are presented.

2. Orbiting Axi-symmetric tori in a Kerr spacetime

We consider axially symmetric configurations orbiting in the equatorial plane of a central Kerr BH with mass parameter M and dimensionless spin $a/M \in [0, 1]$ The Kerr metric tensor can be written as

$$ds^2 = -dt^2 + \frac{\rho^2}{\Delta} dr^2 + \rho^2 d\theta^2 + (r^2 + a^2) \sin^2 \theta d\phi^2 + \frac{2M}{\rho^2} r(dt - a \sin^2 \theta d\phi)^2, \quad (1)$$

$$\rho^2 \equiv r^2 + a^2 \cos^2 \theta, \quad \Delta \equiv r^2 - 2Mr + a^2,$$

where $\{t, r, \theta, \phi\}$ are the Boyer-Lindquist (BL) coordinates; the horizons $r_- < r_+$, and the outer static limit r_ϵ^+ are respectively given by:

$$r_\pm \equiv M \pm \sqrt{M^2 - a^2}; \quad r_\epsilon^+ \equiv M + \sqrt{M^2 - a^2 \cos^2 \theta}. \quad (2)$$

The extreme Kerr black hole has spin-mass ratio $a/M = 1$, while the non-rotating limiting case $a = 0$ is the Schwarzschild metric. In general there is $r_+ < r_\epsilon^+$ on $\theta \neq 0$ and $r_\epsilon^+ = 2M$ in the equatorial plane ($\theta = \pi/2$). Metric tensor (1) is independent of ϕ and t , as consequence of this the covariant components p_ϕ and p_t of a particle four-momentum are conserved along the geodesics² and we can introduce the constants of motion

$$E \equiv -g_{\alpha\beta} \xi_t^\alpha p^\beta, \quad L \equiv g_{\alpha\beta} \xi_\phi^\alpha p^\beta, \quad (3)$$

where $\xi_t = \partial_t$ is the Killing field representing the stationarity of the Kerr geometry and $\xi_\phi = \partial_\phi$ is the rotational Killing field. Thus E , is interpreted as the total energy of timelike test particle

²We adopt the geometrical units $c = 1 = G$ and the $(-, +, +, +)$ signature, Greek indices run in $\{0, 1, 2, 3\}$. The four-velocity satisfy $u^\alpha u_\alpha = -1$. The radius r has unit of mass $[M]$, and the angular momentum units of $[M]^2$, the velocities $[u^t] = [u^r] = 1$ and $[u^\theta] = [u^\phi] = [M]^{-1}$ with $[u^\phi/u^t] = [M]^{-1}$ and $[u_\phi/u_t] = [M]$. For the seek of convenience, we always consider the dimensionless energy and effective potential $[V_{eff}] = 1$ and an angular momentum per unit of mass $[L]/[M] = [M]$.

coming from radial infinity, as measured by a static observer at infinity, while L is the axial component of the angular momentum of the particle. Line element (1) is also invariant under the application of any two different transformations: $x^\alpha \rightarrow -x^\alpha$ for one of the coordinates (t, ϕ) , or the metric parameter a , and therefore the test particle dynamics is invariant under the mutual transformation of the parameters $(a, L) \rightarrow (-a, -L)$. This makes possible to limit the analysis of the test particle circular motion to the case of positive values of a for corotating ($L > 0$) and counterrotating ($L < 0$) orbits with respect to the black hole.

To start of exploration of the accretion sequences we consider a one-species particle perfect fluid (simple fluid), described by the energy momentum tensor

$$T_{\alpha\beta} = (\varrho + p)u_\alpha u_\beta + p g_{\alpha\beta}, \quad (4)$$

where ϱ and p are the total energy density and pressure, respectively, as measured by an observer moving with the fluid whose four-velocity u^α is a timelike flow vector field. Then set up the problem symmetries, assuming to be $\partial_t \mathbf{Q} = 0$ and $\partial_\phi \mathbf{Q} = 0$, for a generic tensor \mathbf{Q} . Consequently the fluid dynamics is described by the *continuity equation* and the *Euler equation* as follows

$$\begin{aligned} u^\alpha \nabla_\alpha \varrho + (p + \varrho) \nabla^\alpha u_\alpha &= 0, \\ (p + \varrho) u^\alpha \nabla_\alpha u^\gamma + h^{\beta\gamma} \nabla_\beta p &= 0, \end{aligned} \quad (5)$$

where $h_{\alpha\beta} = g_{\alpha\beta} + u_\alpha u_\beta$ and $\nabla_\alpha g_{\beta\gamma} = 0$ (Pugliese&Montani, 2015; Pugliese et al., 2012), moreover we assume fluid toroidal configurations centered on the plane $\theta = \pi/2$, and defined by the constraint $u^r = 0$, with a barotropic equation of state $p = p(\varrho)$. No motion is assumed also in the θ angular direction ($u^\theta = 0$). The continuity equation is identically satisfied as consequence of these conditions and the Euler equation in (5) reads

$$\frac{\partial_\mu p}{\varrho + p} = -\partial_\mu W + \frac{\Omega \partial_\mu \ell}{1 - \Omega \ell}, \quad W \equiv \ln V_{eff}(\ell) \quad (6)$$

$$\begin{aligned} \text{where } V_{eff}(\ell) = u_t &= \pm \sqrt{\frac{g_{\phi t}^2 - g_{tt} g_{\phi\phi}}{g_{\phi\phi} + 2\ell g_{\phi t} + \ell^2 g_{tt}}} \\ \text{and } \ell &= \frac{L}{E}. \end{aligned} \quad (7)$$

The function W in Eq. (6) is Paczynski-Wiita (P-W) potential, Ω is the relativistic angular frequency of the fluid relative to the distant observer, and $V_{eff}(\ell)$ provides an *effective potential* for the fluid, assumed here to be characterized by a conserved and constant specific angular momentum ℓ (see also Lei et al. (2008); Abramowicz (2008)).

Similarly to the case of the test particle dynamics, the function $V_{eff}(\ell)$ in Eq. (6) is invariant under the mutual transformation of the parameters $(a, \ell) \rightarrow (-a, -\ell)$, therefore we can limit the analysis to positive values of $a > 0$, for *corotating* ($\ell > 0$) and *counterrotating* ($\ell < 0$) fluids and we adopt the notation (\pm) for counterrotating or corotating matter respectively. Therefore, the accretion tori corotate $(-)$ or counterrotate $(+)$ with respect to the Kerr BH, for $\ell_\mp a \geq 0$ respectively. As a consequence of this, considering the case of two orbiting tori, (i) and (o)

respectively, we need to introduce the concept of *lcorotating* tori, $\ell_i \ell_o > 0$ (es: Figs 1)-*Third panel*, and *lcounterrotating* tori, $\ell_i \ell_o < 0$ —see Figs 1-*Bottom-panel*. The tori can be both corotating, $\ell a > 0$, or counterrotating, $\ell a < 0$, with respect to the central Kerr attractor fPugliese&Stuchlík (2015). The configurations are regulated by the balance of the hydrostatic and centrifugal factors due to the fluid rotation and by the curvature effects of the Kerr background, encoded in the effective potential function V_{eff} . The set of these configurations (macro-configurations) is studied as ringed accretion disks in Pugliese&Stuchlík (2015, 2016a). Examples of integrations for these configurations are shown in Figs 1 (see also Fig. 3).

The procedure adopted in the present article borrows from the Boyer theory on the equipressure surfaces applied to a torus (Boyer, 1965), where the Boyer surfaces are given by the surfaces of constant pressure or³ $\Sigma_i = \text{constant}$ for $i \in (p, \varrho, \ell, \Omega)$ (Boyer, 1965; Frank et al., 2002), where the angular frequency is indeed $\Omega = \Omega(\ell)$ and $\Sigma_i = \Sigma_j$ for $i, j \in (p, \varrho, \ell, \Omega)$. Many features of the tori dynamics and morphology like their thickness, their stretching in the equatorial plane, and the location of the tori are predominantly determined by the geometric properties of spacetime via the effective potential V_{eff} . The boundary of any stationary, barotropic, perfect fluid body is determined by an equipotential surface, i.e., the surface of constant pressure that is orthogonal to the gradient of the effective potential. The toroidal surfaces are the equipotential surfaces of the effective potential $V_{eff}(\ell)$, considered as function of r and θ , solutions $\ln(V_{eff}) = c = \text{constant}$ or $V_{eff} = K = \text{constant}$. The couple of parameters (ℓ, K) uniquely identifies each Boyer surface. According to Eq. (6), the maximum of the hydrostatic pressure corresponds to the minimum r_{min} of the effective potential V_{eff} , and it is the torus center r_{cent} . The fluids instability points are located at the minima of the pressure and therefore maxima r_{Max} of V_{eff} . Equation $\partial_r V_{eff} = 0$ can be solved for the specific angular momentum of the fluid $\ell(r)$ —Fig. 2-*bottom*. This curve provides information about the center of the torus r_{cent} and possible critical points r_{Max} , while we can calculate the values of the curve K as $K_{crit} = V_{eff}(\ell(r))$ specifying the solution topology. These solutions, if they exist, represent non equilibrium configurations which may be closed C_x , for an accreting torus with accretion point r_x , or open O_x which are associated to some “proto-jet” matter configurations⁴, with critical point r_j (see Fig. 3 and also Pugliese&Stuchlík (2016a)). In general we use the notation $()$ and $()_x$ to indicate any equilibrium or critical configuration without any further specification of its topology. Finally C stands for a closed equilibrium configuration whose (stress) inner and outer edges are r_{in} and r_{out} respectively. Then there is $r_{in} \in \Delta r_{crit}$, where $\Delta r_{crit} \equiv [r_{Max}, r_{min}]$ and $r_{out} > r_{min}$.

³More generally $\Sigma_{\mathbf{Q}}$ is the surface $\mathbf{Q} = \text{constant}$ for any quantity or set of quantities \mathbf{Q} .

⁴The role of “proto-jet” configurations, which in fact correspond to limiting topologies for the closed or closed cusped solutions associated with equilibrium or accretion, is still under investigation. More generally, in this model the open surfaces have been always associated with the jet emission along the attractor symmetry axis—see for a general discussion (Kozłowski et al., 1978; Abramowicz et al., 1978; Sadowski et al., 2016; Lasota et al., 2016; Lyutikov, 2009; Madau, 1988; Sikora, 1981; Stuchlík et al., 2000).

The range $\lambda^i = r_{out}^i - r_{in}^i$ is the elongation on the equatorial plane of a C disk and, in a tori couple, $\bar{\lambda} = r_{in}^o - r_{out}^i$ is the spacing between the outer C_o and inner C_i torus of the couple. For colliding tori there is $\bar{\lambda} = 0$.

Tori are strongly constrained by the Kerr geometry *geodesic structure*⁵: this comprises the *notable radii* $r_N^\pm = \{r_\gamma^\pm, r_{mbo}^\pm, r_{mso}^\pm\}$ made by the *marginally stable circular orbit*, r_{mso}^\pm , the *marginally bounded circular orbit*, r_{mbo}^\pm and the *marginal circular orbit* (photon orbit) r_γ^\pm -Fig. 4-Upper- (Pugliese et al., 2011, 2013).

It is simple to see that, consistently with most of the axisymmetric accretion tori models, the (*stress*) *inner edge* r_{in} of the accreting torus is at $r_x \in]r_{mbo}, r_{mso}]$, while the torus outer Roche lobe is centered at $r_{cent} > r_{mso}$ (Krolik&Hawley, 2002; Bromley et al., 1998; Abramowicz et al., 2010; Agol&Krolik, 2000). From now on given r_* , we adopt the notation for any function $\mathbf{Q}(r) : \mathbf{Q}_* \equiv \mathbf{Q}(r_*)$, thus for example $\ell_{mso}^+ \equiv \ell^+(r_{mso}^+)$.

These radii stand as one of the main effects of the presence of strong curvature of the background geometry. In fact, let indexes $i \in \{1, 2, 3\}$ refer to the following ranges of angular momentum $\ell \in \mathbf{Li}$. We find that 1. for fluid specific angular momentum ℓ in $\mp \mathbf{L1}^\pm \equiv [\mp \ell_{mso}^\pm, \mp \ell_{mbo}^\pm[$, topologies (C_1, C_x) are possible, with accretion point in $r_x^\pm \in]r_{mbo}^\pm, r_{mso}^\pm]$. 2. For $\mp \mathbf{L2}^\pm \equiv [\mp \ell_{mbo}^\pm, \mp \ell_\gamma^\pm[$, topologies (C_2, O_x) are possible, with unstable point $r_j^\pm \in]r_\gamma^\pm, r_{mbo}^\pm]$. 3. For $\mp \mathbf{L3}^\pm \equiv \ell \geq \mp \ell_\gamma^\pm$, only equilibrium torus C_3 exists—see Fig. 5. The toroidal surfaces are characterized by $K_\pm \in [K_{min}^\pm, K_{Max}^\pm[\subset]K_{mso}^\pm, 1[\equiv \mathbf{K0}$. Otherwise, there can be funnels of material, associated to matter jets, along an open configuration O_x^\pm with $K_{Max}^\pm \geq 1$ ($\mathbf{K1}^\pm$).

Constraints in this model are provided by the conditions of no-penetration of matter ($\bar{\lambda} \neq 0$ -absence of collision) and by the geometric constraint for the equilibrium configurations determined by the geometric properties of the Kerr background reflected by the geodesic structure. We distinguish four types of unstable couples of orbiting configurations (*states* of the macro-configurations): the *proto-jet-proto-jet* (**J-J**) systems, corresponding to couples of open cusped surfaces, the *proto-jet-accretion* (**J-A**) systems, where the proto-jet can follow or precede the accretion point, and finally the *accretion-accretion* (**A-A**) systems, where matter can accrete onto the attractor from several instability points. Finally we consider also the case of the *proto-jet-equilibrium* (**J-C**) systems, and the *accretion-equilibrium* (**A-C**) systems. We prove that states depend on the dimensionless spin of the attractor, the relative rotation of the tori with respect to the attractor, the relative rotation of the fluids in the tori, strongly differentiating between ℓ corotating and ℓ counterrotating fluids. After studying five fundamental states, we shall consider the possible combination of these states, reorganizing the investigations for ringed disks consisting of more than two rings, i.e. with configuration of order greater than two. An interesting task of this investigation is the search for a possible proto-jet-accretion correlation in the states of the ringed

⁵It is worth specifying that this strong dependence of the model on the geometric properties of spacetime induced by the central attractor enables us to apply to a certain extent the results found here to different models of accretion disks (Abramowicz&Fragile, 2013).

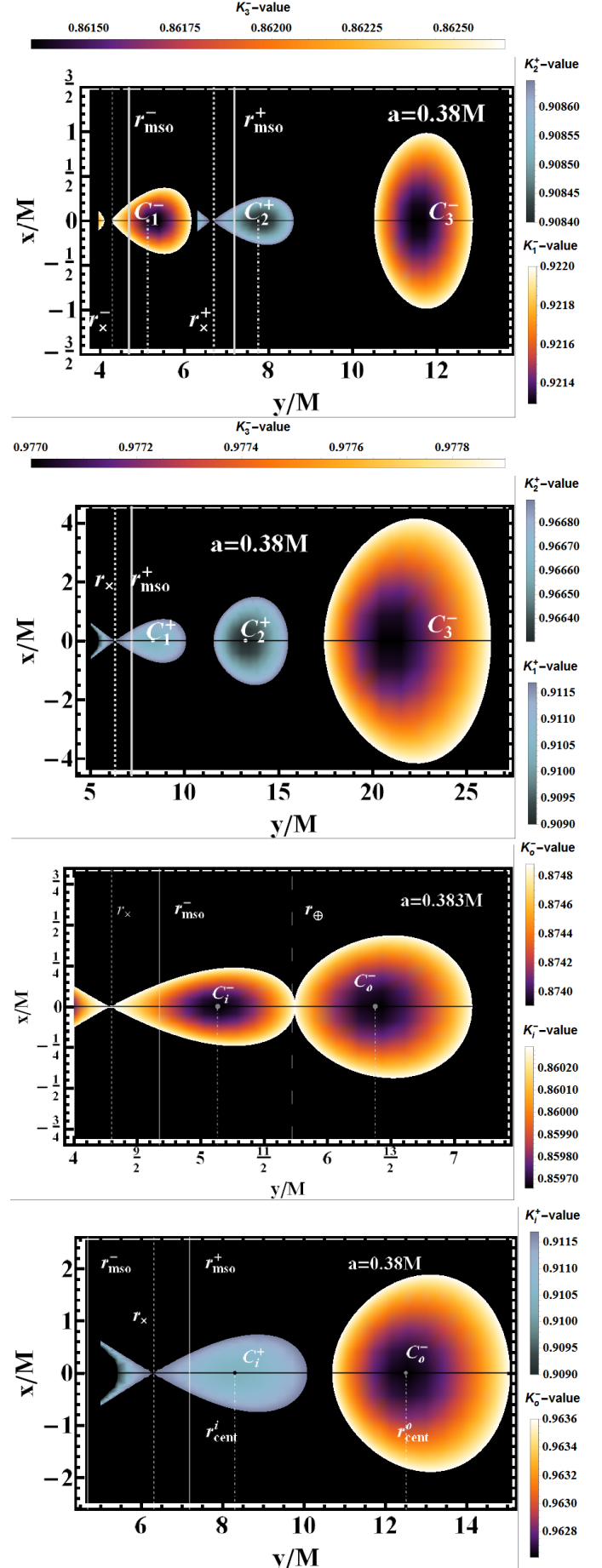


Figure 1: Density plots. *Upper-first panel*: $C_x^- < C_x^+ < C^-$ configurations; *Upper-second panel*: $C_x^+ < C^+ < C^-$ configurations. *Third panel*: colliding corotating tori $C_x^- < C^-$, *Bottom panel*: couple $C_x^+ < C^-$. (x, y) are Cartesian coordinates.

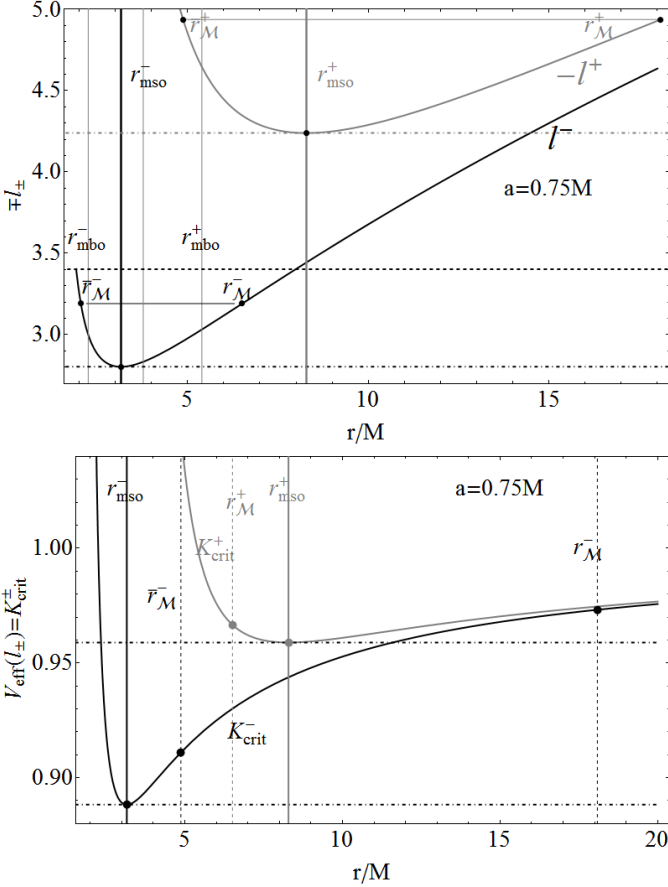


Figure 2: Spacetime spin $a = 0.75M$. The outer horizon is at $r_+ = 1.66144M$. Curves of the fluid specific angular momentum $\pm\ell^\pm$ (upper panel) and $K_{crit}^\pm = V_{eff}(\ell^\pm)$ of critical points of the effective potentials at different angular momenta (bottom panel) as functions of r/M . r_M^\pm the maximum points of derivative $\partial_r(\mp\ell^\pm)$ respectively. Corotating case ($-$), black curves, and counterrotating case ($+$), gray curves, are shown. Minimum of the curves, signed by points, set the vales of the functions $(\ell(r), K_{crit}(r))$ valuated at marginally stable orbits r_{mso}^\pm : toroidal configurations associated with critical points of the pressure are possible only for $\mp\ell_\pm \geq \mp\ell_{mso}^\pm$ and $K^\pm \geq K_{mso}^\pm$ respectively.

disks. Thus, we introduce the concept of *geometrical correlation* between two configurations of a state, when the two surfaces may be in contact, in accordance with the constraints of the system. When a contact between two configurations occurs, feeding or collision phenomena happen, leading eventually to a topological transition of the ring state and, in the end, of the entire macro-configuration. Consequentially we face the problem of the *state evolution*: an initial couple of configurations (starting state) could evolve towards a transition of the surface topologies following an evolutive line from the initial state. We show that in some cases equilibrium configurations can only lead to proto-jet configurations and not to the accretion.

In the following, we will use also the symbols \leq ; we intend the ordered sequence of maximum points of the pressure, or $r_{min} = r_{cent}$, minimum of the effective potential which corresponds to the configuration center. Therefore, in relation to a couple of rings, the terms “internal” (inner- i) or “external” (outer- o), will always refer, unless otherwise specified, to the

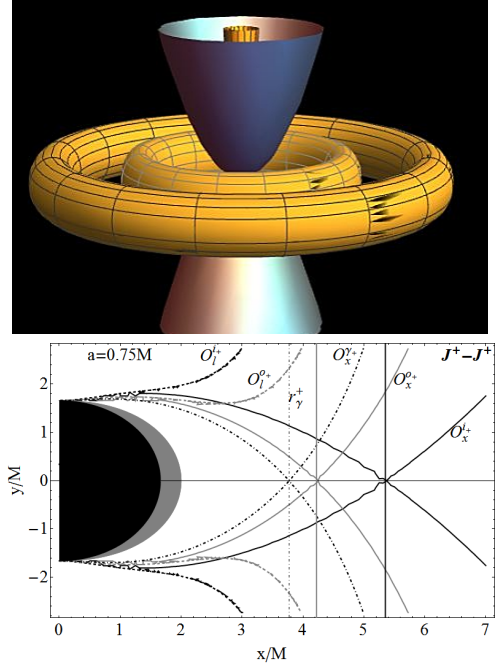


Figure 3: Upper panel: Pictorial representation of a ringed accretion disk with open O_x surfaces. Bottom panel: Spacetime spin $a = 0.75M$, ℓ corotating sequences, $\ell_i \ell_j > 0$, of counterrotating open configurations $\mathbf{J}^+ - \mathbf{J}^+$ $\ell_i a < 0 \forall i, j$. Decomposition including open-crossed sub-configurations (γ -surface) O_x^γ , open cusped with angular momentum ℓ_γ . The outer horizon is at $r_+ = 1.66144M$, black region is $r < r_+$, gray region is $r < r_\epsilon^+$, where r_ϵ^+ is the static limit, and r_γ^+ is the photon orbit on $\Sigma_{\pi/2}$. For O_x^{O+} there is $\ell_o = -5.62551$ and $K_o = 1.28775$, for O_x^{O+} there is $\ell_i = -4.66487$ and $K_i = 1.00272$. The open surfaces O_x^{O+} and O_x^{O+} are limiting solutions without critical points.

sequence ordered according to the center location. r_{cent} ; then with symbols $>$ and $<$, we refer to the sequentiality according to the location of the *minimum* points of the pressure, or r_{Max} , maximum point of the effective potential $r_x^- < r_x^+$.

We organize our analysis dividing discussion in the section (3) for the ℓ corotating sequences and Section (4) for the ℓ counterrotating sequences. For easy of reference we listed in Table (1) major Kerr BH spin values defined during this analysis. In Appendix A we provide proof of the some assertions used in Secs (3) and (4), and a more general discussion of some results. We study inclusions⁶ of the notable radii $r_N^\pm \in ()_\pm$ and $r_N^\pm \in ()_\mp$. This analysis sets location of the disk inner edge with respect to the geodesic structure r_N , according to the fluid specific angular momentum.

3. ℓ corotating sequences

We consider the case of ℓ corotating sequences focusing first on a couple of ℓ corotating configurations and then extending

⁶ $r_\bullet \in ()$ means the inclusion of a radius r_\bullet in the configuration $()$ (location of $()$ with respect to r_\bullet) according to some conditions; \notin is non inclusion; in general \gg ! intensifier a reinforcement of a relation \gg , indicating that this is a necessary relation which is *always* satisfied.

Table 1: Major Kerr **BH** spin values defined during the analysis. Details on the relevance of the 21 selected values of the **BH** spins can be found in the text.

$a_{\mathcal{N}_2} \equiv 0.172564M : -\ell_{mso}^+ = \ell_{mbo}^-$	$a_o^* = 0.201697M : \ell_{mso}^- = \ell^-(r_{mbo}^+)$	$a_l \equiv 0.3137M : r_{mbo}^- = r_{\gamma}^+$
$a_{l_a} \equiv 0.372583M : r_{mso}^- = r_{mbo}^+$	$a_{\mathcal{N}_1} = 0.382542M \in]a_{l_a}, a_{\mathcal{N}_a}[: \ell_{\gamma}^- = -\ell_+(r_{mso}^-)$	$a_{\mathcal{N}_0} \equiv 0.390781M : \ell_{\gamma}^- = -\ell_{mbo}^+$
$\check{a}_s \equiv 0.401642M : \check{\ell}_s = \ell_{\gamma}^-$	$\check{a}_{\mathcal{N}} \approx 0.461854M : \ell^-(r_{mso}^+) = \ell_{mbo}^-$	$a_{\mathcal{N}} \approx 0.5089M : -\ell_{mso}^+ = \ell_{\gamma}^-$
$a_l^* = 0.618034M : \check{\ell}_+ = \ell_{2+}^-$	$d_{\gamma-}^{\beta} \equiv 0.628201M : \ell_{\beta}^- = \ell_{\gamma}^-$	$a_{\gamma+}^- \equiv 0.638285M : r_{\gamma}^+ = r_{mso}^-$
$a_1 \approx 0.707107M : r_{\gamma}^- = r_{\epsilon}^+$	$a_o = 0.728163M \in]a_1, \check{a}_{\mathcal{N}}[: \ell_{mbo}^- = \ell^-(r_{mbo}^+)$	$\check{a}_{\mathcal{N}} = 0.73688M : \ell^-(r_{mso}^+) = \ell_{\gamma}^-$
$a_{\gamma-}^{\Gamma} \equiv 0.777271M : \ell_{\Gamma}^- = \ell_{\gamma}^-$	$a_b^- \approx 0.828427M : r_{mbo}^- = r_{\epsilon}^+$	$a_o^{\gamma} = 0.867744M \in]a_b^-, a_{\mathcal{M}}^-[: \ell_{\gamma}^- = \ell^-(r_{mbo}^+)$
$a_{\mathcal{M}}^- \equiv 0.934313M : \ell_{\gamma}^- = \ell_{\mathcal{M}}^-$	$a_2 \approx 0.942809M : r_{mso}^- = r_{\epsilon}^+$	$\check{a} \equiv 0.969174M : \check{\ell}^- = r_{\gamma}^-$

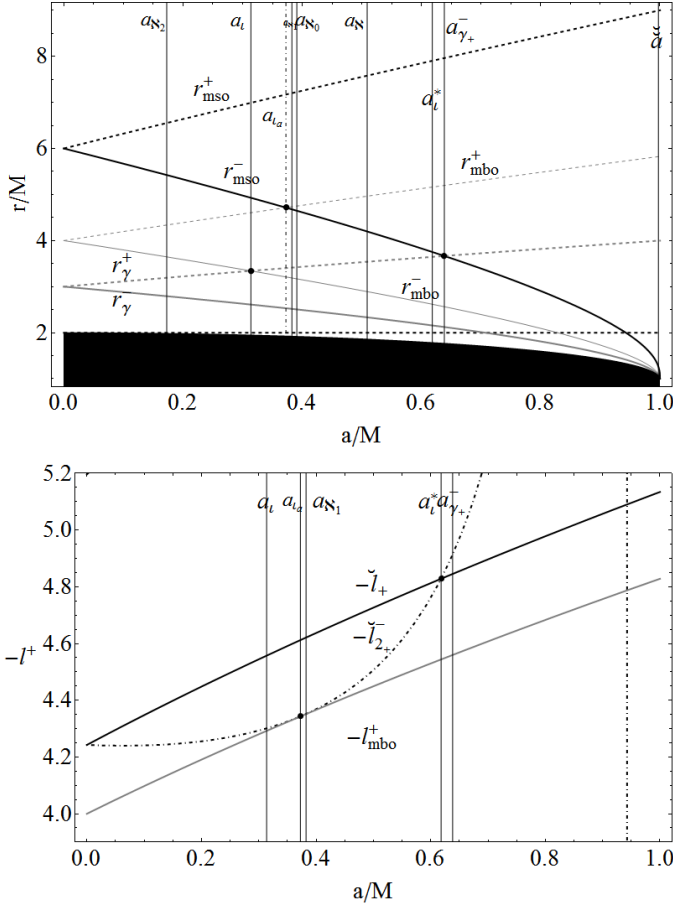


Figure 4: Upper panel: the notable radii $r_{\mathcal{N}}^{\pm} = \{r_{\gamma}^{\pm}, r_{mbo}^{\pm}, r_{mso}^{\pm}\}$, for the corotating (–) and counterrotating (+) orbits. Radii r_{γ}^{\pm} are the photon orbits, r_{mbo}^{\pm} the marginally bounded orbits and r_{mso}^{\pm} the marginally stable orbit. Black region is $r < r_+$, r_+ being the outer horizon. Bottom panel: specific angular momentum for counterrotating $\ell^+ < 0$ orbits on the marginally bounded orbit $-\ell_{mbo}^+$ and the curves $-\check{\ell}_{2+}^-$, as evaluated in r_{mso}^- . There is $\check{\ell}_{2+}^- : V_{eff}(\check{\ell}_{2+}^-, r_{mso}^-) = 1$ where $-\check{\ell}_{2+}^- \in]-\ell_{mbo}^+, -\check{\ell}_2^+]$. The specific angular momentum $\check{\ell}_+ : V_{eff}(\check{\ell}_+, r_{mso}^+) = 1$.

our investigation to the multiple configurations of the decomposition of order $n > 2$. Figure 1-third panel shows a colliding couple of corotating configurations, and Fig. 1-second panel shows an inner couple of counterrotating tori in a three tori configuration, the inner rings are in accretion.

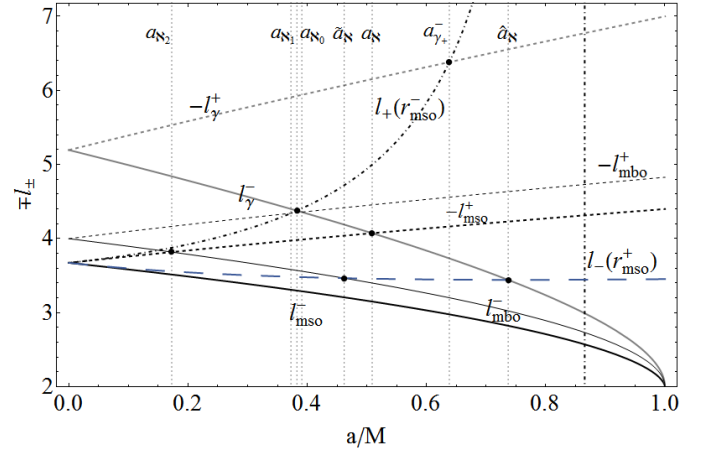


Figure 5: Specific angular momentum for corotating $\ell^- > 0$ and counterrotating $-\ell^+ > 0$ orbits on the notable radii $r_{\mathcal{N}}^{\pm} = \{r_{\gamma}^{\pm}, r_{mbo}^{\pm}, r_{mso}^{\pm}\}$, for the corotating (–) and counterrotating (+) orbits. Where r_{γ}^{\pm} are the photon orbits, r_{mbo}^{\pm} the marginally bounded orbits and r_{mso}^{\pm} the marginally stable orbit. Spins are shown where a cross occurs.

We point out that

$$\begin{aligned} \text{if } ()_i < ()_o, \quad \text{where } \ell_i \ell_o > 0, \\ \text{then } ()_i > ()_o, \quad \text{where } () \in \{C, C_x, O_x\}, \end{aligned} \quad (8)$$

see Fig. 2. For the *ordered* sequences of surface, with the notation $<$ or $>$, we intend the ordered sequence of maximum points of the pressure or r_{min} , minimum of the effective potential and the disk centers for the closed sub-configurations (Pugliese&Stuchlík, 2015). In relation to a couple of rings, the terms “internal” (equivalently inner) or “external” (equivalently outer), will always refer, unless otherwise specified, to the sequence ordered according to the location of the centers. Then, if $C_i < C_j$ for $i < j$, C_i is the inner ring, closest to attractor, with respect to C_j , and there is $r_{cent}^i \equiv r_{min}^i < r_{min}^j \equiv r_{cent}^j$. Within these definitions, the rings (C_i, C_{i+1}) and (C_{i-1}, C_i) are *consecutive* as $C_{i-1} < C_i < C_{i+1}$ (Pugliese&Stuchlík, 2015). The symbols $>$ and $<$ refer instead to the sequentiality between the ordered location of the *minimum* points of the pressure, or r_{Max} , maximum point of the effective potential, if they exist, which are the instability points of accretion, $r_x = r_{Max}$ for C_x topologies, or of launching of proto-jets, $r_{Max} = r_J$ for the open cusped topologies (proto-jets). Where, due to definition, it is always $r_{min}^i < r_{min}^o$. For an ℓ corotating sequence, this definition *implies* also $r_{Max}^i > r_{Max}^o$, therefore, for the ℓ corotating

sequences it is always $O_i < O_o$ and $O_i > O_o$.

The third inequality in Eq. (8) makes sense when the potential function has a maximum point, that is for ℓ_i and ℓ_o in **L1** or **L2**. The nearest to the source is the open surface launching point $r_{Max} = r_J$ or the accretion point $r_{Max} = r_x$, and largest is the magnitude of the fluid specific angular momentum. The largest is the radius of the maximum pressure point and more stretched on the equatorial plane is the configuration, regardless of its topology.

In what follows we will specify relation (8) in different cases, fixing the topology of the couple $(O_i - O_o)$: in Sec. (3.1) we shall consider the couple of open configurations (**J[±]-J[±]**). The couple (**A - J**), formed by a configuration in accretion and an open configuration in O_x topology, are studied in Sec. (3.2) for the case where the opened cusped topology is the outer one of the pair. In Sec. (3.3), the case in which the inner configuration of the couple has open topology is investigated. Section (3.4) describes the couple formed by a disk in equilibrium and an open outer surface (according to the location of minima of the effective potential). Section (3.5) concentrates on the couple where the open surface is the inner one. Some remarks on the couples (**C - A**) are addressed in Sec. (3.6), closing this section.

This section covers the ℓ corotating sequences of rings. We shall always intend the relations between magnitudes of the specific angular momentum, if not otherwise specified.

3.1. The ℓ corotating proto-jet-proto-jet (**J-J**) systems

In this section we consider a couple of ℓ corotating open cusped configurations with P-W instability points (r_{Max}^o, r_{Max}^i) where

$$\begin{aligned} O_x^i < O_x^o \quad \text{implies} \quad O_x^i > O_x^o, \quad |\ell_i| < |\ell_o|, \quad \ell \in \mathbf{L2}, \\ r_J \in]r_\gamma, r_b], \quad \mathbf{K}_i \in]1, \mathbf{K}_o[, \end{aligned} \quad (9)$$

for the state of the ℓ corotating couple $O_x^\pm - O_x^\pm$. Here we determine the evolutive lines for different black hole attractors.

In the sequences of open configurations, we will mainly deal with the critical points. It will be then convenient to introduce the *criticality indices* \hat{i} , univocally associated to the couple (r_{Max}^i, ℓ_i) , where i is as usual the configuration index univocally associated to (r_{min}^i, ℓ_i) ⁷. As relation (8) stands, we can consider $\hat{i}(i)$ as a decreasing function of the configuration index i or $\partial_i \hat{i}(i) < 0$. In other words, Eq. (9) can be written in the criticality indexes as $O_x^i > O_x^o$ and $O_x^o > O_x^i$ as $|\ell_i| = |\ell_\delta| < |\ell_o| = |\ell_i|$. The function $\hat{i}(i)$ has inverse in a restriction of the variation domain of the configuration index. In fact, the configuration index set is far more vast of the set of the criticality indexes containing, for example, the surfaces with momentum in **L3**. However we might say that the function $\hat{i}(i)$ could be inverted in **L1** and **L2**, taking into account that the disk does not include necessarily the critical points when $K < K_{Max}$ (in other words, the rank $r_x \in [0, n]$).

⁷It is intended that no confusion will arise by a possible overlap of two ℓ counterrotating configurations.

In principle, there is an infinite number of ℓ corotating critical open funnels, i.e. $n_J^{Max} = \infty$. As mentioned in Pugliese&Stuchlík (2015), we can introduce definition of configuration density δn , i.e., the density of maximum points of pressure in a fixed orbital range Δr , $\delta n \equiv n|_{\Delta r} / \Delta r$. The configuration density naturally depends on the specific angular momentum parameter and particularly on the matrix of displacements, here considered at constant step κ ⁸. The density is generally a decreasing function of the step $|\kappa| > 0$. Similarly, we can introduce a *criticality density* δn_{Max} as the density of P-W points. Specifically we now consider the density δn_J as the density of P-W launching points of proto-jets in Δr_J . In the particular case of ℓ corotating matter, the following relations hold:

$$\begin{aligned} \partial_{\delta Q} \delta n < 0, \quad \partial_{\delta Q} \delta n_J < 0 \quad \text{with} \quad \delta Q \in \{\delta|\ell|, \delta K\}, \\ \partial_{\delta Q} \Delta r_J^{i,o} > 0 \quad \Delta r_J^{i,o} \equiv r_J^i - r_J^o > 0, \end{aligned} \quad (10)$$

where δK and $\delta|\ell|$ give the magnitude of the difference of the K parameter and the specific angular momentum $|\ell|$ of the ℓ corotating rings, and $\Delta r_J^{i,o}$ is the distance between the two launching points—see Fig. 3 ($\delta|\ell|$ is constant displacement $|\kappa|$ in accordance with Pugliese&Stuchlík (2015)). Here and in the following, by $\partial_B Q > 0$ we mean the quantity Q increases as the quantity B increases and viceversa.

The increase of the criticality (configuration) density corresponds to an increase, at fixed orbital range, of the O_x configurations number in the ℓ corotating sequence. This corresponds to an increase in the magnitude of the specific angular momentum as the launch point r_J is closer to the surface O_x^\pm , cusped surface with angular momentum ℓ_γ^\pm —Fig. 3: additional specific angular momentum is required to the orbiting matter for the formation of a new ℓ corotating launching point of proto-jets, inner with respect to the first O_x^i of the $\{O_x^i\}_i$ sequence, increasing thus inwardly the criticality density δn_J , while approaching the threshold $O_x^\ell = O_x^\gamma$. In other words, the fluid specific angular momentum magnitude decreases *outwardly* in the decomposition.

However, the specific angular momentum that has to be provided for a shift of the critical point inwardly, is not constant with the dimensionless spin of the black hole. It is strongly diversified for the two ℓ counterrotating sequences, and does not in general grow regularly with the configuration index (or decreases with the criticality index) (Pugliese&Stuchlík, 2015). In fact, there exists a maximum value with respect to configuration index (or equivalently with respect to the radius) for configurations with center of maximum hydrostatic pressure in $r_M^\pm > r_{mso}^\pm$, and specific angular momentum $\ell_M^\pm > \ell_{mbo}^\pm$ respectively.

In terms of the criticality indices \hat{i} , one has $\partial_i \ell < 0$, with $\partial_i^2 \ell = 0$ for a configuration with specific angular momentum magnitude $\ell_M > \ell_{mbo}$ and centered in r_M . Indeed, since $r_M^\pm > r_{mso}^\pm$, the radii r_M^\pm can be minimum points of the effective potential, but *not* maximum points. Then ℓ_M is a minimum

⁸For example, by adopting the antisymmetric displacement matrix $\epsilon_{[i,i+\kappa]} = \kappa \epsilon$ (with $\epsilon = \text{constant}$ and step of the decomposition $\kappa \geq 1$), introduced in Pugliese&Stuchlík (2015).

(maximum) value for the function $\partial_i \ell_i$ ($\partial_i \ell_i = \partial_i \hat{i} \partial_i \ell_i$).

The two ℓ counterrotating sequences of ℓ corotating open configurations with specific angular momenta $\ell_{\mathcal{M}}^{\pm}$, have generally different topologies associated with their critical phase. Indeed, for the counterrotating fluids in the geometries $a \in]0, M]$, we have $-\ell_{\mathcal{M}} \in]-\ell_{mbo}^+, -\ell_{\gamma}^+[\equiv \mathbf{L2}^+$; therefore, the critical configurations with $\ell = \ell_{\mathcal{M}}^+$ always correspond to the proto-jets O_x^+ .

Conversely, this is not always the case for the corotating fluids where, at higher spin of the attractor, i.e., $a \geq a_{\mathcal{M}}^- \equiv 0.934313M$, there is $\ell_{\mathcal{M}}^- \in \mathbf{L3}^-$ when there are no critical topologies. Whereas in the geometries with $a \in [0, a_{\mathcal{M}}^-]$, we have $\ell_{\mathcal{M}}^- \in \mathbf{L2}^-$, and only critical configurations O_x^- are possible. Moreover, this also means that the supplying specific angular momentum to be provided for a further inner launch point of proto-jet (according to the criticality index \hat{i}), decreases constantly with the criticality index (or constantly increases with the configuration index) in the geometries of the faster attractors⁹, as in those spacetimes, there is no minimum of $\partial_i \ell^-$ in $\mathbf{L2}^-$. One can conclude that the specific angular momentum to be supplied in the disk for an inner (corotating) proto-jet launch point grows uniformly with the radius (and uniformly with the configuration index)- $\partial_i^2 \ell_J > 0$ for very fast attractors. But the surplus of specific angular momentum needed to locate the proto-jets in the inner regions (moving the center outwardly) increases more and more slowly in the far away regions¹⁰, where the Newtonian limit could be considered and, as asymptotically $\lim_{r \rightarrow \infty} \ell' = 0$ with $\lim_{r \rightarrow \infty} \ell^{\pm} = \pm\infty$, the quantity $\delta \ell_{i+j,i}$ is approximately constant with the radius.

The existence of the couple $(r_{\mathcal{M}}, \ell_{\mathcal{M}})$ is a relativistic effect, also present in the static case $a = 0$, but for a rotating attractor this is strongly differentiated from an albeit minimal intrinsic rotation of the gravitational source. In the static limit, there exists a maximum of $\partial_r \ell$ for $r_{\mathcal{M}} = (6 + 4\sqrt{3})M$, the spread between the two ℓ counterrotating cases appears only when $a \neq 0$, and becomes obviously more and more pronounced with increasing spin of the attractor. In general, however, the increase of specific angular momentum decreases with increasing of r and $R = r/a$ where, at the limit of very large R , there is no distinction between the two ℓ corotating sequences. This is therefore a feature of the toroidal rotating fluids strongly affected by the dragging of the spacetime. Indeed, the difference $\partial_r(\ell^+ + \ell^-)$ goes to zero as $a = 0$ and r goes to infinity¹¹. In terms of the configuration and criticality density we have:

1. $\partial_r \delta n(r)|_{\delta_i} \geq 0$ for $r \leq r_{\mathcal{M}}$ and (11)
2. $\partial_r \delta n_J(r)|_{\delta_i} \leq 0$ for $r \leq \bar{r}_{\mathcal{M}}$.

The first relation of Eq. (11) is always verified for all specific angular momentum ranges \mathbf{Li} , whereas the second of Eq. (11) makes sense only for $\ell \in \{\mathbf{L1}, \mathbf{L2}\}$.

For these specific angular momenta we can consider the radii to be $\bar{r}_{\mathcal{M}} \equiv r_{Max}(\ell_{\mathcal{M}})$ the critical radii associated with the spe-

cific angular momentum $\ell_{\mathcal{M}}$, coupled with the center $r_{\mathcal{M}}$. The plot of $\bar{r}_{\mathcal{M}}$ as function of a/M , will be analogue to the plot of $r_{\mathcal{M}}$ as function of a/M , but rotated along an axis parallel to $r = \text{constant}$ and located in the orbital range according to $\ell_{\mathcal{M}}$ in the ranges \mathbf{Li} ¹².

Similarly to the case of the equilibrium ringed disks, we can explain the significance of the presence of the $r_{\mathcal{M}}$ points and of Eq. (11) in terms of density of critical points. Assuming that increase of the specific angular momentum in magnitude within the macro-configuration is adjusted for constant displacement (κ constant), and $\partial_i \hat{i} < 0$ (we mean to say that one quantity decreases where the other increases, repositioning the labels such that $i \rightarrow \hat{o}$ and viceversa $o \rightarrow \hat{i}$), one has $\epsilon_{[\hat{i}\hat{j}]} = -\epsilon_{ij} = \epsilon_{ji}$ and $\epsilon_{\hat{i}+\hat{k},\hat{i}} = \hat{k}\epsilon > 0$. We note that the configuration density, directly related to κ , is maximal at $r_{\mathcal{M}}$. Let $\bar{r}_{\mathcal{M}} = r_J < r_{\mathcal{M}} = r_{cent}$ be the (proto-jet) instability point associated with $r_{\mathcal{M}}$. This point is always present in the counterrotating case and for corotating fluids orbiting attractors with $a < a_{\mathcal{M}}^-$. The couple of critical points $(\bar{r}_{\mathcal{M}}, r_{\mathcal{M}})$ is an intrinsic property of the specific geometry and it is function of a/M only, as such it is unique for each attractor. It follows that the disk centers are more spaced in the region $r > r_{\mathcal{M}}$ (lower density of the index configuration), and viceversa at $r < r_{\mathcal{M}}$; the rings are closer together as they approach $r_{\mathcal{M}}$. In a neighborhood of $r_{\mathcal{M}}$, the configuration density $\delta n|_{\kappa} \approx \delta n_{\mathcal{M}}$ is highest—Fig. 2. Similarly, rewriting all in terms of the criticality density δn_J , we would say that, under the conditions given by the displacement matrix with step κ constant¹³, as the launching points are more spaced (lower criticality density) in $]r_{\gamma}, \bar{r}_{\mathcal{M}}[$, and decreasing as they move towards the inner O_x^- surface at $r < \bar{r}_{\mathcal{M}}$. At $r_J > \bar{r}_{\mathcal{M}}$, the launching points are getting closer, as they approach $\bar{r}_{\mathcal{M}}$ from the outer regions, or $r_J \in]\bar{r}_{\mathcal{M}}, r_{mbo}[$. It follows that, in a neighborhood of $\bar{r}_{\mathcal{M}}$, the corresponding criticality density $\delta n_J|_{\kappa} \approx \delta n_{\mathcal{M}}$ is *minimal*.

This means that, in a ringed model where the specific angular momentum varies (almost) monotonically with a constant step κ , two remarkable points in the distribution of matter appear: the $r_{\mathcal{M}}$, where the density of stable configurations (or density of the maximum hydrostatic pressure) reaches maximum, and the corresponding point $\bar{r}_{\mathcal{M}}$ where the density of proto-jet launch shall be at minimum. We recall that $(r_{\mathcal{M}}, \bar{r}_{\mathcal{M}})$, are uniquely fixed by the attractor geometry and the sense of the fluid rotation with respect to the geometry. Therefore, it would be possible to deduce both the spin of the attractor and the sign of rotation of the fluid relative to this from the knowledge of one of the points of $(r_{\mathcal{M}}, \bar{r}_{\mathcal{M}})$ and the surfaces with specific angular momentum $\ell \in \{\ell_{\gamma}, \ell_{mbo}, \ell_{mso}\}$.

For very fast attractors with $a > a_{\mathcal{M}}^- = 0.934313M$, there is $\ell_{\mathcal{M}}^- = \ell_{\gamma}^-$, and no maximum of density of the corotating fluid in open topologies exists; then, in the conditions provided by the assumption of κ constant, the set of critical points constantly increases approaching the critical γ -surface configuration (with specific angular momentum $\ell \in \{\ell_{\gamma}, \ell_{mso}, \ell_{mbo}\}$). We specify that the assumption of constant step κ has been here adopted as

⁹For *fast* (*slow*) attractors we intend Kerr attractors with high (small) values of the dimensionless spin with respect to some reference values of a/M , fixed considering the geodesic spacetime structure.

¹⁰In $r \gg r_{\mathcal{M}}(a)(i \gg i_{\mathcal{M}})$, as discussed in Pugliese&Stuchlík (2015).

¹¹However, for $a/M \approx 0$, it is $\approx 2(a/M)(3r/M - 2)/(r/M - 2)^3$.

¹²The couple $(r_{\mathcal{M}}, \bar{r}_{\mathcal{M}})$ corresponds to the couple of indices (i, \hat{i}) .

¹³It is indeed immediate to argue the relation in the assumptions $\kappa = \text{constant}$ and $\epsilon = \text{constant}$.

the most elementary and illustrative example of displacement matrix, the extension of these considerations to a general displacement law, with a generic ϵ_{ij} matrix, could be developed in a rather straightforward manner.

All the considerations involving very fast attractors for corotating fluids can be interpreted as an indication of the role played by the intrinsic rotation of the attractor in the formation of the corotating proto-jets. In this respect, it is worth noting that the following relations hold

$$\begin{aligned} Q_M^+ &> Q_M^-, \quad \Delta r_J^\pm < \Delta r_x^\pm, \quad \delta r_J^\pm < \delta r_x^\pm, \quad \delta \ell_J^\pm > \delta \ell_x^\pm, \\ \delta \ell_s^- &< \delta \ell_s^+, \quad s \in \{J, x\}, \quad Q_M \in \{r_M^\pm, \mp \ell_M^\pm, K_M^\pm\}, \quad a_* \equiv a/M \\ \partial_{a_*} \delta Q_s^\pm &\geq 0, \quad \delta Q^\pm \in \{\delta r^\pm, \delta \ell^\pm\}, \quad \partial_{a_*} Q_M^\pm \geq 0. \end{aligned} \quad (12)$$

Relations (12) highlight various properties of the ℓ counterrotating sequences and the role of the black hole spin in the formation of the decompositions.

However, before moving to the analysis of the two isolated subsequences¹⁴, we need to clarify the role of the two orbits \bar{r}_M^\pm . Considering Eq. (12), we have $Q_M^+ > Q_M^-$ that means a greater specific angular momentum and K -parameter is required for the matter in stable orbit to reach a maximum pressure point, see also Pugliese&Stuchlík (2015). In general, there is $r_{min}^+ > r_{min}^-$. Then for $\ell_\pm \in \mathbf{L2}^\pm$, the solution $\mp \partial_r \ell^\pm = 0$ has only one maximum point, i.e., \bar{r}_M is not a solution of $\mp \partial_r \ell^\pm = 0$, but every critical point of maximum is associated to a minimum, and in this sense we consider \bar{r}_M to be a minimum point as associated to the critical point r_M .

More generally, without restricting the analysis to the $\ell_\pm \in \mathbf{L2}^\pm$ case, if $r_{min}^- < r_{min}^+$, then necessarily $\ell^- < -\ell^+$, but the relation between the maximum points has still to be established. However, if $\ell^- \in]\ell_{mso}^-, -\ell^+[$, then it can be either $r_{min}^- < r_{min}^+$ or $r_{min}^- \in]r_{min}^+, \bar{r}_-]$ where $\bar{r}_- : \ell^-(\bar{r}_-) = -\ell^+$.

If $\ell^- > -\ell^+ > \ell_{mso}^+$, then necessarily $r_{Max}^- < r_{Max}^+ < r_{mso}^+ < r_{min}^+ < r_{min}^-$. But if $\ell^- < -\ell^+$, then neither the maximum or the minima are fixed and it can be either $C^- < C^+$ or $C^+ < C^-$ for each $r_{Max}^- < r_{Max}^+$ or $r_{Max}^+ < r_{Max}^-$.

To summarize, considering also Fig. 2: if $r_{min}^+ > r_{min}^-$, then $-\ell^+ > \ell^-$. But it is simple to see that we can obtain $r_{Max}^+ > r_{Max}^-$ or $r_{Max}^- > r_{Max}^+$. For example, the last case occurs for r_{min}^- being very close to r_{mso}^+ and a great separation in $(\ell^+ + \ell^-)$. Thus if $r_{min}^- \in [r_{mso}^+, r_{min}^+]$ and $\ell^- \in]\ell_{mso}^-, \ell^-(r_{min}^+)[$, if $r_{Max}^- : \ell_{mso}^- < \ell^- < \ell^-(r_{min}^+)$ there is $\partial_{r_{min}^-} r_{Max}^- > 0$, see also Pugliese&Stuchlík (2015); Pugliese&Montani (2015). However, this would make sense for matter orbiting around sufficiently slow attractors $A_i^< \equiv [0, a_i]$, where $a_i \equiv 0.3137M$.

In other words, knowing the relation between the points of maximum pressure, we could ignore the sequentiality according to the minimum points of pressure. This information is indeed important to determine the relative position of the

two ℓ corotating sequences also in the case of consecutive sequences. Part of these considerations will be resumed in Appendix A.

For attractors with higher spins, at $r > r_M$, for the corotating sub-configurations the Newtonian limit is reached in regions closer to the source, and with lower specific angular momenta magnitude with respect to the counterrotating ones. This is in agreement with the fact that the spacetime spin clearly distinguishes the two types of fluids, where the relativistic effects are essentially determined by the rotation of the Kerr attractor. In the first place, as discussed above, the radius corresponding to the minimum critical density δn_J is, for corotating fluids, always closer to the source than for the counterrotating proto-jets. For corotating matter, this point approaches the source as the attractor spin increases, and the specific angular momentum required for the launch of a corotating proto-jet decreases with this. With increasing black hole spin, the magnitude of the specific angular momentum required for a corotating proto-jet decreases and is decreasing in relation to those corresponding to the counterrotating case.

The situation is indeed just the opposite for the O_x^+ surfaces where, with increase of the black hole spin, the point of minimum proto-jet density moves outwards, confining these configurations in regions more and more distant from the source, and requiring also increasing magnitude of the specific angular momentum. It is then possible to prove that the K_M -parameter, associated to the momenta ℓ_M , shows an analogue behavior. This would suggest that the black hole spin distinguishes the two types of matter, by favoring the formation of corotating proto-jets with respect to the counterrotating ones.

In order to fully characterize the role of the dragging effects with respect to the $(J...J)$ ℓ corotating sequences, it is important to analyze the ranges of the variation for the parameters of the proto-jet configurations. Higher specific angular momentum in magnitude is required to set the matter in open funnels than for the accretion. In any Kerr geometry, the orbital region where the open funnels O_x are possible is the closest to the attractor, being inner with respect to the accretion regions (at $\mathbf{L1} < \mathbf{L2}$) and in general it is smaller: the orbital range allowed for an accretion point is larger than that where the proto-jet launch (r_J) can be formed. The extension of the specific angular momentum range possible for the accretion, i.e. the measure of $\mathbf{L1}$, is less than the measure of the $\mathbf{L2}$ range for the jets. These properties are important in the characterization of the critical points sequences, and the determination of the criticality density: we could conclude that the accretion phases are favored with respect to the instable proto-jets.

We could suppose that the proto-jet of open funnels arises at the final stage of the formation of an accretion disk which increases its elongation, approaching the source, or the O_x surface could also arise being non-correlated in any way by the accretion phase. In the model we are considering, this can be achieved keeping $\ell \in \mathbf{L2}$ fixed for a disk C_2 , or fixed in the range $\mathbf{L2}$, with increasing K (growing up of the density due, for example, to the interaction with the surrounding material, with the consequent increase in the disk size and elongation), or decreasing the specific angular momentum from a starting config-

¹⁴The definition of isolated and mixed subsequences were introduced in Pugliese&Stuchlík (2015), here we remind that ℓ counterrotating sub-sequences of a decomposition of the order $n = n_+ + n_-$, are *isolated* \widehat{C}_s if $C_{n_-} < C_{1_+}$ or $C_{n_+} < C_{1_-}$ and *mixed* \widehat{C}_m if $\exists i_+ \in [1_+, n_+] : C_{1_-} < C_{i_+} < C_{n_-}$ or viceversa $\exists i_- \in [1_-, n_-] : C_{1_+} < C_{i_-} < C_{n_+}$.

uration C_3 in **L3**, losing specific angular momentum (in magnitude) and then moving inwards. Finally, starting by a model in **L1**, with topology C_1 or C_x^1 , an open critical surface could be the consequence of an increase of specific angular momentum magnitude (due feeding matter for example, or even for a direct interaction with the source (Pugliese&Montani, 2015), as the disk C_1 , or in the critical topology C_x^1 , lies in the orbital region closer to the source). A possible mechanism for the feeding of matter and increasing momentum for the $(\circ)_1$ disks, with the consequent shift of the critical point from Δr_x to $\Delta r_J < \Delta r_x$, could take place in these multiple ringed systems, for feeding from external surface to $(\circ)_1$, for example in the C_o^n ringed disks.

The case of starting data in **L1** is particularly interesting as the proto-jet launch is related in a direct way to the accretion phase. On the other side, from starting data in **L2** or **L3**, the emergence of the instability points r_J are not directly related with the accretion, and then the chronological lines have different evolutionary histories.

However it is worth to note that the configurations C_1 could evolve directly, without an accretion stage, towards an O_x^2 topology. A transition from C_1 or C_x^1 , requires an increase of the disk specific angular momentum, shifted accordingly from **L1** to **L2**. The disk surface will increase the elongation (but also the density) by the growing of the K -parameter for the shift from **K0** to **K1**. It is therefore necessary, for the configurations in **L1**, to provide a mechanism able to explain the growth of both the angular momentum and the density. On the other hand, for a starting equilibrium C_3 disks, with angular momentum in **L3**, an evolution towards the launch of an O_x^2 proto-jet implies a transition **L3** to **L2**, therefore a loss of the specific angular momentum and increase in density (because K increases) and size. This can occur due to for example to some feeding by embedding material or also a further outer disk of the configuration. For initial data in **L2**, only an increase of K from **K0** to **K1** is required. From this the formation of O_x^2 proto-jets would seem to be favored starting from an equilibrium disk C_2 or C_3 and not from an accretion phase of a C_x^1 surface.

Further considerations concerning the “transitions” to the final state of open funnels, are given in Appendix A where different aspects of the geometric correlation are addressed, analyzing the location of the inner and outer edges of the disks in the geodesic structure. It is important to point out that these considerations are not based on the analysis of the geometrical correlations, but on the analysis of variation of the specific angular momentum: the orbital region for the proto-jet is internal with respect to orbital range of the accretion.

For corotating fluids orbiting the faster Kerr attractors, the reduced range of possible specific angular momentum (and correspondingly the orbital range) is associated in the **RAD** to a reduced possibility of the multiple proto-jets formation, see Eq. (11), implying clearly a smaller critical density δn_J , implying also a reduced distance between two consecutive proto-jets $\delta r_J \propto \delta \ell_J$ (close together according to a fraction $\delta r_J/n_J \propto \delta \ell_J/n_J$), with a proportionality factor that can be easily assessed, being in general a function of radius. Multiple corotating proto-jets shall be then very close to the horizon, approaching this with increasing dimensionless spin of the attrac-

tor.

The ℓ corotating sequences of corotating proto-jets would be favored (and more spaced) in the case of low spin, due to the greater extension of orbital range Δr_J , and for the greater range of the specific angular momentum **L2**⁻. As we shall see in Sec. (4), in these geometries mixed ℓ counterrotating sequences of proto-jets are possible. Further analysis of the situation for the fast Kerr attractors suggests that the accretion orbital regions, greater in measure than the proto-jet regions in general, tend to have the same extension as the proto-jets orbital regions. Then, for the faster Kerr attractors, we could say that the probability that a slight change of specific angular momentum generates a transition between the two critical (ℓ corotating) topologies (O_x, C_x) increases, inducing therefore a possible causal correlation between proto-jet and accretion that would be thus characteristic of the attractors with large spin. For fast attractors, the orbital distance Δr_J is extremely small, and Δr_J would be negligible (however, in those situations the role of increasing proper distance could be relevant). A special class of “fast” attractors corresponds to the spins $a > a_M^-$. In these geometries, where the dragging effects are significant, the critical density δn_J , at the constant step κ , decreases uniformly in the outward direction, but the orbital range is very narrow with the proto-jet funnels very close and eventually indistinguishable.

We also note that in such spacetimes, this region is entirely contained in the ergoregion Σ_ϵ^+ ; further details will be discussed in Sec. (4) where we will compare the two ℓ counterrotating sequences of proto-jets considering the influence of the dragging effects.

This situation is totally reversed for the counterrotating case. Following arguments similar to the corotating case, we would say in general that the multiple surfaces of counterrotating proto-jets appear in regions further away from the attractor with respect to the sequence of corotating proto-jets.

For $a \in A_t^> \equiv]a_t, M]$, only isolated ℓ counterrotating subsequences of proto-jets may exist, and the maximal distance between the two subsequences, assessed as the distance between the outer open surface O_x^2 of the corotating inner sequence and the first O_x^1 of the outer counterrotating one, increases with the spin. Whereas in the geometries of sufficiently slow attractors $A_t^<$, mixed sequences are possible and they will be investigated in Sec. (4.1) where the ℓ counterrotating couples are addressed. The geometric separation has some effects on the geometrical and causal correlations between the two sequences. It should be noted that, if the corotating proto-jets density increases for the slow attractors, just the opposite holds for the counterrotating fluids. The counterrotating sequences are clearly favored at large distances from the black hole, increasing the orbital range Δr_J and the range of the specific angular momentum $\Delta \ell_J$. Then we should expect the multiple surfaces of counterrotating proto-jets to be separated and spaced apart for a broad differential rotation with orbiting the faster attractors. The possibility of a transition between (O_x^+, C_x^+) topologies is reduced then for the counterrotating matter.

In the sequences of counterrotating proto-jets, a minimum of the criticality density is always present, farther away from

the source in comparison with the corotating fluids. Where the differential rotation, as defined in Pugliese&Stuchlík (2015), is approximately equally spaced in the macro-configuration, the presence of a minimum density would be evident in the multiple sequences of proto-jets, being more significant with decreasing step κ of the sequence.

3.1.1. Final notes on the ℓ corotating proto-jets ($\mathbf{J}^\pm - \mathbf{J}^\pm$)

Considering the ℓ counterrotating subsequences made up by ℓ corotating proto-jets, it is necessary to distinguish between two types of attractors: one set including slow rotating black holes, at $\mathbf{A}_i^<$, detailed in Sec. (4), where the two subsequences can be mixed, and the fast attractors, for $a \in \mathbf{A}_i^>$, where the ℓ counterrotating subsequences *must* be separated. A possible geometric correlation can occur inside each subsequence, or also among the two subsequences. In this last case, we should consider the confinement of the two separated subsequences in the geometries $\mathbf{A}_i^>$, and particularly for $\mathbf{O}_x^{\hat{o}} < \mathbf{O}_x^{\hat{i}}$. The minimum separation between the two sequences becomes significant with the increase of the spin, until the minimum distance has maximum value $r_J^{\hat{o}} - r_J^{\hat{i}} \approx 3M$ for very fast attractors with $a \lesssim M$. Eventually, the states $\mathbf{J-A}$ and $\mathbf{J-C}$, addressed in the next sections, could be seen as precursors of the ℓ corotating $\mathbf{J-J}$ decompositions, induced by a P-W instability for the initial closed topology evolving towards the open cusped one, or possibly for collision and then geometrical correlation. So far we have considered in the study of the multiple open cusped surfaces the only criterion of the density of critical points r_J . Yet another aspect to be considered, is the collimation of the \mathbf{O}_x funnels along the rotation axis, which could be related to the formation of a collimated proto-jet. The funnels of matter, in the case of very fast attractors and corotating fluids, have an opening angle relative to the axis of rotation that is smaller in comparison with those related to the slower attractors, thus favoring a stronger collimation along the axis. Then, according to the motion of the test particles, a product $\ell a > 0$ is associated to stabilizing effects for the rotating matter, being “attractive” with respect to the proto-jets, because for increasing a/M , or the specific angular momentum $\ell > 0$, the point r_J^- moves inwards. The inverse occurs for the counterrotating case, $\ell a < 0$, which would act “repulsively”, in the sense of favoring the instability of the orbiting matter, since for increasing a/M , but decreasing magnitude of ℓ^+ , the point r_J^+ moves outwards.

3.2. Outer proto-jet: the ℓ corotating proto-jet-accretion ($\mathbf{A-J}$) systems

We consider a couple of ℓ corotating critical configurations, formed by an open surface and an accreting configuration with $r_J < r_x$. We will refer to the scheme $\mathbf{O}_x - \mathbf{C}_x$, for a ℓ corotating couple. We have

$$\begin{aligned} \mathbf{C}_x^i < \mathbf{O}_x^o \text{ implies } \mathbf{C}_x^i > \mathbf{O}_x^o \quad |\ell_i| < |\ell_o| \quad \ell_o \in \mathbf{L2}, \\ |\ell_i| \in \mathbf{L1}, \quad K_i \in \mathbf{K0}, \quad K_o \in \mathbf{K1}. \end{aligned} \quad (13)$$

We note that the conditions in (13) are always verified for the ℓ corotating couples. In terms of the criticality indices, we can

express Eq. (13) with $\mathbf{O}_x^{\hat{i}} < \mathbf{C}_x^{\hat{o}}$ where $\ell_i \in \mathbf{L2}$ and $\ell_o \in \mathbf{L1}$.

In an evolutive interpretation, the \mathbf{O}_x^o configuration could model the final stage of a \mathbf{C}_x disk and, as pointed out in Sec. (3.1), the evolution towards an \mathbf{O}_x surface from a \mathbf{C}_x^i one requires an increase of the specific angular momentum magnitude during the time. This could be the consequence, for example, of feeding of the disk $\mathbf{C}_x^i \in \mathbf{C}_x^n$ in a ringed structure \mathbf{C}_x^n , from a consecutive and outer ring of the decomposition (Pugliese&Stuchlík, 2015).

A different situation for the critical couple in Eq. (13) could occur when the two P-W instability points are very close, $r_x^{\hat{o}} \gtrsim r_J^{\hat{i}}$, or even coincident. However, this last case can be possible *only* for an ℓ counterrotating couple giving rise to a possible geometrical and causal proto-jet-accretion correlation.

As specified before, in general a geometrical correlation in the $\mathbf{A}^\pm - \mathbf{J}^\pm$ couple could be favored when the distance between the specific angular momenta ranges is small, and then a slight change of ℓ in one of the configuration could lead to correlation or to a topological transition, for loss of specific angular momentum with the formation of a \mathbf{C}_x^i disk, or for increase of $|\ell|$, with the formation of an \mathbf{O}_x^o surface. However, it should be noted that a small step κ , element of the displacement matrix $\epsilon_{oi} \gtrsim 0$, always corresponds to a small difference $r_{min}^o - r_{min}^i = f_{min}(\epsilon_{oi}) \gtrsim 0$ and, for $\ell \in \mathbf{L1}$ or $\mathbf{L2}$, it corresponds also to the difference $r_{Max}^o - r_{Max}^i = f_{Max}(\epsilon_{oi}) \lesssim 0$, where (f_{min}, f_{Max}) are not independent functions of the step κ (Pugliese&Stuchlík, 2015). This is not always true in the ℓ counterrotating case.

More specifically, according to Eq. (12), a correlation for corotating fluids, $\mathbf{A}^- - \mathbf{J}^-$, is more likely to occur in the geometries of very fast attractors, where the ranges of possible specific angular momentum, $\ell_{Max}^s - \ell_{min}^s$ for $s \in \{J, K\}$ (correspondingly the differences $\ell_{Max}^J - \ell_{Max}^K - (\ell_{min}^J - \ell_{min}^K)$), are very small. Conversely, in the spacetimes of slower attractors, this difference is highest. One could conclude that the topology of the corotating orbiting matter is more stable for slow attractors, at least for sufficiently low specific angular momentum (the surface topology remains unaffected by sufficiently small change in the specific angular momentum), where $r_{cent}^- \gtrsim r_{ms}^-$.

If the disk center moves outward, then it is inevitable that also for the slower attractors the \mathbf{C}_x^- disk expands in the equatorial plane (increasing elongation at almost constant difference $K_- - K_{min}^-$), and it eventually acquires a critical morphology, see also Appendix A.

The situation is just the opposite for the counterrotating fluids: the configurations orbiting the slower attractors are more likely to give rise to a proto-jet-accretion correlation, while in the geometries of faster attractors, a clear geometrical separation among the configurations can occur. The range $\ell_{Max}^{x+} - \ell_{min}^{x+}$ remains approximately constant with increasing spin of the attractor, even if ℓ_{min}^{x+} increases. On the other hand, the range of the specific angular momentum for a counterrotating proto-jet increases, and therefore, the difference $\ell_{Max}^{J+} - \ell_{Max}^{K+} - (\ell_{min}^{J+} - \ell_{min}^{K+})$ increases, and analogously for the respective orbital ranges. As a consequence of this, the orbital distance between the two surfaces remains generally significant, even for very slow attrac-

tors with $a \approx 0$ (indeed the minimum range for counterrotating fluids is approximately the maximum range for the corotating ones).

In conclusion, a correlation among the ℓ corotating $\mathbf{A}^- - \mathbf{J}^-$ configurations is facilitated in the geometries of faster attractors, while a correlation in the counterrotating $\mathbf{A}^+ - \mathbf{J}^+$ configurations is in general less likely to occur with increasing spin. Therefore, the ℓ corotating proto-jet-accretion correlation should be more evident for corotating matter orbiting the fast attractor, and an increase of the black hole spin should favor a possible correlation.

To properly characterize a possible causal correlation, it is important to characterize the distance between the two critical points of the couple. The \mathbf{C}_x^1 configuration could be close to the inner proto-jet point r_J , with flooding of material towards the inner critical point r_J , and supply of specific angular momentum. These phenomena would lead to an increasing separation among the two surfaces \mathbf{O}_x and \mathbf{C}_x . In fact, the proto-jet point r_J shifts inwards. Conversely, the maximum pressure point $r_{min}^{x_1}$ of the accreting disk losing its specific angular momentum, will approach the radius r_{mbo} , reducing its elongation by decreasing $K = K_{Max}^{1_x}$. However, the minimum point of hydrostatic pressure, $r_{Max}^{1_x}$, will move outwards. This could eventually lead to a negative-feedback effect which, after certain time, might even stop the feeding (see also [Appendix A](#)). The final result of this very simplified scenario would turn in a couple made by a small outer disk, eventually in equilibrium, and an inner configuration in proto-jet with increased specific angular momentum.

As discussed in [Sec. \(3.1\)](#), in principle it is possible that an infinite number of $J...J$ couples could be formed. On the other hand, a possible ℓ corotating $\mathbf{C}_x - \mathbf{C}_x$ couples would violate the principle of non-penetration of matter (at the first Roche lobes, as the two ℓ corotating configurations would contain the same r_{mso}). Therefore, in the multiple $\mathbf{A} - \mathbf{J}$ couples, there would be a ℓ corotating subsequence of a number n_J of open funnels, as considered in [Sec. \(3.1\)](#), and one (outer) accreting configuration. The geometric correlation could be then between the \mathbf{C}_x^1 configuration and $\mathbf{O}_x^{\hat{1}} < \mathbf{C}_x^{\hat{0}}$.

Therefore, an ℓ corotating proto-jet cannot be formed from the feeding of material from an outer (ℓ corotating) surface, through a P-W point on a stable inner configuration or on an accreting inner one. An open cusped surface may be formed instead from a \mathbf{C}_2 or $(\mathbf{O})_1$ configuration, after a (hypothetical) collision with an outer equilibrium disk at higher specific angular momentum, which is increasing its mass for example due to interaction with the embedding environment, or by some other collisional phenomena occurring in the macro-configuration. These situations are discussed in more details in [Appendix A](#), where different situations for corotating or counterrotating couples orbiting attractors of different classes are explored. In [Appendix A.2](#), the location of r_{out} , outer edge of the disk, is also investigated; here we present some general considerations based on the results proved there. Firstly, as a disk in equilibrium can contain the marginally stable orbit (but not the marginally bounded orbit as detailed in [Appendix A.1.1](#), the inner margin of the disk in equilibrium can be close to the in-

ner ℓ corotating proto-jet point, $r_{in} = r_{mbo} + \epsilon$ with $\epsilon > 0$. The inclusion¹⁵ $r_{mso}^{\pm} \in \mathbf{C}_i^{\pm}$ implies some restrictions on the specific angular momentum of the disk, different for the corotating and counterrotating fluids, and ultimately distinction between different attractors—[Appendix A.1.1](#). In general, for larger specific angular momentum magnitude (such that $r_{in} = r_{mbo} + \epsilon$), the disk would be significantly extended outward, it would have a very large elongation¹⁶ λ , with $r_{cent} - r_{in} \gg r_{out} - r_{in}$, and the surface, for increase in size (also at almost constant specific angular momentum) might become opened, being unstable but not reaching an \mathbf{O}_x topology.

We finally note that an immersion of a \mathbf{C}_i disk in a \mathbf{C}_x^i one, where $\pm(\ell_i^{\mp} - \ell_x^{\mp}) > 0$, could lead to an increase in size and in the specific angular momentum magnitude of the inner disk, and eventually to transition of \mathbf{C}_x^1 to a \mathbf{O}_x^2 topology. This can happen in fact only with sufficient supply of specific angular momentum for the \mathbf{C}_x^1 surface. However, the increase of specific angular momentum magnitude is a necessary but not sufficient condition for the occurrence of a topological transition. In fact, the disk may be stabilized by moving outwards the center of maximum pressure with a $K \in \mathbf{K0}$ (however for $|\ell_o|$ very large, also K_o can be very large, as there is $\partial_{\ell} K_{crit} > 0$ and, for ℓ_o very close to ℓ_{mso} , the parameter K_o will be close to the minimum K_{mso}). The specific angular momentum cannot be too large, being proportional to the distance among the centers or, $\partial_{\delta\ell} \delta r_{min} > 0$. Thus, as confirmed in [Appendix A](#), there will be an upper bound on the suitable range of specific angular momentum magnitude.

We conclude this analysis describing the configurations in the Newtonian limit. The specific angular momentum of the equilibrium configuration could be $\ell \in \mathbf{L3}$ for a stable \mathbf{C}_3 disk centered in $r > \bar{r}_\gamma \gg r_{mso}$, with $\bar{r}_\gamma > r_\gamma : \ell(\bar{r}_\gamma) = \ell_\gamma$, where there is also $\partial_{\delta\ell} \delta K_{crit} > 0$, and $\partial_{\delta r_{crit}} \delta K_{crit} > 0$. However, according to the discussion in [Pugliese&Stuchlík \(2015\)](#), even if the inequality $\bar{r}_\gamma > r_{mso}$ is always verified in every geometry, for the corotating fluids orbiting fast attractors, this cannot be considered necessarily as an indication of the location of this radius in a region where the Newtonian limit could be applied. This situation can be inferred from [Fig. 6](#), where the radii \bar{r}_γ^{\pm} , have been plotted for different attractors, emphasizing their location with respect to the geodesic structure of the spacetime and the radii $r_M^{\pm} > r_{mso}^{\pm}$. [Fig. 6](#) confirms that $\bar{r}_\gamma^{\pm} \gg r_{mso}^{\pm}$ for the counterrotating fluids in any geometry, and for the corotating case only at $a \ll M$. Then it is clear that $\bar{r}_\gamma^+ \gg r_M^+$ for any attractor spin, while the situation is different in the corotating case. Considering an attractor with $a = a_M^- : \ell_\gamma^- = \ell_M^-$, we have $\bar{r}_\gamma^- = r_M^-$ and

¹⁵The inclusion notation, (\in, \notin) and $\in!$, will be widely used in [Appendix A](#). The use of $\bar{r} \in ()$, for the radius \bar{r} and any surface $()$, means that there can be found proper K or ℓ parameters such that this property is satisfied. The symbol $\in!$ is a reinforcement of this inclusion, indicating that this is a necessary relation which is *always* satisfied. The symbol \notin (meaning non-inclusion) does not generally have any intensifier (!), as this analysis is to underline the possibility of inclusion and the condition for this to be satisfied.

¹⁶The definition of elongation of a ring and ringed accretion disk was introduced in [Pugliese&Stuchlík \(2015\)](#), here we recall that in general for an accretion disk the elongation range is defined as $\Lambda \equiv [r_{in}, r_{out}]$ and the disk elongation on the equatorial plane as $\lambda = r_{out} - r_{in}$, where r_{in} (r_{out}) are the inner (outer) edge of the disk.

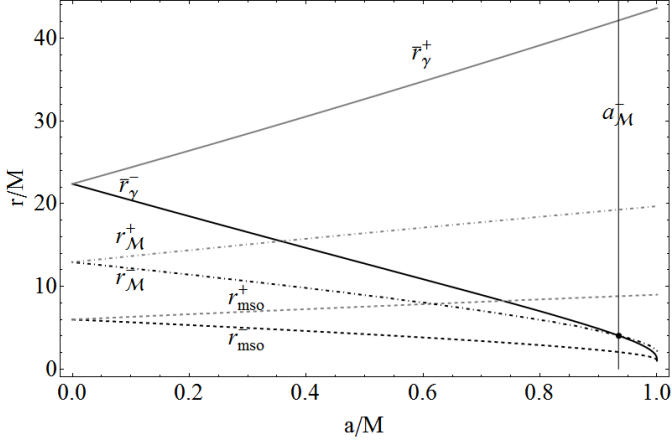


Figure 6: The panel shows the marginally stable orbits r_{mso}^{\pm} , the radii r_M^{\pm} (orbits of maximum growing of the specific angular momentum magnitude, as function of a/M) and the radii $\bar{r}_{\gamma}^{\pm} > r_{\gamma}^{\pm}$: $\ell_{\pm}(\bar{r}_{\gamma}^{\pm}) = \ell_{\gamma}^{\pm}$, as functions of the black hole spin-mass ratio a/M . For $a = a_M^- \approx 0.9343M$: $\ell_{\gamma}^- = \ell_M^-$ there is $r_M^- = \bar{r}_{\gamma}^-$.

a_M^- could be seen as the infimum of the spin range where it is not possible to consider the inequality $\bar{r}_{\gamma} \gg r_{mso}^-$, and then the region where a Newtonian limit could be considered.

The radii \bar{r}_{γ}^{\pm} (points of maximum hydrostatic pressure) are the solutions of the algebraic fourth degree equation:

$$\begin{aligned} \partial_r V_{eff}|_{\ell_{\gamma}^{\pm}} = 0, \quad \bar{r}_{\gamma}^{\pm} : a^2(a - \ell)^2 - 4(a - \ell)^2 r + \\ 2(a - 2\ell)(a - \ell)r^2 - \ell^2 r^3 + r^4|_{\ell_{\gamma}^{\pm}} = 0, \end{aligned} \quad (14)$$

in dimensionless quantities. We note that actually the second equation, solved for each r in terms of the parameters ℓ and a , is able to provide all the extremes of the effective potential and thus also the minimum and maximum points of the hydrostatic pressure. Specifically we can write the solutions \bar{r}_{γ}^{\pm} as

follows¹⁷:

$$\begin{aligned} \bar{r}_{\gamma}^{\pm} \equiv \frac{1}{12} \left[\sqrt{3}h_3 + 3\ell^2 + \sqrt{6}(-2^{2/3}h_2 - 2^4(a - 2\ell)(a - \ell) \right. \\ \left. + 3\ell^4 - \frac{2^{10/3}(2a^2 - 3a\ell + \ell^2)^2}{h_2} + \right. \\ \left. \frac{3\sqrt{3}[2^5(a - \ell)^2 - 8(a - 2\ell)(a - \ell)\ell^2 + \ell^6]}{h_3} \right]^{1/2} \end{aligned} \quad (15)$$

$$\begin{aligned} h_3 \equiv (2^{5/3}h_2 - 2^4(a - 2\ell)(a - \ell) + 3\ell^4 + \\ \frac{2^{13/3}(2a^2 - 3a\ell + \ell^2)^2}{h_2})^{1/2}; \end{aligned}$$

$$h_2 \equiv \left[h_1 + \sqrt{h_1^2 - 2^8(2a^2 - 3a\ell + \ell^2)^6} \right]^{1/3};$$

$$\begin{aligned} h_1 \equiv -(a - \ell)^2 [2^7 a^4 - 5.2^6 a^3 \ell + 16\ell^2 (\ell^2 - 3^2) + \\ 8a\ell (3.2^4 + 13\ell^2) - 9a^2 (48 - 8\ell^2 + 3\ell^4)]. \end{aligned} \quad (16)$$

3.3. Inner proto-jet: the ℓ corotating proto-jet-accretion (**J-A**) systems

The ℓ corotating couples $O_x^i < C_x^o$, are *not* possible. In fact their existence should imply that $|\ell_i| < |\ell_o|$, where $\ell_o \in \mathbf{L2}$ and, on the other hand it has to be $\ell_i \in \mathbf{L3}$ that is contradictory.

We conclude the discussion on the ℓ corotating couples with an inner open surface J_x , noting that in a ℓ corotating couple with an accretion point and a proto-jet, the launching point r_J must be the *inner* with respect to the accretion point r_x , implying that it has to be a **A-J** couple, with a possible correlation between the two surfaces.

We note finally that, given a correlated couple O_x or C_x , an overflow of matter occurs, with the consequent decrease of specific angular momentum magnitude and the value of K parameter. This may lead to a series of accretion stages with a progressive “drying” of the disk¹⁸.

¹⁷Notice that this different behavior with respect to the spin suggests, as indeed can be immediately verified, that the equation associated to the problem (14) is not completely re-parameterizable as a function of the dimensionless quantities $R \equiv r/a$ and $\bar{\ell} \equiv \ell/a$, but the equations explicitly depend on a/M . The couples $(R, \bar{\ell})$ are used for example in Pugliese&Montani (2015), to identify the Newtonian limit and underline the emergence of the properly relativistic and dragging effects.

¹⁸Suppose that a C_x disk is characterized by the couple of parameters (ℓ_a, K_{Max}^a) with $\ell_a \in \mathbf{L1}$ and $K_{Max}^a < 1$, and critical points (r_{min}^a, r_{Max}^a) of the hydrostatic pressure. Decreasing the specific angular momentum in magnitude and also K_{Max} , the disk might return to an equilibrium phase with topology C, here labeled by the superscript b , with $r_{min}^b < r_{min}^a$, $r_{Max}^b > r_{Max}^a$, and also $K_b \leq K_{Max}^b < K_{Max}^a$ (it can be also $K_b = K_{Max}^b - \epsilon \lesssim K_{Max}^b$). This transition, from a cusped C_x to a C topology, should be a continuous process. The initial topology could also involve an open surface O_x , resulting therefore in a proto jet-accretion transition, as decreasing of specific angular momentum magnitude may involve a transition from **L2** to **L1**, or proto-jet-equilibrium configuration transition with angular momentum in **L2** or **L1**. A second new phase of instability may be induced by the interaction of the new surface with the surrounding matter, present in the macro-configuration as it was in its initial phase, prior the transition, or by some other mechanism.

3.4. Outer proto-jet: the ℓ corotating equilibrium disk-proto-jet (C-J) systems

We consider the ℓ corotating C-J couple, with only one P-W instability point r_J , associated to the outer O_x^o proto-jet. We obtain

$$\begin{aligned} C_i < O_x^o \quad \ell_i < \ell_o \quad r_{min}^i < r_{min}^o \quad K_i < 1 \quad \ell_o \in \mathbf{L2}, \\ \text{thus } O_x^o < C_i, \quad r_J^o = r_{in}^+ - \epsilon_r \quad (17) \\ \text{where } \epsilon_r > 0, \quad \ell_i \in \{\mathbf{L1}, \mathbf{L2}\}. \end{aligned}$$

In fact, there is $r_{Max}^o < r_{Max}^i < r_{mso} < r_{min}^i < r_{min}^o$. This last relation is a property of any ℓ corotating subsequence, and it also assures that, since r_{Max}^o must necessarily exist being associated to O_x^o , and as $\ell_i < \ell_o$, for definition, then $\ell_i \in \{\mathbf{L1}, \mathbf{L2}\}$. The inequality $O_x^o < C_i$ of Eq. (17), and then the location of the inner edge of the inner disk, is guaranteed by the fact that, considering the topologies (O_x^o, C_i), we find $r_{Max}^o < r_{mbo} < r_{mso} < r_{min}^i < r_{min}^o$. However, as Eq. (A.2) and Eq. (A.3) hold, then the inner edge of the C_i disk has to be external to the launching point of the proto-jet, r_J . In other words, the disk in regular topology is *entirely* contained in the orbital region $r > r_J$, which finally validates Eq. (17).

Under these circumstances, a viable correlation among these configurations can take place, for example, for possible impact of the funnels¹⁹ O_x^o on the internal surface C_i . Or a geometrical correlation may occur by action of the surface C_i approaching the critical point r_J , for loss of specific angular momentum ℓ_i and increasing of the parameter K_i . However, as discussed in Appendix A, by the analysis of the possible inclusion relation $r_{mso} \in C_i$, the investigation of this case may require additional restrictions on the specific angular momentum ℓ_i . In fact, for particular specific angular momenta of the rings, and depending of the kind of attractor they are orbiting, some rings are *entirely* confined in the region $r > r_{mso}$, and then the two surfaces in Eq. (17) are necessarily geometrically (and causally) separated. Particularly the situation is summarized in Eq. (A.6) for the C_1^\pm disk, in Eq. (A.10,A.11,A.12) for the corotating C_2^- disks and in Eq. (A.14) for the C_2^+ counterrotating disk. This study has been done in all details in Appendix A.1.2, here we report the general results based on the parameter conditions for the confinement of the two surfaces in separated orbital regions and the main idea under these results.

Then, for $\ell_i \in \mathbf{L1}$ Eq. (A.6) holds, thus for sufficiently large (in magnitude) $\ell_i \in \mathbf{L1}$ and sufficiently large density $\mathbf{K0}$, the inner margin of the C_i^\pm disks can approach the orbits r_{mbo}^\pm (the gap between r_{in}^i and r_{mbo} can be in fact exactly evaluated). Conversely, for $\ell_i \in \mathbf{L2}$, the situation is much more complicated as it essentially depends on the range of specific angular momentum and, for the corotating disks C_i^{2-} , also on the different classes of attractors: we may be able, from the couple (17), to establish, if the ringed disk is made up by counterrotating or corotating fluids and, in this last case, also to identify the class of the attractor.

¹⁹We stress that this statement requires the study of proto-jet surfaces along the rotation axis.

The case C_i^{2-} is described by Eq. (A.10,A.11,A.12). For attractors with sufficiently high spin, as in Eq. (A.12), the situation is similar to the C_i disks with $\ell_i \in \mathbf{L1}$, and a geometric correlation between the couple may occur. In the geometry of the slower attractors, in order to have a correlation, it is necessary to balance the dragging effects due to the slower spin of the attractor by a sufficiently low disk specific angular momentum (in magnitude), namely in the range \mathbf{II} as specified by Eq. (A.11). Whereas, for high enough specific angular momenta, i.e., $\ell_i \in \mathbf{L2}$, the two disks cannot be geometrically correlated, see Eq. (A.10).

For the counterrotating fluids of the couple $C_i^{2+} < O_x^{2+}$, orbiting any Kerr black hole attractor, Eq. (A.14) holds. The situation is, in general, analogous to the case of C_2^- disks but, in the counterrotating case, for specific angular momentum sufficiently high in magnitude, the two surfaces are geometrically separated, while for the lower values of $|\ell_i^+|$, there can be a geometrical correlation in any Kerr geometry. It has to be specified that, for the C_i disk, one has to consider the role of the elongation parameter $K_i > K_{min}^i \in \mathbf{K0}$, which indeed constitutes an additional free parameter of the system. In the unstable surface (in open or closed topology), this is uniquely determined by the specific angular momentum of the fluid, thereby reducing, in the cusped topologies, the number of free parameters to the only angular momentum ℓ .

If the two surfaces are geometrically separated, and therefore no correlation is possible, then no feeding of matter, or any matter penetration after collision, can occur from a C_i disk to an O_x^o configuration.

As for the multiple ℓ corotating configurations with topology C and O_x , regulated by Eq. (17), there can certainly be two ℓ corotating subsequences formed by surfaces with equal topologies, respectively, with configuration of order n_J and decreasing magnitude of specific angular momentum with r_J , and of order n_c for the closed topologies with the specific angular momentum increasing with the orbit r_{min} . However, for the considerations outlined before, the subsequences will be isolated and separated by the orbit r_{mbo} . Further considerations, of the corotating or counterrotating nature of the fluids and different classes of attractors are provided in Appendix A.

3.5. Inner proto-jet: the ℓ corotating proto-jet-equilibrium disk (J-C) systems

We close this part on ℓ corotating systems with an inner open cusped configuration, by considering the couple $O_x^i < C_o$. But it is easy to see that existence of such a couple, similarly to the $O_x^i < C_x^o$ one, leads to a contradiction, and we can finally conclude that any ℓ corotating couple (J-C) must be described by Eq. (17).

3.6. The ℓ corotating accretion-equilibrium disk (A-C) systems

We add here some notes on the ℓ corotating couples made up by a disk in accretion and a configuration in equilibrium. This case was discussed in detail in Pugliese&Stuchlík (2015). Let

us suppose that the disks are C_a^x and C_b , then it has to be

$$\begin{aligned} K_a \in \mathbf{K0}, \quad K_b \in \mathbf{K0}C_b \not\prec C_x^a \quad \ell_a \ell_b > 0 \quad \pm \ell_b^\mp < \pm \ell_a^\mp, \\ \ell_a \in \mathbf{L1}, \quad \ell_b \in \mathbf{L1}, \end{aligned} \quad (18)$$

$$C_x^a < C_b \quad \ell_a \ell_b > 0 \quad \pm \ell_a^\mp < \pm \ell_b^\mp, \quad \ell_a \in \mathbf{L1}, \quad \ell_b \in \mathbf{Li}. \quad (19)$$

If the equilibrium surface C_b would be the inner one of the couple, in contradiction with Eq. (18), it is immediate to prove that it would violate the non-penetration of matter, as shown below. We note that $r_{mbo} < r_{Max}^a < r_{mso}^-$. But we know, from the assumption on the specific angular momentum $\ell_{b/a} < 1$, that $r_{Max}^a < r_{mso}^- < r_{min}^b < r_{min}^a$, implying that this configuration is not possible because there would be a penetration of the first Roche lobe. Therefore $C_x^a \not\prec C_b$ and $C_x^a < C_b$, that is reflected in Eq. (19).

We now focus on Eq. (19): the specific angular momentum ℓ_b of the configuration in equilibrium can be, in principle, in any range \mathbf{Li} . However, in order to establish if the condition of non-penetration of matter is really preserved, it is necessary to establish the location of the outer edge of C_x^a and of the inner edge of C_b disk. This analysis has been addressed in all detail in Appendix A.1.1. This discussion points out significant distinctions between the ℓ corotating couples made up respectively by corotating and counterrotating fluids.

In general, the two surfaces will be separated for sufficiently large momentum ℓ_b as compared to ℓ_a (in magnitude), and for K_b small enough at fixed ℓ_b (while $K_a = K_{Max}^a$ is uniquely determined by the specific angular momentum ℓ_a). The specific angular momentum ℓ_b should be sufficiently high for $r_{mso} \notin C_b$ at any K_b . Obviously, this inclusion relation will also be determined by the K_b value, at least for some specific angular momenta: the situation does indeed depend of the specific angular momentum range $\ell_b \in \mathbf{Li}$ and the class of the attractor. In some cases, it will depend especially on the corotating or counterrotating nature of the disk. This issue is detailed in Eq. (A.6), for specific angular momentum $\ell_b^\pm \in \mathbf{L1}^\pm$, in Eqs (A.10–A.12) for the corotating disk C_b^- with $\ell_b^- \in \mathbf{L2}^-$. Whereas for counterrotating disks Eq. (A.14) holds.

Finally, for counterrotating disks, with $\ell_b^+ \in \mathbf{L3}^+$, Eq. (A.20) holds, and then one can always find a K_b such that the two configurations are separated. Viceversa, for the C_3^a disks, Eq. (A.18) and Eq. (A.19) apply, distinguishing fast and slow attractors.

We conclude this section by noting that the couple in (19) could be seen perhaps as a precursor of the ℓ corotating couple $C_x - C_x$, briefly discussed on the sidelines of Sec. (3.2). But in fact, considering the topology of the couple, and taking account of the requirement of non-penetration of matter, a possible evolution of a C_b disk towards the C_x phase, which would imply a variation of one or both K_b and ℓ_b parameters, would be non correlated to the inner configuration. Indeed, the inner C_x^a disk would be correlated to the onset of an accretion phase of the C_b configuration only by increasing its own specific angular momentum ℓ_a and therefore the parameter K_{Max}^a , which is not expected. A final note regards the decompositions of order greater than two with a seed couple $C_x^a < C_b$. From the former analysis we conclude that the ‘‘additional’’ configurations would

be in equilibrium and therefore in the outer orbital regions with respect to C_x^b .

4. ℓ counterrotating sequences

The situation for a ℓ counterrotating couple, with a critical configuration, is determined by the two families of the notable radii $r_{\mathcal{N}}^\pm$ of the geodesic structure of the spacetime and by the associated specific angular momenta $\ell_{\mathcal{N}}^\pm$. The discussion of this case turns to be more articulated than the ℓ corotating case investigated in Sec. (3). Some of the results considered here will be discussed more deeply in Appendix A.2, where the location of the notable radii $r_{\mathcal{N}}^\pm \in ()_{\mp}$ is considered with respect to the configurations $()_{\mp}$.

Here we will first consider the couples of fixed topology and rotation with respect to the central attractor, providing rather stringent constraints on the decomposition. Then, by considering the couple of configurations as a seed for a decomposition of order $n > 2$, we investigate the configurations made up by more disks. To simplify the notation we introduce the total angular momentum \mathcal{L} and total \mathcal{K} parameter of the couple. Examples of ℓ counterrotating tori are in Figures 1-Upper and Bottom, also the outer couple of non accreting tori in Second panel.

4.1. The ℓ counterrotating proto-jet-proto-jet ($\mathbf{J}-\mathbf{J}$) systems

We consider a couple of ℓ counterrotating opened-crossed configurations. It has to be

$$\begin{aligned} \mathcal{L} = \mathbf{L2}^- \cup \mathbf{L2}^+, \quad \mathcal{K} = \mathbf{K1}^- \cup \mathbf{K1}^+ \text{ for } a > a_i \quad \text{O}_x^+ > \text{O}_x^- \\ (\mathbf{J}^+ - \mathbf{J}^-), \quad a_i : r_{mbo}^- = r_\gamma^+, \text{ for } a < a_i \quad \text{O}_x^+ > \text{O}_x^- \quad (20) \\ (\mathbf{J}^+ - \mathbf{J}^-) \text{ or } \text{O}_x^+ < \text{O}_x^- \quad (\mathbf{J}^- - \mathbf{J}^+), \quad (21) \end{aligned}$$

see Fig. 5. For the smaller attractor spin values, Eq. (21) holds and, as we have $r_{mbo}^- > r_\gamma^+$, a $(J - J)$ couple can be in the state $\text{O}_x^+ < \text{O}_x^-$ or also $\text{O}_x^+ > \text{O}_x^-$. But in the geometries determined by the larger spin values, where $r_{mbo}^- < r_\gamma^+$, Eq. (20) stands, and the inner proto-jet *must* be corotating i.e. the only possible state for this couple is $\mathbf{J}^+ - \mathbf{J}^-$.

In the following discussion we will refer to the results in Eq. (12) for the ℓ corotating couples, which also emphasizes some properties of the density δn_J of unstable points r_j^\pm .

The separation between the ℓ counterrotating subsequences of launching points increases with a/M . This could indicate that the black hole spin favors the launch of corotating material. For large vales of the spin, the inner proto-jets should be mainly regulated by the dragging effects of the Kerr spacetime, and more generally by the curvature effects, while the outer and counterrotating sequence shall be mainly regulated by the centrifugal effects (where $\ell \in \mathbf{L2}^+$), and especially by the PW instability (in r_j^+) due to the high values of the K parameter (indeed $K = K_{Max}^2$ is fixed by the specific angular momentum ℓ_2), regulating both the elongation on the equatorial plane and the disk density²⁰.

²⁰Then one should certainly consider, especially for these sequences, the role played in the unstable states by other factors typically characterizing the evolution of the accretion disks, such as electromagnetic effects, which were not included in the model adopted here for each ring.

In a possible evolutionary scheme, where the attractor is not meant to be isolated but interacting with the surrounding material, a possible increase of its dimensionless spin a/M should have a stabilizing effect for the corotating material, eventually “separating” the two ℓ corotating sequences, as the counterrotating one could fill, according to the discussion in [Pugliese&Montani \(2015\)](#); [Pugliese&Stuchlík \(2015\)](#), the regions far away from the source.

As mentioned also in Sec. (3.1), matter in the critical O_x^- topology penetrate the ergoregion Σ_ϵ^+ in the equatorial plane for sufficiently fast Kerr attractors. The funnels of material will eventually cross the static limit with an initial velocity $\dot{\phi} > 0$, following a possible energy extraction process. The static limit r_ϵ^+ is, on $\theta = \pi/2$, independent of a -but not of M . More precisely, we have

$$\begin{aligned} r_j^- \in \Sigma_\epsilon^+ \quad \text{for } a \in [a_1, a_b^-], \quad \text{and } r_j^- \in \Sigma_\epsilon^+ \\ \text{for } a \in [a_b^-, M], \\ \text{where } a_1/M \equiv 1/\sqrt{2} \approx 0.707107; \quad a_b^-/M \equiv 2(\sqrt{2} - 1) \approx 0.828427; \\ a_1 : r_\gamma^- = r_\epsilon^+; \quad a_b^- : r_{mbo}^- = r_\epsilon^+ \end{aligned}$$

see Fig. 4 and [Pugliese&Quevedo \(2015\)](#). At $a > a_2$, the maximum of the hydrostatic pressure will be in Σ_ϵ^+ where $a_2/M \equiv 2\sqrt{2}/3 \approx 0.942809$ and $a_2 : r_{mso}^-(a_2) = r_\epsilon^+$.

This fact confirms that the dragging effects are dominant in the corotating case, while the centrifugal component of the effective potential would become predominant in the counterrotating fluids with respect to the corotating case.

Considering Eq. (12), we can draw first conclusion by saying that the unstable points r_j^\pm in $\mathbf{L2}^\pm$ cannot be geometrically correlated in the geometries of fast attractors ($\mathbf{A}_i^> : a > a_i$), but a geometric correlation may occur in the geometries of the slower attractors ($\mathbf{A}_i^< : a < a_i$), where the launching points may also be coincident ($r_j^+ \approx r_j^-$). In fact the orbital region $\Delta r_j^\pm \equiv \Delta r_j^- \cap \Delta r_j^+$ is rather narrow, $\Delta r_j^\pm \lesssim M$, and such that $\partial_a(\Delta r_j^\pm) < 0$.

The considerations outlined here relate primarily to the orbital ranges eligible for sequences of cusped open ℓ counterrotating topologies. It is worth to note that, as the O_x^\pm configurations are not closed, the characterization of such multiple decomposition is indeed a one-dimensional problem, reduced to the location of the r_j^\pm points in a bounded but continuous range of variation of Δr_j^\pm . In other words, this is not an extended matter problem and, as also discussed in Sec. (3.1) for the ℓ corotating proto-jets, for every ℓ corotating subsequences, the order n_j^\pm can be infinite in principle.

Obviously, considering the geodesic structure of the spacetime the possible multiple ℓ counterrotating decomposition of proto-jets, orbiting fast attractors with $a > a_i$, are necessarily isolated, as it is clear from Eq. (22). Then there is an inner corotating sequence of $(J\dots J)^-$ configurations, and an outer one made up by the counterrotating proto-jets $(J\dots J)^+$. The ℓ counterrotating sequences may be characterized by a more or less wide spacing, and the counterrotating sequence will be more or less extended, considering the distance $[r_j^{\hat{n}_j^+}, r_j^{\hat{n}_j^+}] \in \Delta r_j^+$, with respect to the corotating sequence which is confined in an

orbital region increasingly smaller as the attractor dimensionless spin increases—Fig. 4. The minimum separation between the two subsequences is $\Delta r_{j+}^- \equiv r_\gamma^+ - r_{mbo}^-$, which states evidently maximum in the case of extreme geometry. A possible geometric correlation between two ℓ counterrotating proto-jets will depend on the distance Δr_{j+}^- .

Mixed configurations, on the other hand, are possible for sufficiently slow attractors i.e. $a < a_i$; this is quite small class of attractors, compared to the class of black hole sources at higher spin. Small values of a/M favor mixed configurations, as the orbital region $\Delta r_{j+}^\pm \equiv -\Delta r_{j+}^- = r_{mbo}^- - r_\gamma^+$ (and the corresponding specific angular momentum range) is minimum in the geometry a_i , where the mixed sequences are possible, and maximum in the static Schwarzschild geometry. We can write, with regards with the orbital location:

$$(J\dots J)^-(22)(J\dots J)^+ < (J\dots J)^+. \quad (23)$$

The outer, ℓ corotating sequence $(J\dots J)^+$ of counterrotating proto-jets, is bounded in the orbital region $\Delta r_j^+ - \Delta r_{j+}^\pm$, with maximum measure in the geometry $a = a_i$ and null in $a = 0$. This is followed by the inner region of mixed sequences $(J\dots J)^\pm$ in Δr_{j+}^\pm , and the finally the ℓ corotating inner isolated sequence $(J\dots J)^-$.

We now address the problem of a possible initial state for the couples in the state (20) or (21). A more detailed discussion can be found in [Appendix A](#). For each ℓ corotating subsequence, the considerations outlined in Sec. (3.1) apply. The evolution from a closed crossed topology C_x of an accretion configuration to the topology O_x of the open funnels, requires an increase (in magnitude) of the specific angular momentum to ensure the transition $\mathbf{L1}$ to $\mathbf{L2}$ and an increase of the K -parameter with a shift $\mathbf{K0}$ to $\mathbf{K1}$. Whereas, starting from a closed topology, an analogue transition occurs if the initial data on the specific angular momentum are in $\mathbf{L1}$ or $\mathbf{L2}$. Conversely, if the starting data for the closed configurations are in $\mathbf{L3}$, then the K parameter increases from $\mathbf{K0}$ to $\mathbf{K1}$, but the specific angular momentum ℓ decreases with a transition from $\mathbf{L3}$ to $\mathbf{L2}$. However, as any equilibrium disk C_\pm can never contain the marginally bound orbit r_{mbo}^\pm , as stated in Eqs (A.1,A.2,A.3); this transition implies a stretching of the disk towards the attractor, moving inward the point of maximum of the hydrostatic pressure, if the disk is located in the outer region with larger centrifugal barrier ($\ell \in \mathbf{L3}$), or viceversa, the shifting of the disk center outwards, from the initial data in $\mathbf{L1}$. The initial configuration with specific angular momentum in $\mathbf{L2}$ will not necessarily give rise to a shift of the center of maximum pressure, but it will change morphology and topology as consequence of the transition $\mathbf{K0}$ to $\mathbf{K1}$.

These considerations derive mainly from the analysis of the geodesic structure of spacetime. Correspondingly one can observe arrangement of the eligible specific angular momenta for the ℓ counterrotating couple of proto-jets in $\mathbf{L2}^\pm$, as summarized in Eq. (12). The two ℓ counterrotating subsequences of proto-jets have been discussed extensively in Sec. (3.1).

We mention that associated to the orbital region Δr_{j+}^\pm , where the mixed decompositions are possible, is also the region of common specific angular momentum $\Delta \ell_{j+}^\pm \equiv -\mathbf{L3}^+ \cap \mathbf{L3}^-$. This

has the remarkable implication that in the mixed decomposition, it will tend to have a ratio $\ell_{+/-} \sim -1$, for sufficiently close points r_J^\pm , up to the extreme situation where the attractor has spherical symmetry. This fact is particularly relevant when one considers that in this orbital region a geometric correlation between the elements of the mixed sequence is possible. One can also see this situation directly through the analysis of the curves of specific angular momentum $\mp \ell^\pm$ which should approach in the spacetimes where $a < a_i$. This means that, when correlated, the ℓ counterrotating open cusped surfaces have specific angular momentum approximately close in magnitude.

We remind also that there are no solution $\bar{r} : \ell_{+/-} = -1$, but certainly there is an appropriate couple $\bar{r}_\pm : \ell^+(\bar{r}_+) = -\ell^-(\bar{r}_-)$ where, for $a < a_i$, we have $\bar{r}_- < \bar{r}_+ < r_{mso}^- < r_{mso}^+$ or $r_{mso}^- < r_{mso}^+ < \bar{r}_+ < \bar{r}_-$. Finally, we refer to the discussion of Sec. (3.1), for the characterization of these structures in the Newtonian limit, as defined through the couples $r_{\mathcal{M}}^\pm$ and the corresponding instability points $\bar{r}_{\mathcal{M}}^\pm$.

4.2. The ℓ counterrotating proto-jet-accretion (J-A) systems

The ℓ counterrotating couples of cusped topologies, made up by a proto-jet and a accreting closed disk, can be analyzed by considering the following four states:

4.2.1. **State I:** $C_x^+ > O_x^-$

First, we focus on the couple $C_x^+ > O_x^-$: a counterrotating closed configuration with an outer accretion point and an inner instability point r_J^- , with open configurations corotating with the black hole. It has to be:

$$\begin{aligned} \mathcal{L} &= \mathbf{L1}^+ \cup \mathbf{L2}^- \quad \Delta r_J^- \cap \Delta r_x^+ = \emptyset, \quad \text{then} \quad C_x^+ > O_x^- \\ \text{and} \quad C_x^+ &\not> O_x^- \quad \text{as there is} \quad \Delta r_J^- < \Delta r_x^+. \end{aligned} \quad (24)$$

We shall focus on a possible geometrical correlation between the two configurations for action of the outer counterrotating disk in accretion to the inner corotating open proto-jet configuration.

We note that the critical points are located in the regions Δr_x and Δr_J : in the first case, the P-W accretion point r_x^+ corresponds to the inner margin of the outer Roche lobe. The minimum distance between the points $r_x^+ > r_J^-$ is $\inf(r_x^+ - r_J^-) = r_{mbo}^+ - r_{mbo}^- > 0$ for $a > 0$. Even if the critical points (r_x^+, r_J^-) are geometrically separated, when the outer counterrotating configuration reaches the critical topology, the matter falls towards the attractor and, as the state is $O_x^- < C_x^+$, this leads to a possible interesting scenario with the counterrotating matter accreting with super-Eddington luminosity on the O_x^- corotating configuration.

However, associated to the O_x^- configuration, in the region $r > r_e^+$, there will be an inner surface (second and inner Roche lobe) embracing the black hole, which therefore could match the second lobe of the outer C_x^+ one, with the consequent collision of counterrotating material with specific angular momentum, generally, greater in magnitude than the specific angular momentum ℓ^- .

The macro-configurations of order $n > 2$, with seed couple as in Eq. (24), will be made by the isolated sequences of couples

in Eq. (24) with $n_x^+ = 1$ and the criticality order n_J^- up to infinity. For the discussion on the inner $(J\dots J)^-$ sequences, we refer to Sec. (3.1).

Clearly, both the parameters K_{Max}^\pm are uniquely fixed by the momenta ℓ_\pm respectively (we recall then that the lines of constant K_{crit}^\pm , provide exactly the inner and outer edges of the closed critical configurations).

Considering the radial distances Δr_J^- , and $\Delta \ell_J^-$, we could conclude that the multiple corotating proto-jets are favored at lower spin, requiring however in general also a larger specific angular momentum, see Eq. (12). Therefore, a larger centrifugal component gives rise to launches of open funnels (in Pugliese&Montani (2015) it has been proposed in terms of the rationalized specific angular momentum ℓ/a , which emphasizes the relevance of the ratio between the ‘‘orbital’’ specific angular momentum and the attractor spin in regulating the disk morphology and evolution).

At high values of spin, the multiple corotating proto-jets are disadvantaged, while they are possible with lower specific angular momentum, as discussed in Sec. (3.1). For the counterrotating matter in closed (cusped) topology, we find $\inf(r_x^+ - r_J^-) \in [M, 6M[$ as the black hole spin $a \in [0, M]$. It is then $\partial_{-\ell_2^+} K_{Max}^+ > 0$ for $\ell_2^+ \in \mathbf{L2}^+$, see Eq. (12).

In this respect, the more relevant effects for the interaction between the $C_x^+ > O_x^-$ systems could occur for lower vales of spin, where an increase of the criticality density δn_J at constant step κ occurs, and the orbital range Δr_J^- is larger. Concerning the specific angular momentum at $a > a_{\mathcal{N}}$, there is $-\mathbf{L1}^+ \cap \mathbf{L2}^- = \emptyset$ and $-\mathbf{L1}^+ > \mathbf{L2}^-$, with orbital range $\delta r_x^+ > \delta r_J^-$, which increases with increasing attractor spin. Moreover, according to Eq. (22), there is $r_J^- \in \Sigma_\epsilon^+$, being inaccessible to any possible contact with the counterrotating matter.

For attractors with spin $a < a_{\mathcal{N}}$, the situation is less articulated and the separation between the orbital regions decreases, being never zero, and the specific angular momentum $-\mathbf{L1}^+$ decreases while $\mathbf{L2}^-$ increases. As discussed above, in these spacetimes possible interaction between the two configurations could be more relevant.

Then one has $-\mathbf{L1}^+ \cap \mathbf{L2}^- \neq \emptyset$ in $]a_{\mathcal{N}0}, a_{\mathcal{N}}[$, and $a_{\mathcal{N}0} : \ell_\gamma^- = -\ell_{mbo}^+$, where $-\ell_1^+ < \ell_2^-$ is possible; in this case, the critical points r_x^+ and r_J^- are closer, favoring therefore a correlation. Finally, at $a \in]a_{\mathcal{N}2}, a_{\mathcal{N}0}[$, there is $-\mathbf{L1}^+ \subset \mathbf{L2}^-$, while for $a < a_{\mathcal{N}2}$, very close to $a = 0$, there is a range of counterrotating specific angular momentum lower in magnitude than the corotating ℓ^- one—see Fig. 5 and Fig. (4).

4.2.2. **State II:** $C_x^+ < O_x^-$

This case is ruled out by Eq. (24) and this couple is not allowed. Therefore, corotating open funnels of matter and counterrotating accreting configurations must be regulated according to Eq. (24).

4.2.3. **State III:** $C_x^- < O_x^+$

We consider the possible presence of counterrotating funnels of matter, launched from a point r_J^+ , with an ‘‘inner’’ closed con-

figuration in accretion C_x^- , or

$$\begin{aligned} C_x^- < O_x^+ \quad r_x^- < r_J^+, \quad \ell^- \in \mathbf{L1}_- \quad \ell^+ \in \mathbf{L2}_+, \\ r_{mbo}^- < r_x^- < r_{mso}^- < r_{out}^- < r_J^+ < r_{mbo}^+ < r_{mso}^+. \end{aligned} \quad (25)$$

The conditions (25) imply a condition on the location of the outer edge r_{out}^- of the accreting C_x^- disk, which should satisfy the last sequence of inequalities in (25). On the basis of these considerations only, we could say that this couple would be possible in the geometries of the fastest attractors, however at higher spins this is the *only* state possible for the elements of the couples (C_x^-, O_x^+) . Therefore we could say

$$\mathbf{A}_{a_i}^> : \quad a > a_{i_a} \quad C_x^- < O_x^+; \quad \mathbf{A}_{a_i}^< : \quad a < a_{i_a} \quad C_x^- \not< O_x^+, (26)$$

where the spin a_{i_a} is introduced in Eq. (A.27). One could consider this state as the opposite with respect to the state $C_x^+ > O_x^-$, analyzed in point **I** above.

As made explicit in Eq. (26), the situation depends on the attractor characteristics and one could say that the couple $C_x^- < O_x^+$ is a characteristic of the geometry of the fast attractors. At lower spins the problem of the location of the outer margin of the corotating disk in accretion with respect to the launching point becomes relevant, and an overlapping of material with the outer configuration is possible. However, considering the last inequality of Eq. (25), we recall that since the inner configuration is closed, it makes sense to enquire if the *outer* edge of the disk in accretion, that is r_{out}^- , can be near the outer critical point r_J^+ , where this kind of situation would lead to collisions. This issue is partially discussed in Appendix A.2. In any case, a possible correlation could emerge from an interaction between the outer edge r_{out}^- and the outer critical point r_J^+ .

In order to provide some constraints on the parameters of C_x^+ , we should investigate the inclusion relation $r_{mbo}^+ \in C_x^+$. This problem is fully addressed in the last point of Appendix A.2.2, fully responding to this problem by providing the relations in Eq. (A.60) and following discussion. Since the last circular orbit is the lower boundary of the orbital range Δr_J^+ , we should consider the inclusion $r_J^+ \in ()^-$, as discussed in Appendix A.3.

We close this section with some general considerations. The configurations (C_x^-, O_x^+) , regulated by Eq. (25), can evolve independently without geometrical contact. On the other hand, from the analysis of the total specific angular momentum and the orbital ranges, we can infer a classification in different sets of attractors where it could be more likely to observe such critical configurations. The first set is defined for geometries $a > a_{\gamma^+}$, introduced and characterized in Eq. (A.34), where at $a = a_{\gamma^+} > a_{i_a}$ we have $r_{mso}^- = r_{\gamma^+}^+$, and the critical points (r_x^-, r_J^+) are geometrically separated by the distance $r_{\gamma^+}^+ - r_{mso}^-$ increasing with the spin, see Fig. 4. This is a subset of the class of attractors $\mathbf{A}_{a_i}^>$.

Increasing the dimensionless spin, the geometric separation increases, and the minimum distance is at most $\approx 4M$ for $a \approx M$.

We can then read the situation in terms of the specific angular momentum. The analysis of the specific angular momentum range $\mathbf{L2}^+ \cup \mathbf{L1}^-$ shows an interesting situation; there is $-\mathbf{L2}^+ \cap$

$\mathbf{L1}^- = \emptyset$ and $-\mathbf{L2}^+ > \mathbf{L1}^-$, $\mathbf{L1}^- < -\mathbf{L2}^+$, and $-\mathbf{L2}^+$ increases with the spin increasing, while $\mathbf{L1}^-$ decreases with increasing a/M — see Eq. (22).

As a consequence of this fact, if there is a collision between these two systems, then the specific angular momentum of the open configuration in funnels is always larger in magnitude than the counterrotating one in accretion. From these results one can easily draw some general conclusions on the multiple surfaces generated from the seed $C_x^- < O_x^+$ in Eq. (25), considering that one might have a ℓ corotating sequence of $(\mathbf{J}^+ \dots \mathbf{J}^+)$ proto-jets.

4.2.4. State IV: $C_x^- > O_x^+$

The couple $C_x^- > O_x^+$, formed by an inner proto-jet of counterrotating matter and an outer accretion corotating ring, can exist only in the geometries of the slow attractors, i.e., for $a \lesssim 0.6M$ where $r_{mso}^- > r_{mbo}^+$. In fact, as stated in Eq. (26), the couples $C_x^- > O_x^+$ are forbidden at higher spins:

$$\mathbf{A}_{a_i}^> : \quad a > a_{i_a} \quad C_x^- \not> O_x^+; \quad \mathbf{A}_{a_i}^< : \quad a < a_{i_a} \quad C_x^- > O_x^+, (27)$$

see also Fig. 4. The results of this section are expanded and deepened in the last point of Appendix A.2.2 and in Appendix A.3, where the inclusion relations $r_{mbo}^+ \in C_x^-$ and $r_{\gamma^+} \in C_x^-$ will be analysed. At $a < a_{i_a}$, it is always possible to find ℓ_1^- small enough for $r_{min}^- \approx r_{mso}^-$, and then $K_{Max}^{1-} < 1$ small enough to get a small critical elongation λ_x^{1-} , having $r_{mso}^- > r_{mbo}^+$. We have then $r_x^{1-} \in]r_{mbo}^+, r_{mso}^-]$, while $r_J^+ \in]r_{\gamma^+}^+, r_{mbo}^+]$ that is Eq. (27). For the exact conditions we refer to the study of the inclusion relations of Eq. (A.60) and Fig. A.16.

The geometric separation between these configurations increases with increasing spin of the attractor. Then an interaction is possible due to a geometric correlation and favored for low spins and large (great elongation and great density) corotating disks C_x^{1-} , whereas smaller disks C_x^{1-} are favored at higher spin $a \lesssim a_{i_a}$. Indeed, in this last case the outer corotating matter accreting onto the black hole could impact on the inner counterrotating matter, which is unstable according to the P-W model.

Considering that the specific angular momentum of the couple is $\mathcal{L} = \mathbf{L1}^- \cup \mathbf{L2}^+$, it is clear that the specific angular momentum of the counterrotating matter will be in magnitude greater than the specific angular momentum of the inner corotating one. Therefore, the location of the couples (C_x^-, O_x^+) clearly distinguishes the two classes of attractors, according to Eq. (26) and Eq. (27).

Considering the decomposition of order $n > 2$, generated by the seed couple $C_x^- > O_x^+$ in Eq. (25), one could consider couples at fixed topologies with multiple copies of $C_x^- > O_x^+$ and an outer sequence of $(\mathbf{J}_+ \dots \mathbf{J}_+)$. The orbital region of the open sequence is therefore more reduced while approaching the limit $a = 0$.

We now focus on the possible initial states for the couple $C_x^- > O_x^+$, making referring to Fig. 7. As this is a ℓ counterrotating couple, the starting state could be, for example, $C^- > ()^+$, where the topology of the counterrotating configuration remains to be fixed, specifically among the topologies (C^-, C_x^-) for the corotating fluids and $\{C^+, C_x^+, O_x^+\}$ for the counterrotating ones. The general scheme is then provided by

Fig. 7, which does not consider all the constraints imposed by the geodesic structure of the $\mathbf{A}_{a_i}^<$ spacetimes. To prevent any penetration of material, each initial couple shall be such that $(^-) > (^+)$. Being counterrotating, their formation can occur independently and therefore they can take place at different phases. All the possible initial states and evolutive lines, lead-

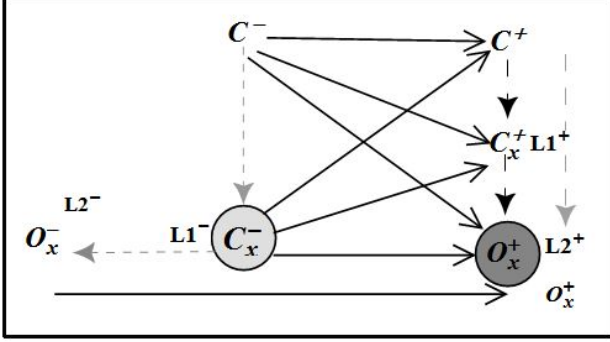


Figure 7: The ℓ counterrotating couple $C_x^- > O_x^+$ (circled), allowed only in the Kerr geometry with $a < a_{ia}$. Dashed arrow-lines show the evolution of the individual configuration, starting from the initial state and pointing to the final state. Black continuum arrow-lines indicate the status of the couple in a specific evolutionary phase, the direction of the arrow is in accordance to the sequentiality relation $>$ (maximum of the hydrostatic pressure sequentiality), in the order of configuration (and criticality). Where uniquely fixed, the region of specific angular momentum is indicated close to each configuration. We assume that O_x^\pm configurations have an initial state in closed topology, but it is indeed possible that the outer configuration C^- could be formed after the formation of O_x^+ .

ing to the final couple in (27), are shown. However, some of the lines of evolution are to be suppressed due to the dynamical structure of the $\mathbf{A}_{a_i}^<$ geometries and the conditions of non-penetration of matter. It is clear that the couple with C^- as initial state, with $\ell^- \in \mathbf{L3}^-$, is always possible, but if $\ell^- \in \mathbf{L1}^-$, then different constraints have to be considered. The initial state in $\mathbf{L3}^+$ will be disadvantaged by the simultaneous presence of an outer $(^-)$ configuration. The analysis of specific constraints of the evolutive lines of Fig. 7 is straightforward and it follows directly the arguments of Appendix A and we will not focus more on it here. The analysis of Fig. 7 also shows the possible evolutive lines of the corotating configurations which would bring the system to the state $O_x^- > O_x^+$, reflected in Eq. (21).

4.3. The ℓ counterrotating accretion-accretion (A-A) systems

For a couple of ℓ counterrotating accreting disks it has to be:

$$C_x^- < C_x^+ \quad (\text{and} \quad C_x^- < C_x^+) \quad \forall a \in]0, M], \quad \mathcal{L} = \mathbf{L1}^- \cup \mathbf{L1}^+. \quad (28)$$

In fact, for the attractor spins, $a > a_{ia}$ (at $a_{ia} : r_{mso}^- = r_{mbo}^+$), the inequality in Eq. (28) could not be inverted to create a hypothetical couple $C_x^+ < C_x^-$, as $\Delta r_x^- < \Delta r_x^+$ and $\Delta r_x^- \cap \Delta r_x^+ = \emptyset$, see also Pugliese&Montani (2015); Pugliese&Stuchlík (2015).

In the spacetimes of the slower attractors we find $r_{mbo}^+ < r_{mso}^-$, and therefore $\Delta r_x^- \cap \Delta r_x^+ \neq \emptyset$.

However, in such spacetimes, an hypothetical couple $C_x^- > C_x^+$, would violate the condition of non penetration of matter in the outer Roche lobes of C_x^\pm : in fact $r_{mbo}^- < r_{mbo}^+ < r_x^+ < r_x^- < r_{mso}^- < r_{mso}^+ < r_{cent}^+$.

Thus, according to Eqs (A.28,A.30), in the geometries $\mathbf{A}_{a_i}^<$ a proper specific angular momentum has to be selected (small enough in magnitude) for the outer C_x^+ disk satisfying the condition $r_{mso}^- \notin C_1^+$.

In conclusion, Eq. (28) holds for the slower attractors $\mathbf{A}_{a_i}^<$ under the restrictions (A.30) on C_x^\pm .

Furthermore, one should consider also the location of the outer edge r_{out}^- of the corotating disk in accretion with respect to the outer accretion point r_x^+ . For sufficiently small specific angular momentum ℓ_1^- (corresponding to smaller accretion disks), K_{Max}^{1-} will be small enough for the disk C_x^- being not extending to include r_j^+ . Further details on the conditions on the K_1 parameter can be found also in Pugliese&Stuchlík (2015). We refer also to the analysis and discussion in Appendix A.3 and particularly Fig. A.16.

In the couple $C_x^- < C_x^+$, penetration of matter occurs from the material of the outer accreting ring C_x^+ to the inner one C_x^- : the case of two disks in accretion clearly results in a penetration of matter affecting the inner lobe of the outer ring and the outer lobe of the inner ring. In this case, the counterrotating matter is accreting onto the corotating one: the two configurations in the C_x^\pm topology could have independent origins and evolutions up to the collision phase, giving rise then to a geometric correlation, and a consequent instability induced on the inner disk from the outer disk in accretion.

The specific angular momentum $-\mathbf{L1}^+$ is certainly larger than $\mathbf{L1}^-$ for sufficiently high spins $a \gtrsim a_{N2}$ therefore in particular also for attractors $a \in]a_{N2}, a_{N1}[$ —see Fig. 5. The outer disk could therefore be characterized by a larger elongation, $\lambda_x^+ > \lambda_x^-$, and correspondingly a greater density. For the slower attractors, the situation is just the opposite and $\Delta \ell_x^+ \cup \Delta \ell_x^- \neq \emptyset$.

Regarding the separation between the two configurations in the first Roche lobe, we should consider the relations from Eq. (A.60)—the inclusion relation implies $r_{mbo}^+ \notin C_x^+$. As $r_x^+ > r_{mbo}^+$, the two configurations are separated by the orbit r_{mbo}^+ . The counterrotating disk C_1^+ can approach this value as much as the specific angular momentum $-\ell_1^+$ increases in $-\mathbf{L1}^+$. For the slower attractors, this spacing will be reduced, according to the relation $\Delta r_x^- \cap \Delta r_x^+ \neq \emptyset$. The spacings $\bar{\lambda}_{i+1,i}$ in general increase with the attractor spin and decrease with the increasing magnitude of the specific angular momentum (corresponding to a decrease of their elongation) see Pugliese&Stuchlík (2015).

4.4. The ℓ counterrotating equilibrium disk-accretion (C-A) systems

In this section we study the couples (C – A) of ℓ counterrotating configurations formed by a closed regular configuration and a configuration in accretion. This case has been also studied in some detail in Pugliese&Stuchlík (2015), where it was considered a single point of instability within the ringed macro-configuration C_x^n .

The multiple configurations with a seed couple (C-A) would be made by an ℓ corotating sequence of regular closed surfaces in equilibrium, whose location and rotation with respect to the attractor are fixed in accordance with the specific state of the couple (C – A).

What is significant here is that, in general, in the decompositions with an inner sequence of corotating or counterrotating fluids in equilibrium, the configuration density (at κ constant) will be smaller in the geometries of the slower attractors for counterrotating disks, and in the field of faster attractors for the corotating ones. But the configuration density turns to be generally lower for the corotating fluids, predicting therefore that the multiple surfaces of this kind are not favored. However, the conditions from the geodesic structure for the existence of these configurations and the condition of no-penetration of matter are very stringent and give a clear indication of these limits.

As in this case there are all closed configurations, it will be convenient to make reference to the configuration index. Consider then the following four states:

4.4.1. State I: The $C^+ - A^-$ systems

This state of the decomposition is easily ruled out. Indeed, its existence would imply:

$$\begin{aligned} C_x^- > C^+ \quad (r_{min}^{1-} > r_{min}^+) \quad r_x^- \geq r_{out}^+, \\ \mathcal{L} = \mathbf{Li}^+ \cup \mathbf{LI}^- \quad \mathcal{K} = K_+^< \cup K_{Max}^{1-}. \end{aligned} \quad (29)$$

This configuration is *not* possible:

$$\begin{aligned} r_{mso}^- > r_x^- > r_{mbo}^-, \quad r_x^- \geq r_{out}^+ > r_{mso} \\ \text{but it is } r_{mso}^- < r_{mso}^+ \quad \text{therefore } C_x^- \not\geq C^+. \end{aligned} \quad (30)$$

Considering Eq. (30,26,27) and Eq. (28), we conclude that the C_x^- configuration of ℓ counterrotating closed couple (29) *must* be the inner one.

4.4.2. State II: The $A^- - C^+$ systems

This second state of the ℓ counterrotating couple ($A - C$) is formed by a corotating disk in accretion and a counterrotating one in equilibrium. According to Eq. (30), we have

$$\begin{aligned} C_x^- < C^+ \quad (r_{min}^{1-} < r_{min}^+) \quad r_x^{1-} \leq r_{in}^+, \\ \mathcal{L} = \mathbf{Li}^+ \cup \mathbf{LI}^- \quad \mathcal{K} = K_+^< \cup K_{Max}^{1-}. \end{aligned} \quad (31)$$

Therefore, the outer counterrotating C^+ disk is in equilibrium and the inner corotating one C_x^- is in accretion.

These two configurations can be geometrically separated and they could evolve independently, at least from some time, unless the outer one is not reaching its unstable mode, according to (26), for open counterrotating proto-jets, leading then to the topological transition $C^+ \rightarrow O_x^+$.

Therefore, a topological shift towards the couple $C_x^- - O_x^+$ is possible, with $\mathbf{Li}^+ = \mathbf{L2}^+$, only in the geometries of higher $a > a_a$.

Or, as Eq. (28) holds, the couples $C_x^- < C^+$ could term in a final $A - A$ system with $\mathbf{Li}^+ = \mathbf{L1}^+$. The couple (31) then, representing an initial stage for the states $C_x^- - O_x^+$, when $a > a_a$, or for the states $C_x^- - C_x^+$ for $a \in]0, M]$. This closes the analysis of a possible interaction, with consequent change in the topology of the outer configuration, in the initial state C^+ .

However, a geometric correlation between the elements of the couple would be possible also at fixed topologies, for collisions and penetration of matter due, for example, to an increas-

ing elongation (magnitude of specific angular momentum $-\ell^+$ in any of $-\mathbf{Li}^+$, or growing of K_+ at fixed ℓ^+), or increasing the specific angular momentum of the accreting matter $\ell_1 \in \mathbf{LI}^-$, increasing therefore its critical elongation (also) outwards (we recall that for each cusped configuration the elongation K is uniquely determined by the matter specific angular momentum). These couples are detailed in Appendix A.2. It could be significant therefore, to discuss the existence of possible constraints for the spacing $\bar{\lambda}_{+,-}$ between this couple.

According to Eq. (A.1,A.2,A.3) it has to be $r_{in}^+ \geq r_{out}^- > r_{mso}^-$ and there is $r_{in}^+ > r_{mbo}^+$.

We should now consider the situation with respect to the outer margin r_{out}^+ . Under the conditions provided by the latest relation of Eq. (A.30) we can find that, for slow attractors ($a < a_a$), counterrotating configurations satisfy the condition $r_{mso}^- \in C_1^+$. Then a geometric correlation with an overlapping of material from the outer to the inner configuration of the couple $C_x^- < C^+$ can certainly occur, if the magnitude of the specific angular momentum ℓ^+ is sufficiently high, accordingly to the constraints provided by Eq. (A.30).

On the other hand, we note that $\mathbf{LI}^- < -\mathbf{Li}^+$ for $a > a_{\mathcal{N}2}$, although the K_+ parameter of the counterrotating disk, can be significantly lower than the K_- parameter of the inner disk.

At lower spins, $a < a_{\mathcal{N}2}$ the situation is not uniquely determined and one needs to distinguish between different specific angular momentum regimes \mathbf{Li} : in fact at $a < a_{\mathcal{N}2}$ we have $\Delta\ell_x^1 \cap (-\Delta\ell_1^+) \neq \emptyset$, and consequently $-\ell_1^-/\ell_1^+ > 1$, while the measures of $-\mathbf{L2}^+$ and $-\mathbf{L3}^+$ are larger than that of $\mathbf{L1}^-$.

To complete this analysis, we consider the location of the radius r_{mbo}^+ with respect to the configuration C_x^- , and of r_{mso}^+ with respect to C^+ .

One would think that it may be always possible to find a sufficiently high specific angular momentum to locate, for example, the center of a *corotating* accreting disk, C_x^- , on the orbit r_{mbo}^+ , as proved in Appendix A.2 and stated in Eq. (A.66) and the following²¹.

However, we have proved that a corotating disk in accretion must have a specific angular momentum $\ell_1 \in \mathbf{LI}^-$. But for these disks, and a fortiori for C_1 (which has lower K_-), the density and elongation could be not sufficient to induce a gravo-hydrostatic instability. Therefore these disks are all contained in $]r_{mbo}^+, r_{mbo}^-]$. In other words, it could be $r_{out}^- < r_{mbo}^+$, implying that the supremum of the spacing is at higher spin $A_a^>$, and it

²¹We can explicit the general idea of this argument as follows: for the couple $C_x^- < C^+$, there is $r_{mbo}^- < r_x^- < r_{mso}^- < r_{out}^- < r_{in}^+ < r_{min}^+ < r_{out}^+$, having to make sure there is non-null distance $r_{in}^+ - r_{out}^-$ where $r_{in}^+ > r_{mbo}^+$. Then, if $r_{mbo}^+ \in C_x^-$, which means $r_{out}^- > r_{mbo}^+$, it is possible to choose a specific angular momentum ℓ^- and ℓ^+ large enough in magnitude, because the distance is zero or negative. On the other side, there is $r_{mbo}^+ > r_{mso}^-$ only for spacetimes of class $A_a^>$, which implies that in these geometries we have $r_{mbo}^- < r_x^- < r_{mso}^- < (r_{mbo}^+ < r_{out}^-) < r_{in}^+$, where the brackets signify a commutation between the terms (r_{mbo}^+, r_{out}^-) . Then the inclusion $r_{mbo}^+ \in C_x^-$ is clearly favored in the case of attractors $A_a^<$ where $r_{mbo}^- < (r_x^- < r_{mbo}^+) < r_{mso}^- < r_{out}^- < r_{in}^+$. Thus, one could inquire if $r_{mso}^- \in C^+$ in the spacetimes $A_a^>$, and this is considered in Eq. (A.30,A.40, A.42,A.48). For faster attractors, $A_a^>$, there is $r_{mso}^- \notin C^+$ implying that these two surfaces are always separated. Whereas for slower attractors the situation is different and collision could take place for $|\ell|$ sufficiently high, according to Eq. (A.47) and Eq. (A.30).

increases with the spin (this fact might be expected also from general considerations about the influence of the spin of the black hole on the ℓ counterrotating couples, discussed in more points here and in detail in [Pugliese&Stuchlík \(2015\)](#)).

It is also possible to provide a rough estimation of the distance $r_{mbo}^+ - r_{mso}^-$ as minimum spacing, but the infimum of this spacing, for this class of attractors, is reached in the geometry $a = a_{ia}$. Therefore, this property may be used as tracing to identify the spin class the attractor belongs to.

One can also read this situation in the following way: for higher spins, the topologies C_x° of order $n = 2$, with the couple $C_x^- < C^+$, could not be possible, and therefore a geometric (and consequently a causal) correlation cannot occur in this couple whose sub-configuration will evolve independently, at least until the outer counterrotating configuration will not change topology. However, Eqs (A.1,A.2,A.3) prohibit the penetration of r_{mbo}^- in the corotating disk.

For the counterrotating disk in open topologies, with $\mathbf{K1}^+ \cup \mathbf{L2}^+$, there is the instability point $r_J^+ \leq r_{mbo}^+$, and matter collision can occur as described in the point **III** $C_x^- < O_x^+$.

We can conclude that at higher spin a correlation between the outer counterrotating matter and the inner disk in accretion (as $\lambda_x = \sup \lambda$, a fortiori this will be true also for a possible inner closed and regular topology) occurs if the outer configuration is open, $(\)^+ = O_x^+$ (we note that $r_x^+ > r_{mbo}^+$ for the cusped closed configuration). Finally this analysis is completed in [Appendix A.3](#) with the discussion of the location of r_γ^\mp in the $(\)_\pm$ configurations.

4.4.3. State III: The $C^- - A^+$ systems

These couples are described by the conditions

$$\begin{aligned} C^- < C_x^+ \quad (r_{min}^- < r_{min}^{1+}) \quad r_x^+ \geq r_{out}^-, \\ \mathcal{L} = \mathbf{Li}^- \cup \mathbf{L1}^+ \quad \mathcal{K} = K_-^< \cup K_{Max}^{1+}. \end{aligned} \quad (32)$$

It is clear that in this case a correlation in the couple $C^- < C_x^+$ must exist, for the *outer* disk C_x^+ is accreting on the attractor and therefore a collision with the *inner* C^- corotating disk will certainly occur.

This couple could even be considered as a precursor of an ℓ counterrotating $\mathbf{A} - \mathbf{A}$ couple, as analyzed in Eq. (28), where it was proved that $C_x^- < C_x^+ \forall a \in]0, M]$, or also of a $\mathbf{A} - \mathbf{J}$ configuration, considered as point **III**, where $C_x^- < O_x^+$, implying the outer configuration opening in proto-proto-jet.

Decreasing the specific angular momentum $-\ell^+ \in -\mathbf{L1}^+$, or increasing $K_- \in \mathbf{K0}$ or ℓ^- for the topology C^- , the spacing between the two surfaces will in general decrease as $\partial_{|\ell|} r_{Max} < 0$, $\partial_{|\ell|} r_{min} > 0$ and $\partial_{|\ell|} r_{out}^x > 0$.

For the conditions in Eq. (32), it has to be $r_{mbo}^- < r_{in}^- < r_{min}^- < r_{out}^- < r_x^+ < r_{min}^+$, with $r_{mbo}^- < r_{mbo}^+ < r_x^+$. Therefore it is important to consider the relative position of the radii r_{mso}^\pm and $r_{mbo}^\pm \in C^-$.

This has been partially faced in [Pugliese&Stuchlík \(2015\)](#) and addressed in detail in this article in [Appendix A.2](#) by Eq. (A.60). From Eq. (A.3) it follows that $r_{mbo}^+ \notin C_x^+$, thus we can certainly find separated couples $C^- < C_x^+$ (meaning here $r_{out}^- < r_x^+$) in the geometries $\mathbf{A}_{ia}^>$, where in fact $r_{mbo}^+ \in]r_{mso}^-, r_{mso}^+]$,

and one can find a sufficiently small momentum $\ell^- \in \mathbf{L1}^-$ for $r_{cent} \in]r_{mso}^-, r_{mbo}^+]$.

However in this case we need to deal also with the location of the outer boundary of the inner corotating disk C^- to establish if configurations C^- with $r_{out}^- < r_{mbo}^+$ are possible. This condition is sufficient but *not* necessary for the separated disks. We addressed his problem in Eq. (A.69), which ensures the validity of this result for fluids with momentum $\ell^- \in \mathbf{L1}^-$ and, in the other cases, for different classes of attractors. Here we introduce the general idea behind the main arguments.

As discussed in [Appendix A.2](#), we need to distinguish the class of attractors $\mathbf{A}_{ia}^<$ at $a \in [0, a_{ia}]$ and $\mathbf{A}_{ia}^>$ with $a \in]a_{ia}, M]$ respectively.

In general, if $\ell = \ell_{mso}^- + \epsilon_\ell$ then $r_{min}^- = r_{mso}^- + \epsilon_{r_{min}}$, where $\epsilon_{r_{min}} = \epsilon_{r_{min}}(\epsilon_\ell) > 0$ and $\epsilon_\ell > 0$ (analogously for the maximum points with $\epsilon_{Max} < 0$, and in general $\epsilon_{r_{min}} \neq \epsilon_{r_{Max}}$ ([Pugliese&Stuchlík, 2015](#)), thus ensuring the disk is small enough or placed far enough from the marginally bounded orbit, as $r_{in}^- < r_{mbo}^+$, in the geometries $\mathbf{A}_{ia}^<$, and $r_{out}^- > r_{mbo}^+$ for $\mathbf{A}_{ia}^>$.

Thus K_- could be sufficiently small to consider $r_{mbo}^+ \notin C^-$, but this must imply $\ell^- \in \mathbf{L1}^-$ (from the definition of $\mathbf{L1}^-$).

On the other side, increasing ℓ^- towards $\ell^-(r_{mbo}^+)$, see [Fig. A.10](#), the center with maximum hydrostatic pressure approaches r_{mbo}^+ at $a > a_{ia}$, or the minimum of the pressure for attractors $\mathbf{A}_{ia}^<$. The ring has to have a K_- parameter smaller and smaller to ensure the disk does not include r_{mbo}^+ . Therefore, we can say that these disks not including r_{mbo}^+ , are nor favored at low K for low specific angular momentum.

For attractors with $a \in]0, a_{ia}[$, an increase of the spin acts against the formation of these configurations, that are favored instead for higher spins, and thus also the larger K for the multiple configuration, according to the analysis of Eq. (A.69).

Indeed, $r_{mso}^- < r_{min}^- < r_{out}^- < r_x^+ < r_{mso}^+$ and $r_{mbo}^+ < r_x^+$. Thus one can always find an $-\ell^+ \in -\mathbf{L1}^+$ sufficiently small, and a small ℓ^- , accordingly to allow a separated couples.

The decompositions of higher order than $n = 2$ would be possible, for example, with an inner ℓ corotating sequence of *corotating* disks in equilibrium, and one outer with respect to C_x^+ , formed by corotating or counterrotating fluids in equilibrium.

4.4.4. State IV: The $A^+ - C^-$ systems

These systems are defined by the relations:

$$\begin{aligned} C_x^+ < C^- \quad (r_{min}^{1+} < r_{min}^-) \quad r_{in}^- \geq r_{out}^+, \\ \mathcal{L} = \mathbf{Li}^- \cup \mathbf{L1}^+ \quad \mathcal{K} = K_-^< \cup K_{Max}^{1+}. \end{aligned} \quad (33)$$

In this case the *outer* disk is C^- in equilibrium, and the counterrotating *inner* disk is in accretion. It has to be $r_{mbo}^+ < r_x^+ < r_{mso}^+ < r_{min}^+ < r_{out}^+ \leq r_{in}^- < r_{min}^-$. These configurations have also been discussed in details in [Pugliese&Stuchlík \(2015\)](#).

A geometric correlation between the two configurations is possible, and therefore a causal correlation, as a consequence of a shift inward of the outer disk, due to lost of specific angular momentum or to an increase of $K_- \in \mathbf{K0}$, with the fixed center but longer elongation. An increase of specific angular momentum magnitude $-\ell^+ \in -\mathbf{L1}^+$, would also produce a shift outward of the outer margin r_{out}^+ . Eventual emergence

of an instability of the disk in regular topology C^- , leading to the couple $C_x^+ < C_x^-$, cannot occur but following the collision with the inner counterrotating disk C_x^+ already in accretion (as $r_{mso}^+ < r_{mso}^-$).

In fact, Eq. (28) holds, indicating that $C_x^- < C_x^+$ and therefore $C_x^- \neq C_x^+$, from which it results that the couples $C^+ - A^-$, according to the definition Eq. (29), *could not* evolve into the topology $A^+ - A^-$. For the faster attractors, $a > a_{\mathcal{N}_1}$, such a kind of couple is forbidden for the geodesic structure of the spacetime and, for the slower attractors, $a < a_{\mathcal{N}_1}$, from the condition of non-penetration of matter.

As we have mentioned above, a further possibility of correlation occurs for the action of the *inner* unstable configuration, due to increasing specific angular momentum $-\ell^+ \in -\mathbf{L1}^+$ and consequently increasing K_+ , with a consequent shift outward of the center of maximum pressure and of the outer boundary.

As can be seen from Fig. 4, these couples can be always possible, within the necessary condition $r_{mso}^+ \notin C_-$, if ℓ^- is sufficiently large and K sufficiently close to the minimum (lower density), with $\ell^+ \in \mathbf{L1}^+$ low enough (in magnitude) for the non-penetration of matter condition will be satisfied. We can specify these limits considering Eqs (A.57, A.58 A.59).

By referring to Fig. A.10, we need to distinguish between the attractors $\check{A}_*^<$ with spin $a < \check{a}_*$, and the geometries of the faster attractors $\check{A}_*^>$ with $a > \check{a}_*$. Together with the further restriction, for increasing ℓ^- and decreasing $-\ell^+$, to avoid the condition $r_{out}^+ \in C^-$, uniquely fixed by the specific angular momentum ℓ^+ . In any case, we still consider the non-penetration of matter from the outer Roche lobes of the two configurations as described by the second relation of Eq. (32).

4.5. The ℓ counterrotating equilibrium disk-proto-jet (C-J) systems

We will consider a couple formed by an equilibrium configuration and a configuration opened in proto-jet.

As specified in Sec. (4.2) and Sec. (4.4), multiple surfaces formed by couple seed, shall contain two ℓ corotating sequences at equal topology. In general, at constant κ , the density of the inner sequence with regular and closed topologies will be small particularly at high spin a/M for co-rotating fluids. Below are discussed several limitations and considerations on the possible orbital extension for such sequences. The following four cases occur:

4.5.1. Case I: The $C^+ - J^-$ systems

This case is described by the condition

$$C^+ < O_x^- \quad (r_{min}^+ < r_{min}^-) \quad \text{with} \quad r_{out}^+ \not\leq r_J^- \quad \text{and} \\ r_{in}^+ \geq r_J^-, \quad \mathcal{L} = \mathbf{L1}^+ \cup \mathbf{L2}^-, \quad \mathcal{K} = \mathbf{K0}^+ \cup \mathbf{K1}^-, \quad (34)$$

that is, in order to avoid any overlap of material, and considering the geodesic structure of the spacetime as in Fig. 4, the equilibrium C^+ disk has to be entirely contained in the region $r > r_J^-$, but with $r_{min}^+ < r_{min}^-$, as it comes from the definition $C^+ < O_x^-$. This is in contrast with the state $C^- < O_x^+$, analyzed in Eq. (36), where there is still a closed inner configuration.

Therefore $r_J^- < r_{mbo}^- < r_{mbo}^+ < r_{in}^+ < r_{min}^- < r_{out}^+$, the third inequality is a consequence of Eq. (A.1,A.2,A.3) and $r_{cent}^- > r_{mso}^+$.

The couples of Eq. (34) could be always geometrically separated. However, the closed C^+ configuration cannot change topology towards the transition $C^+ > J^+$ as this would imply a transition where the closed configurationf changes topology creating a couple $J^- - J^+$ or $J^- - A^+$ considered above. In any case, it has to be $r_J^- < (r_J^+ < r_{min}^-) < r_{min}^-$ or $r_J^- < (r_x^+ < r_{min}^-) < r_{min}^-$. The first inequality is to avoid any penetration of matter, starting the initial condition Eq. (34), the last one follows the definition of the specific state of the decomposition, more probably to be formed at spins $a > a_i$ and $a > a_{l_a}$, as it follows from the geodesic structure in Fig. 4.

4.5.2. Case II: The $J^- - C^+$ systems

We consider the couple

$$O_x^- < C^+ \quad (r_{min}^- < r_{min}^+) \quad \text{with} \quad r_{out}^+ \not\leq r_J^- \quad (35) \\ \text{and} \quad r_{in}^+ \geq r_J^-, \quad \mathcal{L} = \mathbf{L1}^+ \cup \mathbf{L2}^-, \quad \mathcal{K} = \mathbf{K0}^+ \cup \mathbf{K1}^-.$$

Since $r_J^- < r_{mbo}^- < r_{mso}^- < r_{min}^- < r_{min}^+$, the counterrotating closed configurations are separated and remain separated during its evolution (at fixed topology) from the inner (using the criticality index) corotating proto-jet.

Therefore, in both the cases, **I** for the $C^+ - J^-$ systems, and **II**- for the $J^- - C^+$ systems, the outer disk is in equilibrium and the two configurations are geometrically separated.

In this case it has to be $r_J^- < (r_J^+ < r_{min}^-) < r_{min}^-$ or $r_J^- < (r_x^+ < r_{min}^-) < r_{min}^-$.

For these cases to be fulfilled, it must be guaranteed that the specific angular momenta ℓ_{\pm} are ensuring the relations above; we know then that it has to be $\ell^- < -\ell^+$, see also Pugliese&Stuchlík (2015) and Fig. 4.

4.5.3. Case III: The $C^- - J^+$ systems

This state is described by the conditions:

$$C^- < O_x^+ \quad (r_{min}^- < r_{min}^+) \quad \text{with} \quad r_{out}^- \leq r_J^+ \quad \text{or} \\ r_{in}^- \geq r_J^+ \quad \mathcal{L} = \mathbf{L1}^- \cup \mathbf{L2}^+, \quad \mathcal{K} = \mathbf{K0}^- \cup \mathbf{K1}^+. \quad (36)$$

This couple, as in Eq. (34), includes by definition a closed and regular inner surface. In contrast with the cases defined in Eqs (34,35), which are bound in $r_{out}^- \not\leq r_J^+$, by the condition of non-penetration of matter. The state considered here is instead possible as an *alternative* to the relation $r_{in}^- \geq r_J^+$. This means that the corotating disk in equilibrium can be entirely contained in $r > r_J^+$.

This couple can always exist in any geometries but, as in $A_{l_a}^<$, we have $r_J^+ < r_{mbo}^+ < r_{mso}^+ < r_{mso}^- < r_{min}^+$. To avoid any penetration of matter, the configuration should be contained in the region $r > r_J^+$. Thus $r_{out}^- > r_{in}^- > r_J^+$, but there could be a geometric correlation and indeed it can even be $r_{in}^- = r_J^+$.

On the other side, for attractors $A_{l_a}^>$, there is $r_{mso}^- < r_{mbo}^+$ and in this case the corotating ring can be outer or inner to the region $r < r_J^+$. There could be geometric correlation, and indeed

it could be even $r_{out}^+ = r_J^+$. The existence of a geometric correlation should be considered according to the limits provided by the analysis of [Appendix A.2](#) and [Appendix A.3](#).

4.5.4. Case IV: The $J^+ - C^-$ systems

The following conditions hold:

$$\begin{aligned} O_x^+ < C^- \quad (r_{min}^+ < r_{min}^-) \quad \text{with} \quad r_{out}^- \not\leq r_J^+ \quad (37) \\ \text{and} \quad r_{in}^- \geq r_J^+, \quad \mathcal{L} = \mathbf{L1}^- \cup \mathbf{L2}^+, \quad \mathcal{K} = \mathbf{K0}^- \cup \mathbf{K1}^+. \end{aligned}$$

In this case the corotating ring is located in the region $r > r_J^+$, and the surfaces of the couple are geometrically separated, generally by the distance $]r_{mbo}^+, r_{mbo}^-]$. The situation is clearly articulated as it depends on the geodesic structure of spacetime, and therefore it differentiates various classes of attractors.

Using the results of [Appendix A](#), and considering the limiting spins introduced in the analysis and in [Fig. 4](#), we can summarize the situation as follows:

1. At $a < a_t$, we have $r_\gamma^+ < r_{mbo}^- < r_{mbo}^+ < r_{mso}^- < r_{mso}^+ < r_{min}^+ < r_{min}^-$. But $r_J^+ \in]r_\gamma^+, r_{mbo}^+]$ and $r_{mbo}^- \in]r_\gamma^+, r_{mbo}^+]$ $\notin C^-$.

Using [Eqs \(A.6,A.10,A.11\)](#) and [Eqs \(A.13,A.14\)](#), we can say that, for ℓ large enough, and then the minimum point r_{min}^+ far enough, and large K_- , the radius r_{mso}^- can approach the inner edge of the disk (considering also $\mathbf{L3}^-$).

This means that they will be separated by the range $]r_{mbo}^+, r_{mso}^-]$. This is confirmed by [Eq. \(A.60\)](#) and [Eq. \(A.63\)](#) where a similar argument is carried out for the other cases.

2. For $a \in]a_t, a_{t^*}]$, one has $r_{mbo}^- < r_\gamma^+ < r_{mbo}^+ < r_{mso}^- < r_{mso}^+ < r_{min}^+ < r_{min}^-$ thus, by increasing the spin of the attractor, the constraints should be less stringent reducing to the only inclusion $r_{mbo}^+ \in C^-$ and $r_{mso}^- \in C^-$. In this case, one has to consider properly large specific angular momenta ℓ^- and K_- parameter, because an inclusion relation may be then satisfied, in accordance with the above analysis.

At $a \in]a_{t^*}, a_{\gamma^*}]$, see [Fig. 4](#), we find $r_{mbo}^- < r_\gamma^+ < r_{mso}^- < r_{mbo}^+ < r_{mso}^+ < r_{min}^+ < r_{min}^-$. The only condition to be insured is $r_{mso}^+ \notin C^-$. For even higher spin, $\mathbf{A}_{t^*}^+$, which includes the extreme case, there is $r_{mbo}^- < r_{mso}^- < r_\gamma^+ < r_{mbo}^+ < r_{mso}^+ < r_{min}^+ < r_{min}^-$. It remains to establish the condition $r_{mso}^+ \notin C^-$, but also $r_\gamma^+ \notin C^-$.

The inclusion condition with respect to the photon orbit have been investigated in [Appendix A.3](#), and therefore we have to adhere to the conditions in [\(A.75,A.76\)](#).

This analysis confirms that the geometrical correlation, for the contact in $r_J^+ \approx r_{in}^-$, can occur only in specific circumstances, by narrowing both the set of geometries and the range of the fluid specific angular momentum.

Finally, the equilibrium surface is subjected to a change of topology, ending in a critical phase, for example in O_x^- or C_x^- . However, the formation of such a couple from the initial phase in [Eq. \(37\)](#) $O_x^+ < C^-$, with $r_{min}^+ < r_{min}^-$, and $r_x^- \geq r_J^+$ or $r_J^- \geq r_J^+$, or equivalently $O_x^+ > (O_x^-)$, is regulated by the conditions in [Eqs \(20,21\)](#) and [Eq. \(26\)](#) respectively.

5. Phenomenology and observational evidence of RADs

RADs are agglomerates of several accretion tori orbiting very compact objects, following the possibility that several ac-

cretion disks can form around very compact objects as **SMBHs** ($10^6 - 10^9 M_\odot$, M_\odot being solar masses) in **AGNs** embedding. For these very compact objects the curvature effects are relevant and the host can provide for a very rich and active **BH** environment. **RAD** may be originated after different accretion phases in some binary systems or **BH** kick-out, or by local clouds accretion. Concerning the accretion emergence, the maximum number of accreting disks orbiting around one central Kerr **BH** is $n = 2$. A double accretion can be observable only as a couple $C_x^- < C_x^+$ (see [Fig. 1](#)), around all Kerr **BHs** ($a \neq 0$). The couple is subjected to constraints provided here on the fluid angular momentum range (ℓ -parameter) and density (K -parameter)—see also [Pugliese&Stuchlík \(2017b\)](#). However, some “screening”-configurations for such accreting couples can form, constituting a more articulated **RAD** system (\mathbf{xx}) : $C_x^- < C^- < \dots < C_x^+ < C^\pm$, with only *corotating* non-accreting disks between the two accreting tori. Eventually this demonstrates that a screening disk must be always a corotating (non-accreting) torus. These special configurations may be detectable for example as X-ray spectra emission obscuration. On the other hand, if a counterrotating torus is accreting onto the central **BH**, then a **RAD** with a corotating outer torus towards the accretion (i.e. C_1^-), can be observed only as an aggregate of the kind (\mathbf{x}) : $(O_x^- < C_x^+ < C_1^- < C^\pm)$, and orbiting around “slow” **BHs** with $a < 0.46M$. We note that, if the inner torus is C_x^- , then a configuration (\mathbf{x}), or with a string of configurations $(O_x^- < C_x^+ < C_1^- < C^\pm)$, reduces to a special case of (\mathbf{xx}) **RAD**, that is of the kind $C_x^- < C^- < \dots < C_x^+ < C^\pm$ ([Pugliese&Stuchlík, 2017b](#)). This also implies that, during the evolution of the outer corotating torus towards accretion, no such couple can form, prior the emergence of tori collision, eventually reducing the actual possibility to observe a counterrotating accreting disk, in the **RAD** context, and tightening it to the **BH-RAD** early phases of evolution—see also [Pugliese&Stuchlík \(2017b\)](#).

A further relevant aspect of this investigation is to support the need, endorsed also by several other studies, of a more general framework of analysis envisaging the **BH**-disk system as an integrated whole. Evidences of this fact are the ongoing debates on the jet-accretion correlation, the issues of the **BH** accretion rate-disk luminosity, **BH** growth - accretion disk, and **BH**-spin shift-accretion disk correlation.

Results of our analysis, moreover, show the importance of proto-jet-accretion correlation, envisaged here as (**J-A**)-correlation—[Secs \(3.2,3.3\)](#) and [Sec. \(4.2\)](#). Proto-jets are narrow, relatively fast, long matter funnels ([McKinney et al., 2013](#); [Lovellace et al., 2014](#); [Marscher et al., 2002](#); [Maraschi&Tavecchio, 2003](#); [Chen et al., 2015](#); [Yu et al., 2015](#); [Zhang et al., 2015](#); [Sbarato et al., 2014](#); [Coughlin&Begelman, 2014](#); [Maitra et al., 2009](#); [Ghisellini et al., 2014](#); [Fragile et al., 2012](#); [Miller et al., 2012](#); [Abramowicz&Sharp, 1983](#); [Sadowski&Narayan, 2015](#); [Okuda et al., 2005](#); [Ferreira&Casse, 2004](#); [Lyutikov, 2009](#)). Findings of [Secs \(3.1,4.1\)](#) suggest the possibility to detect *structured proto-jets* as sequences of jet-like configurations (or *jet-bundles*), constrained in spacings and relative fluids rotation.

[Appendix A](#) specifies the more general statement according to which the inner edge of an accreting torus is located

in $r_x \in]r_{mbo}, r_{mso}[$ (Krolik&Hawley, 2002; Bromley et al., 1998; Abramowicz et al., 2010; Agol&Krolik, 2000; Paczyński, 2000). We bounded the location of the accretion disk cusp to the variation ranges of the ℓ -parameter and in accordance with the torus evolutionary phases and the **RAD** structure. In turn, in this analysis, we narrowed down the location of the single accretion torus inner edge, showing the strong connection between **RAD** structures and **BH** spins—see also Pugliese&Stuchlík (2017c).

A further phenomenological application of these studies, already mentioned in Pugliese&Stuchlík (2015), regards the possible connection between **RADs** seismology and **QPOs** - the pattern of the possible oscillation modes of the tori aggregate has been provided and related to the evolution of instabilities in **RAD**. **QPOs** are low and high frequency peaks in the power density spectra, studied in missions like **XMM-Newton** (X-ray Multi-Mirror Mission)²² or **RXTE** (Rossi X-ray Timing Explorer)²³. Each torus of the aggregate considered here, has its own axisymmetric and incompressible modes which have been variously associated with the **QPO** emergence. For global oscillations of slender tori in the radial and vertical directions, their frequencies are determined by combinations of the geodesic epicyclic frequencies - for details see Stuchlík et al. (2013). In the **RADs** case, these modes have to be combined with the stratified structure of the **RADs** and its own modes, finally leading to an alteration of the macrostructures elongations and spacings.

In any case, the internal structure of the **RAD** presents a rich multiplicity of situations and different working frameworks. It is clear that in many aspects the physics of **BHs** and its host galaxy would be altered by the relevance of the **RAD** argument in support of the hypothesis of a more complex **BH**-accretion disk system, than is commonly considered. **RAD** accretion in galaxy may produce radiative power outshining the host galaxy itself (note that the **AGNs** accretion disk is encircled by a thick (outer) torus of gas and dust). On the other hand, **AGN** are generally characterized by very fast jets (almost speed of light), which might be connected with an inner **RAD** disk jet launch.

A **RAD** structure analysis demands for an accurate determination of the processes timescales to determine the **RAD** evolution timeline. This issue was detailed discussed in Pugliese&Stuchlík (2017b), where a **RAD** of the order $n = 2$ was considered as an ℓ corotating or ℓ counterrotating couple. This analysis was performed as part of the broadest investigation on the tori collision emergence. In fact, the complexity and variety of the processes characterizing the tori agglomerate can be actually contained in a few evolutionary patterns, heavily depending on the initial data of the single component of the aggregate. The **RAD** timescales were shown then to strongly depend on timescale of tori formation more than from the instability of each torus. Different situations are distinguished according to the relative fluids rotation and the rotation of the **RAD** inner torus with respect to the central **SMBH**. These studies show how, for some couples, an expected final collisional phase occurs, eventually followed by a tori merging with a modification

of the **RAD** internal structure, or a drying-feeding effect with rising of oscillatory modes. Couples (**x**) and (**xx**), are examples where one of the tori approaches the instability, while the evolution of the outer corotating torus inevitably leads to the collision. This situation ultimately ends up constraining the **BH** evolution itself in its environment.

Concerning then the disk *process timescales* in the aggregate, these depend-on and determine the tori model characteristics (as thickness, opacity, accretion rates or instabilities). The determination of the **RAD** timescales should be made by combining the analysis of each **RAD** component timescale with the **RAD** internal oscillation. For the geometrically thick configurations considered here, it is generally assumed that the timescale of the dynamical processes, τ_{dyn} , (regulated by the gravitational and inertial forces, the timescale for pressure to balance the gravitational and centrifugal force) is much lower than the timescale of the thermal ones, τ_{the} , (i.e. heating and cooling processes, timescale of radiation entropy redistribution) that is lower than the time scale of the viscous processes, τ_{vis} , and the effects of strong gravitational fields are dominant with respect to the dissipative ones and predominant to determine the unstable phases of the systems (Font&Daigne, 2002b; Igumenshchev, 2000; Abramowicz&Fragile, 2013), i.e. $\tau_{dyn} \ll \tau_{the} \ll \tau_{vis}$. Thus the effects of strong gravitational fields dominate the dissipative ones, grounding the assumption of perfect fluid energy-momentum tensor—see also Abramowicz&Fragile (2013); Paczyński (1980). Moreover, during the evolution of dynamical processes, the functional form of the angular momentum and entropy distribution depends on the initial conditions of the system and on the details of the dissipative processes: the entropy is constant along the flow and, according to the von Zeipel condition, the surfaces of constant angular velocity Ω and of constant specific angular momentum ℓ coincide (Abramowicz, 1971; Chakrabarti, 1990, 1991; Zanotti&Pugliese, 2014), implying the rotation law $\ell = \ell(\Omega)$, independently by the equation of state (Lei et al., 2008; Abramowicz, 2008). Eventually, this model describes an opaque and super-Eddington, radiation pressure supported accretion disks cooled by advection with low viscosity, where proto-jet configurations are funnels of material with highly super-Eddington luminosity.

Despite the fact that the **RAD** model we used is based on aggregates of thick tori, actually the major significance of **RAD** presence in **BH** host environment should emerge from the “macrostructure-scale”, to be considered in some extents quite independently of the single torus model. **RAD** can be made by aggregate components with very different models, according to the different evolution processes advocated for each torus origin. In this respect, the macrostructure morphology is more decisive, for the point of view of the **RAD**-**BH** system phenomenology, than the model for the each component.

In the following, we briefly consider different observational spots expected to be associated with the **RAD**, and strongly dependent of the **RAD** morphology. Firstly, **RAD** blends the geometry of a thin disk (the **RAD** is generally a geometrically thin disk as demonstrated in Pugliese&Stuchlík (2015)) with the specific characteristics of a geometrically thick disk (for

²²<http://sci.esa.int/science-e/www/area/index.cfm?fareaid=23>

²³<http://heasarc.gsfc.nasa.gov/docs/xte/xtegif.html>

example, high accretion rates), together with a stratified inner structure, a differential relational law and a *knobby*, although axial-symmetric, disk surface (Pugliese&Stuchlík, 2015). In this sense, the macrostructure disrupts the usual “disk-model”-“disk geometry” correlation, especially as regard of the assessment of the accretion rate. First important consequence of this mix of different elements is in the possibility of episodic accretion phases, with super-Eddington accretion rates. This distinctive feature can enter into the debate on the **SMBHs** origin, combining however with drying-feeding processes and screening effects. The already mentioned possibility of structured proto-jet bundles and possible evidences in the **QPOs** analysis are other important fields of application.

On the other hand, from the observational view-point, the need for such multiple systems is actually already stated in the literature, for example in the analysis of screening effects of X-ray emission supposed so far to be induced by some “bubbles” of material orbiting between an accreting disk and its central attractor (Marchesi et al., 2016; Gelli et al., 2007; Marchesi et al., 2017; Masini et al., 2016; DeGraf et al., 2017; Storchi-Bergmann et al., 2017). Results of our investigation, therefore, strongly advocate for a framework shift in the screening X-ray emission study, which is here traced back to the *only* cases (x) and (xx). More generally, the X-ray emission investigation can provide an accurate description of the spectral features of the **RADs** structure. We expect that the tori spacings ($\bar{\lambda}$) and the **RAD** knobby surface would leave traces in a stratified emission spectra. The X-ray emission from **AGNs** has been variously assumed to be related to accretion disk instabilities and surrounding corona. This spectra profile should provide a fingerprint of the ringed disk structure, possibly as a radially stratified emission profile. The simplest structures of this kind are thin radiating rings (Schee&Stuchlík, 2009, 2013; Sochora et al., 2011). Future X-ray spectroscopy may reveal the **BH** accretion ring models as relatively indistinct excesses on top of the relativistically broadened spectral line profile Sochora et al. (2011), arising in a well-confined radial distance in the agglomerate- (Pugliese&Stuchlík, 2015, 2016a; Pugliese&Stuchlík, 2017b). In Karas&Sochora (2010) extremal energy shifts of radiation from a ring near a rotating **BH** were particularly studied: radiation from a narrow circular ring was proved to show a double-horn profile with photons with energy around the maximum or minimum of the range. This energy span of spectral lines is a function of the observer’s viewing angle, the black hole spin and the ring radius.

Eventually, **RADs** might represent an environment of the episodic accretion phases advocated as explanation of the **SMBHs** origin from (intermediate or low mass) **BH** seeds. Formation and evolution of **SMBHs**, especially at cosmological distances (redshift $z \approx 6$), is still an open topic in High Energy Astrophysics. One of the key issues is the identification of the different processes associated with the **SMBHs** origin with very large masses (Volonteri et al., 2007; Volonteri, 2007, 2010; Li, 2012; Oka et al., 2017; Kawakatu&Ohsuga, 2011). Note that recently another fundamental alternative of direct creation of **SMBHs** has been proposed in Stuchlík et al. (2017b), being based on gravitational instability of central region of the

so called trapping relativistic polytropes that could model dark matter galactic halos (Stuchlík et al., 2016).

It should be noted then, that the evaluation of the **SMBHs** spin is strictly correlated with the “masses-problem”. The assessment of the precise value of the spin parameter of the **BH** is connected with the evaluation of the main features of the **BH** accretion disk system, as the **BH** accretion rate or the location of the inner edge of the accretion disk. Several processes have been proposed and analyzed: for example, **BHs** characterized by long and continuous accretion episodes arising due to merging, and involving a relevant spin-shift process (especially in elliptic galaxy), or sequences of small and random accretion episodes occurred after different situations as cloud accretion or also tidal disruption of a star companion (especially in spiral galaxies). These two different situations would, however, lead to two relatively different populations of **BHs** with different masses. Collapse from stellar-mass black holes, **BHs** mergers, accretion of some gas-clouds with low radiative efficiency, are other proposed evolutive patterns. **SMBHs**, originated from some “seeds” ($10^4 - 10^2 M_\odot$) with different evolutive patterns, generally depend on the seed initial mass and on the **BH** environment, needing enough matter for accretion, proper processes timescales, and large initial angular momentum of the accretion disks. An alternative then consists of a succession of accretion episodes from misaligned disks with random **BH** spinning-up and spinning-down, or also a sequence of turning-on and turning-off of super-Eddington accretion phases interspersed with sub-Eddington phases²⁴.

The **RAD** agglomerates, due to their stratified inner structure, are a source of episodic accretions, combined with the effects of tori collisions, accretion obscuration and drying-feeding processes. The macrostructure stands then as promising arena of investigation for **SMBH** formation, following accretion from multi-disks of (x) and (xx) configurations. Efficiency of the **RAD** and its luminosity are not uniquely determined by the inner accreting disk, in fact our investigation shows here evidences that the aggregate structure falsifies this hypothesis, by considering the possibility, albeit restricted to cases (x) and (xx), of screening effects and alternated phases of accretion and collision. Many of the mentioned aggregate characteristics can be easily evaluated under the hypothesis of the thick torus components—see for example Abramowicz (2004); Abramowicz&Straub (2014); Abramowicz et al. (1978); Jaroszynski et al. (1980); Abramowicz (1985, 2004); Abramowicz&Frigile (2013). We can provide a quantification of the key parameters in a special case of **RAD**. This will allow us also to evaluate some trends and determine special aspects of problem space-scales. Considering polytropic fluids with pressure $p = \kappa \varrho^{1+1/n}$, we can evaluate many of the **RAD** characteristics, as the **RAD** thickness (h) and elongations (λ), tori spacings ($\bar{\lambda}$), through an

²⁴A super-Eddington phase may have very low efficiency in converting mass into radiation. We note that the efficiency of a thick torus with $r_x \approx r_{mbo}$ is nearly zero (indeed in the **RAD** model such a torus is subjected to special boundary conditions). This is a general relativistic effect, the binding energy decreases as the inner boundary of the disk moves inwards inside the marginally stable orbit towards r_{mbo} , where $E_{mbo} = 1$.

assessment of the K -parameter only (Pugliese&Stuchlík, 2015). For a single torus, calculations of its polytropic structure can be found in Stuchlík et al. (2009). Furthermore, we can also provide an estimate of the mass-flux, enthalpy-flux (evaluating also the temperature parameter), and the flux thickness—see for example Abramowicz (1985). All these quantities have form $O(r_x, r_s, n) = q(n, \kappa)(W_s - W_x)^{d(n)}$, where $q(n, \kappa)$ and $d(n)$ are different functions of the polytropic index²⁵, $W = \ln V_{eff}$ is Paczynski-Wiita (P-W) potential of Eq. (6), $W_s \geq W_x$ is the value of the equipotential surface, which is taken with respect to the asymptotic value. Consequently, the determinant parameter, in this analysis is $K : W_* = \ln K_*$ for any radius r_* . Therefore, as the cusp approaches the limiting radius r_{mbo} , the potential $W_x \approx 0$, which is the limiting asymptotic value for very large r . The mass flow rate through the cusp (mass loss, accretion rates) \dot{M}_x and the cusp luminosity \mathcal{L}_x (and the accretion efficiency η), measuring the rate the thermal-energy is carried at cusp, are²⁶ as $\mathcal{P} = O(r_x, r_s, n)r_x/\Omega_K(r_x)$. In fact the relativistic frequency Ω reduces to the Keplerian value Ω_K at the edges of the accretion torus, where the pressure forces vanish—see also Figs 8 and 9.

A throughout investigation of these quantities for the **RAD** couples, considered here, is planned for a future analysis, in connection with the analysis of the **SMBH** accretion rates. We provide here some general considerations for a (xx) couple. For this purpose, we can consider the couple (xx) or $C_x^- < C_x^+ < C^-$ of Fig. 1, where there is ($a = 0.38M$, $\ell_o^- = 3.99$, $\ell_o^+ = -3.99$, $\ell_i^- = 3.32$). We do not consider the outer corotating non-accreting torus C^- of the triple system. Notice that in this triple ℓ counterrotating system, the outer C^- disk is not constrained to a higher height with respect to the internal disks, or any equilibrium disk or an ℓ counterrotating accreting couple has no special constraints on the relative height of the tori. This obviously implies a very wide set of possibilities for a knobby **RAD** disk. Then, we can evaluate the tori center (r_{cent}), the cusp location (r_x), the outer margin (r_{out}), the torus elongation on the equatorial plane (λ), the torus height (h), and the tori spacings ($\bar{\lambda}$) as follows: for the counterrotating torus, C_x^+ , there is ($r_{cent}^+ = 7.8195M$, $r_x^+ = 6.645M$, $r_{out}^+ = 8.60278M$, $\lambda^+ = 1.95744M$, $h^+/2 = 0.267283M$), for the corotating torus, C_x^- , there is ($r_{cent}^- = 5.29868M$, $r_x^- = 4.1907M$, $r_{out}^- = 6.18481M$, $\lambda^- = 1.99412M$, $h^-/2 = 0.364584M$). In this specific case, the **RAD** aggregates a set of small tori. Nevertheless, a (xx) couple can be observable orbiting any Kerr **BH**, and the larger is the **BH** dimensionless spin the bigger the tori can grow, while a larger spacing is required. An immediate evaluation shows that the maximum spacing possible for a double accreting tori is $\bar{\lambda}_{max} \lesssim 8M$, in the case of an extreme Kerr **BH** where $a \approx M$. Spacing for the (xx) couple of Fig. 1 is

$\bar{\lambda} \equiv r_x^o - r_{out}^i = 0.460526M$ (Note that the space-scales are in units of **SMBH** masses)—(Pugliese&Stuchlík, 2015). To realize the significance of this data we should note that the spacing parameter $\bar{\lambda}$ is of essential importance for determination of tori collision, the aggregate oscillation and in the analysis of the stratified **RAD** X-ray emission spectra. We also recall that only this case (xx) screening effects are only possible for the corotating tori as follows $C_x^- < C^- < \dots < C_x^+ < C^\pm$. In the next session, we summarize the final methodological considerations and future perspectives of this work.

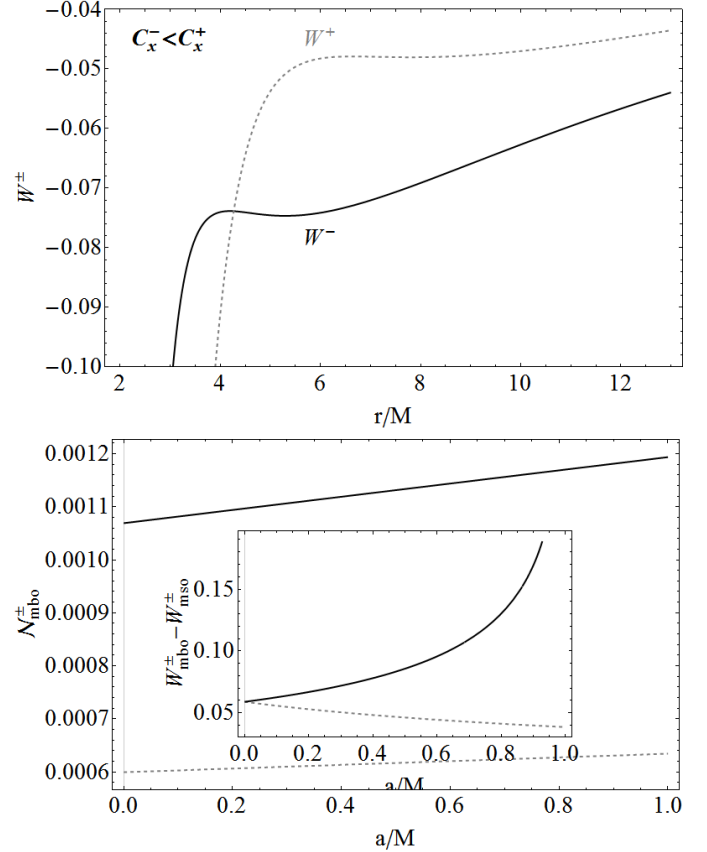


Figure 8: *Upper panel:* Paczynski-Wiita (P-W) potential W^\pm of Eq. (6) as function of r/M ($W = \ln V_{eff}$), for the tori of the couple $C_x^- < C_x^+$ of Fig. 1 respectively, where $a = 0.38M$, $\ell_o^+ = -3.99$ and $\ell_i^- = 3.32$. *Bottom panel:* $N_{mbo} \equiv r_x(W_{mbo} - W_x)^\kappa (\Omega_K(r_x))^{-1}$ as function of a/M . $\Omega_K(r_x)$ is the the Keplerian angular velocity at the cusp r_x , r_{mbo} is the marginally bounded orbit. $\kappa = n + 1 = 4$ has been fixed for an adiabatic fluid with polytropic index $4/3$. *Inside panel:* difference ($W_{mbo}^\pm - W_{mso}^\pm$) (maximum location of inner edge is $r_x \lesssim r_{mso}$), as function of a/M . Quantities are evaluated at fixed ℓ_o^+ and ℓ_i^- . Dashed line is for the accreting torus C_x^+ , black line is for the C_x^- torus.

6. Conclusions

The systems investigated here offer several methodological and observational challenges. Describing a set of virtually separated tori orbiting one attractor as an entire configuration, requires a certain number of assumptions. We distinguish three periods of **BH**-ringed accretion disk life: the first featuring tori formations, a second facing the accretion of one or two tori onto

²⁵More precisely we can say that Enthalpy – flux = $\mathcal{D}(n, \kappa)(W_s - W)^{n+3/2}$, Mass – Flux = $C(n, \kappa)(W_s - W)^{n+1/2}$, while $\mathcal{L}_x/\mathcal{L} = \mathcal{B}/\mathcal{A}(W_s - W_x)/(\eta c^2)$ stands for the fraction of energy produced inside the flow and not radiated through the surface but swallowed by central **BH**. Efficiency $\eta \equiv \mathcal{L}/\dot{M}c^2$, \mathcal{L} representing the total luminosity, \dot{M} the total accretion rate where, for a stationary flow, $\dot{M} = \dot{M}_x$ (Abramowicz, 1985).

²⁶There is $\mathcal{L}_x = \mathcal{B}(n, \kappa)r_x(W_s - W_x)^{n+2}/\Omega_K(r_x)$, accretion rate for the disk is $\dot{m} = \dot{M}/\dot{M}_{Edd}$, while $\dot{M}_x = \mathcal{A}(n, \kappa)r_x(W_s - W_x)^{n+1}/\Omega_K(r_x)$ (Abramowicz, 1985).

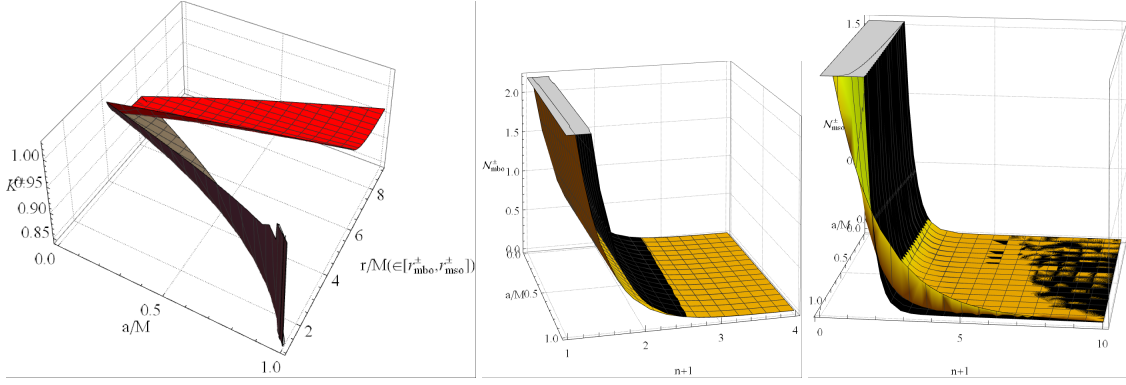


Figure 9: *Left panel*: Parameter $K^\pm \equiv \exp W^\pm$ at the fluid critical specific angular momentum ℓ^\pm for the counterrotating and corotating fluids respectively, as function of $a/M \in [0, 1]$ and the radius $r/M \in [r_{mbo}^\pm, r_{mso}^\pm]$. W^\pm is the Paczynski-Wiita (P-W) potentials. $N_*^\pm \equiv r_* (W_{mbo}^\pm - W_*^\pm)^\kappa (\Omega_K(r_*^\pm))^{-1}$ at $r_* = r_x^\pm$ (*Center panel*) and $r_* = r_{mso}^\pm$ (*Right panel*) as function of a/M and $\kappa = n + 1$, where $\gamma = 1/n + 1$ is the polytropic index, for corotating (yellow surfaces) and for counterrotating (black surfaces) fluids. Ω_K is the Keplerian angular velocity, r_x is the cusp, r_{mbo} is the marginally bounded orbit. The maximum location of inner edge is $r_x \lesssim r_{mso}$. Quantities are evaluated at fixed $\ell_0^+ = -3.99$ and $\ell_1^- = 3.32$ —see also Fig. 8.

the central **BH** and the eventually emerging of tori collisions. Picturing these situations is clearly a risky and complex task.

From observational view point we believe our results may be of significance for the High Energy Astrophysics: these multi-configurations may be at the root of phenomena eventually detectable by the planned X-ray observatory ATHENA, such as the shape of X-ray emission spectra, the X-ray obscuration and absorption by one of the ring, and the extremely energetic radiative phenomena in quasars and **AGNs**. The phenomenology associated with these systems may be very wide. We note that the presence of such structures is capable to substantially modify the single disk scenario, which has been effectively taken so far as the common ground of the High Energy Astrophysics connected with the accretion onto **BHs**. Explanation of some of the most intriguing and unveiled issues of **BH** physics interacting with matter may be reset in this new framework. The single torus paradigm would be then just seen a limit or special case related to an evolutive phase of **BHs** life in their Host. The existence of these objects clearly opens an incredible amount of possibilities to be investigated. As pointed in Pugliese&Stuchlík (2015); Pugliese&Stuchlík (2017b), tori interactions or oscillations can be associated to a variety of phenomena with relevant energy release. The radially oscillating tori of the ringed disk could be related to the high-frequency quasi periodic oscillations observed in non-thermal X-ray emission from compact objects (QPOs), a still obscure feature of the X-ray astronomy related to the inner parts of the disk. The presence of an inner tori may also enter as a new unexpected ingredient in the accretion-jet puzzle, as proposed also in Sochora et al. (2011); Karas&Sochora (2010); Schee&Stuchlík (2009).

There are evidences suggesting what these structures may play a major role in Galaxy dynamics and particularly in **AGNs**. In fact, there are studies in support of the existence of **SMBHs** characterized by multi-accretion episodes during their lifetime in Galaxy cores. Consequently **SMBHs** life may report traces of their host Galaxy dynamics as a diversified feeding of **SMBHs**. These processes may involve for example repeated

galaxy mergers or also interacting binary **BHs**, X-ray binaries or **SMBHs** binary systems. As consequence of these activities, matter around attractor could find an equilibrium configuration as counterrotating and misaligned disks— (Aly et al., 2015; Dogan et al., 2015).

In this analysis we specialize our investigation on sequences of toroidal axi-symmetric (ringed accretion disks) configurations orbiting in the equatorial plane of a central Kerr black hole. From methodological view point, the ringed disks evolutions should arise from the evolution of each torus. Tori in ringed disk may collide and merge, or, eventually the accreting matter from the outer torus of the couple can impact on the inner torus, or the outer torus may be inactive with an active inner torus accreting onto the **BH**, or both tori may be active. Our analysis shows the occurrence of these situations is strictly constrained. We discussed also the emergence of the instability phases for each torus, identifying classes of central Kerr attractors in dependence of their dimensionless spin. Existence and evolution of these structures strongly depends on the black hole dimensionless spin, and the relative rotation of the fluids. This aspect has important implications on the possible observational effects providing a perspective on the phenomena emerging from their dynamics, isolating those situations where actually these configurations may be chased. Finally, the analysis carried out here reduces the range of possibilities in the description of the several possible **RAD** configurations to determination of the $2n$ parameters, where n is the number of tori in the agglomerate, the **RAD** “order”. The (non-constrained) parameters are the fluid specific angular momentum ℓ , and the K -parameter which is related to the torus density and morphology. As explained in Section (5), this parameter is directly connected to some of the main phenomenological aspects might be associated with **RAD**, as the X-ray emission screening and the spacings $\bar{\lambda}$, that would eventually emerge in an emission containing a fingerprint of the **RAD** stratified structure. The K -parameter enters moreover in the evaluation of the **SMBH** accretion rate. Accretion or collision constitute possible scenario

for the entire ringed disk instability. We feature the constraints for the emergence of these situations, foreseen in the occurrence of these disruptive phenomena. These results can then be used in any numerical analysis of more complex situations, sharing the same symmetry of one at last disk to set up the initial data configurations, as it is generally adopted in many GR-HD or GR-MHD dynamical integrations for the single accretion disk case.

Appendix A. Location of the notable radii r_N in the accretion disks: the location of the inner edge of the disk

In this section we provide proof of the some assertions used in Sec. (3) and (4), and a more general discussion of some results.

We address the issue of the location of the notable radii $r_N \equiv \{r_\gamma^\pm, r_{mbo}^\pm, r_{mso}^\pm\}$, defining the geodesic structure of the Kerr spacetime, with respect to the matter distribution $(\circ)_\pm$ with momentum in the range $\mathbf{L}i^\pm$.

This is in fact important particularly in the determination of a possible correlation between the ℓ corotating configurations. We discuss the case of ℓ corotating matter, investigating the inclusion of $r_N^\pm \in (\circ)_\pm$ respectively in Appendix A.1.1 and Appendix A.1.2, and of $r_N^\pm \in (\circ)^\mp$ respectively in Appendix A.2.

It is worth noting here that this investigation actually matches the broader problematic of the location of the inner edge of the disk. Indeed, this investigation will often imply, especially for the inclusion $r_N^\pm \in (\circ)_\pm$, a discussion of the location of these radii with respect to the inner margin of the disk, while the location of the outer edge turns to be important especially for the discussion of the $r_N^\pm \in (\circ)_\mp$ case. This analysis will eventually turn in a set of constraints on the parameters ℓ and K .

We expect that considerations traced here could be applicable also for more general models where the specific angular momentum is not constant along the disk ²⁷.

Appendix A.1. Location of the notable radii $r_N^\pm \in (\circ)_\pm$

In the following, we discuss the location of the marginally bounded orbit $r_{mbo}^\pm \in (\circ)_\pm$ in Appendix A.1.1. Location of the marginally stable orbits $r_{mso}^\pm \in (\circ)_\pm$ is analyzed in Appendix A.1.2, whereas the location of marginally circular orbit $r_\gamma^\pm \in (\circ)_\pm$ is considered in Appendix A.3.

Appendix A.1.1. Location of the marginally bounded orbits r_{mbo}^\pm

We will prove that the marginally bounded orbits r_{mbo}^\pm is *not* included in any disk, for any specific angular momentum in the range $\mathbf{L}i^\pm$, neither in the equilibrium configurations C_i^\pm (with $\ell_i^\pm \in \{\mathbf{L}1^\pm, \mathbf{L}2^\pm, \mathbf{L}3^\pm\}$) or in accretion C_x^\pm (with $\ell_i^\pm \in \mathbf{L}1^\pm$).

There is indeed $r_{mbo}^\pm > r_J^\pm$ for $\ell^\pm \in \mathbf{L}2^\pm$, while for the open cusped configuration O_x with specific angular momentum $\ell = \ell_{mbo}$ we have $K_{mbo} = 1$ and critical point in located in $r_J = r_{mbo}$.

²⁷For example it could be $\ell = \ell(r, \alpha_i)$, where α_i is for a set for parameters, (Lei et al., 2008).

We will assume, for every ℓ , the radial function V_{eff} to be well defined in r_{mbo} and in all the orbital regions considered in this analysis. On the other side, if the effective potential is not well defined in r_{mbo} , as indeed it is in some orbital regions for $\ell \in \mathbf{L}3$, this is sufficient to prove that the marginally bounded orbit can not belong to any configuration regulated by that effective potential.

Appendix A.1.1.1. Configuration C_3^\pm : $\ell_3 \in \mathbf{L}3$.

We start by observing that given a radius \bar{r} located in the orbital range where there is $\partial_{|\ell|} V_{eff}|_{\bar{r}} > 0$ and $V_{eff}^2 > 0$ is well defined then, being $\ell_2 < \ell_3$ for any $\ell_2 \in \mathbf{L}2$ and $\ell_3 \in \mathbf{L}3$, we have $V_{eff}(\ell_3)|_{\bar{r}} > V_{eff}(\ell_2)|_{\bar{r}}$.

But since $\ell_{mbo} = \inf \mathbf{L}2 = \min \mathbf{L}2 \leq \ell_2$, we have $V_{eff}(\ell_3)|_{\bar{r}} > V_{eff}(\ell_{mbo})|_{\bar{r}}$, then $V_{eff}(\ell_3)|_{r_{mbo}} > V_{eff}(\ell_{mbo})|_{r_{mbo}} = 1$, and if ²⁸ $r_{in}^3 = r_{mbo}$ there is $K_3 = 1$ (here in the following we adopt the notation r^i where $i \in \{1, 2, 3\}$ according to the related fluid specific angular momentum ℓ^i respectively).

In fact, it cannot be $r_{in}^3 < r_{mbo}$ and therefore $r_{mbo} \in C_3$, for this to happen, it should be $K_3 > 1$, as the effective potential increases at $r < r_{in}$ without a maximum point.

Therefore we can conclude that:

$$r_{in}^{3\pm} > r_{mbo}^\pm \quad \text{implying} \quad r_{mbo}^\pm \notin C_3^\pm. \quad (\text{A.1})$$

We note that these arguments are quite independent from the corotating or counterrotating nature of the fluid, but depend mainly on the variation range of the momentum magnitude. In fact $\mathbf{L}3$ is the range of higher specific angular momentum magnitude, and one could assume that the distinction in the geodesic structure of the Kerr spacetime between the ℓ counterrotating fluids is higher (as essentially determined by the ratio ℓ/a). However, it should be noted that for $\ell \in \mathbf{L}3$, the centers of the equilibrium disks are placed in a orbital region rather distant from the attractor, namely in $r > \bar{r}_\gamma \gg r_{mso}$, where $\bar{r}_\gamma > r_\gamma : \ell(\bar{r}_\gamma) = \ell_\gamma$, in the region $R = r/a \gg 0$, with the exception of the corotating configurations where, for $a \in [a_M^-, M[$, we find $\bar{r}_\gamma \in [r_M^-, r_{mso}^-[$, see Fig. 6 and discussion in Sec. (3.2).

Appendix A.1.1.2. Configurations C_2^\pm and C_x^\pm : $\ell_2 \in \mathbf{L}2$.

The situation in $\mathbf{L}2$ is as follows: for $\ell_{mbo} = \inf \mathbf{L}2 = \min \mathbf{L}2$ (where $\sup \mathbf{L}2 = \ell_\gamma$), and $r_{mbo} = \sup r_{Max}^2 = \max r_{Max}^2$ (where $\inf r_{Max}^2 = r_\gamma$), similarly to the argumentation for the $(\circ)_3$ configurations, we consider a specific angular momentum $\ell_2 : \ell_{mbo} < \ell_2 \in \mathbf{L}2$, thus $V_{eff}(\ell_2)|_{\bar{r}} > V_{eff}(\ell_{mbo})|_{\bar{r}}$. In particular, $K_2 = V_{eff}(\ell_2)|_{r_{mbo}} > V_{eff}(\ell_{mbo})|_{r_{mbo}} = 1$.

The unstable phase, expected for the equilibrium disks C_2 with specific angular momentum in $\mathbf{L}2$, is the open cusped configuration O_x . If the inner edge r_{in}^2 of the disk C_2 in equilibrium would be r_{mbo} for a $\ell_2 \neq \ell_{mbo}$ then there is $K_2 > 1$ (at $\ell_2 = \ell_{mbo}$

²⁸Note that we are using, along this work, the convention introduced in the end of Sec. (2): in general, the label (i) with $i \in \{1, 2, 3\}$ indicate any quantity \mathbf{Q} relative to the range of specific angular momentum $\mathbf{L}i$ respectively, thus in this case r_{in}^3 is the inner margin of the regular configuration with specific angular momentum $\ell_3 \in \mathbf{L}3$.

the disk is open but this is a special, unstable case). On the other hand, if $r_{mbo} \in C_2$, that is $r_{mbo} < r_{in}^2$, then the following considerations apply: for $\ell_2 \in \mathbf{L2} \exists r_{Max}^2 \in]r_\gamma, r_{mbo}] : K_{Max}^2 \geq 1$ where $r_{mbo} = r_{Max}^2$ only if $\ell_2 = \ell_{mbo}$.

Therefore, at ℓ_2 , r_{Max}^2 being a maximum of the effective potential, the function V_{eff} is increasing in $]r_{Max}^2, r_{mbo}]$ and, being $\ell_2 > \ell_{mbo}$, we have $V_{eff}(\ell_2, r_{mbo}) > V_{eff}(\ell_{mbo}, r_{mbo}) = 1$. As a consequence of this, for the equilibrium closed C_2 disk, there is $K_2 \neq V_{eff}(\ell_2, r_{mbo})$ and as the minimum point is $r_{min}^2 > r_{mso} > r_{mbo}$, then we have $K_2 = V_{eff}(\ell_2, r_{in}) = V_{eff}(\ell_2, r_{out}) < 1$, where $r_{mbo} < r_{in}^2 < r_{min} < r_{out}^2$, and therefore $r_{mbo} < r_{in}^2$.

We finally conclude that

$$\begin{aligned} r_{in}^2 > r_{mbo}^\pm \quad \text{implying} \quad r_{mbo}^\pm \notin C_x^\pm, \quad \text{and} \\ r_J^\pm \leq r_{mbo}^\pm \quad \text{for} \quad O_x^2 \quad \text{thus} \quad r_{mbo}^\pm \in O_x^2. \end{aligned} \quad (\text{A.2})$$

Appendix A.1.1.3. Configurations C_1^\pm and C_x^\pm : $\ell_1 \in \mathbf{L1}$.

For the rings with specific angular momentum $\ell_1 \in \mathbf{L1}$ we will repeat the argument used for the $(O)_2$ configurations.

The unstable configurations for the disks within this data set has topology C_x . Let $\ell_1 \in \mathbf{L1}$, then $\ell_1 < \ell_{mbo} = \sup \mathbf{L1}$. Thus in particular there is $V_{eff}(\ell_1, \bar{r}) < V_{eff}(\ell_{mbo}, \bar{r}) = 1$. In general one could say that $V_{eff}(\ell_1, r_{mbo}) < V_{eff}(\ell_{mbo}, r_{mbo}) = 1$, which does not solve the problem. However as it is $r_{Max}^1 \in]r_{mso}, r_{mbo}]$, then $\partial_r V_{eff} < 0$ for $r \in]r_{Max}^1, r_{mbo}]$. This implies that $r_{mbo} \notin C_x^1$, or $r_{mbo} \notin C_1$.

One can say that since the maximum disk orbital extension occurs for the critical configuration C_x^1 , then it is sufficient to say that for no $\ell_1 \in \mathbf{L1}$ there is $r_{Max}^1 < r_{mbo}$, but $r_{Max}^1 \in [r_{mso}, r_{mbo}]$. Then it follows that r_{mbo} cannot belong to any topology associated to the range $\mathbf{L1}$.

We therefore conclude that

$$\begin{aligned} r_{in}^{1\pm} > r_{mbo}^\pm \quad \text{implying} \quad r_{mbo}^\pm \notin C_1^\pm, \quad \text{and} \\ r_J^\pm \geq r_{mbo}^\pm \quad \text{for} \quad C_x^{1\pm}, \quad \text{thus} \quad r_{mbo}^\pm \notin C_x^{1\pm}. \end{aligned} \quad (\text{A.3})$$

Appendix A.1.2. Location of the marginally stable orbits r_{mso}

An unstable configuration, according to P-W mechanism, must contain the marginally stable orbit, or $r_{mso} \in (O)_x$. Therefore

$$\begin{aligned} r_x^1 > r_{mso} \quad r_{mso} \in C_x^1 \quad \text{for} \quad \ell_1 \in \mathbf{L1}; \quad r_J^2 > r_{mso} \\ r_{mso} \in O_x^2 \quad \text{for} \quad \ell_2 \in \mathbf{L2}. \end{aligned} \quad (\text{A.4})$$

It remains to establish the condition for the marginally stable circular orbit to be contained in a disk of C topology, corresponding to a surface in equilibrium²⁹, considering the specific angular momentum for $\ell \in \mathbf{Li}$.

²⁹In fact, as there is always $r_{min} > r_{mso}$, it is possible to select a value of the K parameter small enough (i.e. $K = K_{mso} + \epsilon_K$ with $\epsilon_K \gtrsim 0$) for $r_{mso} < r_{in}$, and consequently there is $r_{mso} \notin C$. However, if a disk with $\ell \in \{\mathbf{L1}, \mathbf{L2}\}$, admits critical configurations ($r_{Max} < r_{mso}$), then $r_{mso} \in C_x$ or $r_{mso} \in O_x$. The potential function is monotonically decreasing in the region $]r_{Max}, r_{mso}]$, or in a sufficiently narrower left region of the orbit r_{mso} , for specific angular momentum $\ell \in \mathbf{L3}$ where the effective potential admits no maximum. However, this does not ensure that $V_{eff}(r_{mso}) \leq 1$, and therefore this condition does not ensure that the orbit r_{mso} is included in the closed disk. Essentially, this

Appendix A.1.2.1. Configurations C_1^\pm : $\ell_1 \in \mathbf{L1}$.

There is :

$$\forall \ell_1 \in \mathbf{L1} \quad (\text{where} \quad r_{min}^1 > r_{mso} > r_{Max}^1 > r_{mbo}) \quad \text{there is} \\ K_{mso} < V_{eff}(\ell_1, r_{mso}) < V_{eff}(\ell_1, r_{Max}^1) < 1. \quad (\text{A.5})$$

The first inequality of Eq. (A.5) is due to the fact that $\ell_{mso} = \inf \mathbf{L1}$ (and the effective potential is in general an increasing function of the specific angular momentum magnitude (Pugliese&Montani, 2015)). The second inequality is a consequence of the relation $\partial_r V_{eff} < 0$ in $]r_{Max}^1, r_{mso}]$. The third and last inequalities show that, for any $\ell_1 \in \mathbf{L1}$, there is $K_1 = V_{eff}(\ell_1, r_{mso}) < 1 : r_{in}^1 = r_{mso}$, which constitutes the result of this paragraph.

the inner edge of the equilibrium disk C_1 is located on the stable orbit r_{mso} —Fig. A.11. Thus, it is possible to select a set of parameters $K_1 \in]V_{eff}(\ell_1, r_{mso}), K_{Max}[$, for $r_{mso} \in C_1$. This range of parameters increases as the range $r_{Max}^1 - r_{mbo}$ decreases, along with the range $|\ell_{mbo} - \ell_1|$.

We can summarize the situation by saying that:

$$r_{mso}^\pm \in C_1^\pm, \quad r_{mso}^\pm \in !C_x^{1\pm} \quad \forall \ell_1^\pm \in \mathbf{L1}^\pm, \quad (\text{A.6})$$

see also Fig. A.10.

Therefore for Eq. (A.6), the critical configuration must include the marginally stable orbit.

Appendix A.1.2.2. Configurations C_2^\pm : $\ell_2 \in \mathbf{L2}^\pm$.

This case is rather well articulated and enables to analyze deeply a possible correlation between critical ℓ counterrotating sequences of corotating or counterrotating fluids. Firstly, suppose there exists a couple of corotating or counterrotating fluid configurations such that there is a special specific angular momentum $\check{\ell}(a/M) : V_{eff}(\check{\ell}, r_{mso}) = 1$. The exact expression of $\check{\ell}(a/M)$ can be easily found as a solution of a quadratic equation for the variable ℓ — see also Figs A.10, A.12.

We analyze below the different situations for corotating and counterrotating disks decreases.

(1) The corotating disk C_2^-

There is a wide class of rotating attractors defined as

$$\begin{aligned} \check{\mathbf{A}}_< \quad \text{at} \quad a/M \in [0, \check{a}[\quad \text{where} \\ \check{a} \equiv 0.969174M : \check{\ell}_- = r_\gamma^-, \end{aligned}$$

which includes the limiting static case $a = 0$ of the Schwarzschild solution, where $\check{\ell}_- \in \mathbf{L2}^-$. Accordingly, we consider the following two ranges of values of the specific angular momentum

$$\mathbf{I} \quad \ell_2^- \in]\check{\ell}_-, \ell_\gamma^-[\quad \text{when} \quad r_{in}^2 > r_{mso}^- \quad \text{and} \quad (\text{A.7})$$

$$\mathbf{II} \quad \ell_2^- \in]\ell_{mbo}^-, \check{\ell}_-[, \quad (\text{A.8})$$

condition depends on the specific angular momentum and also on the location of r_{mbo} . Moreover, in some cases for $\ell \in \mathbf{L3}$, it is necessary to assess whether the effective potential is actually well defined.

–see Fig. A.10. We analyze the configurations in the two ranges of angular momentum in the following.

I For specific angular momentum sufficiently high, i.e. $\ell_2^- \in]\check{\ell}_-, \ell_\gamma^-[$, when $r_{in}^{2-} > r_{mso}^-$, the disk in equilibrium can never contain the marginally stable orbit or $r_{mso}^- \notin C_2^-$.

II For the configurations with lower specific angular momentum, i.e. $\ell_2^- \in [\ell_{mbo}^-, \check{\ell}_-]$ for $V_{eff}(\ell_2^-, r_{mso}^-) < 1$, it is possible to select, for the equilibrium C_2^- disk, a K_2^- : $r_{in}^{2-} = r_{mso}^-$ or $r_{in}^{2-} < r_{mso}^-$, and therefore $r_{mso}^- \in C_2^-$, being located in the region with extremes $(r_{in}^{2-}, r_{min}^{2-})$ – see Figs A.10. However, in the case

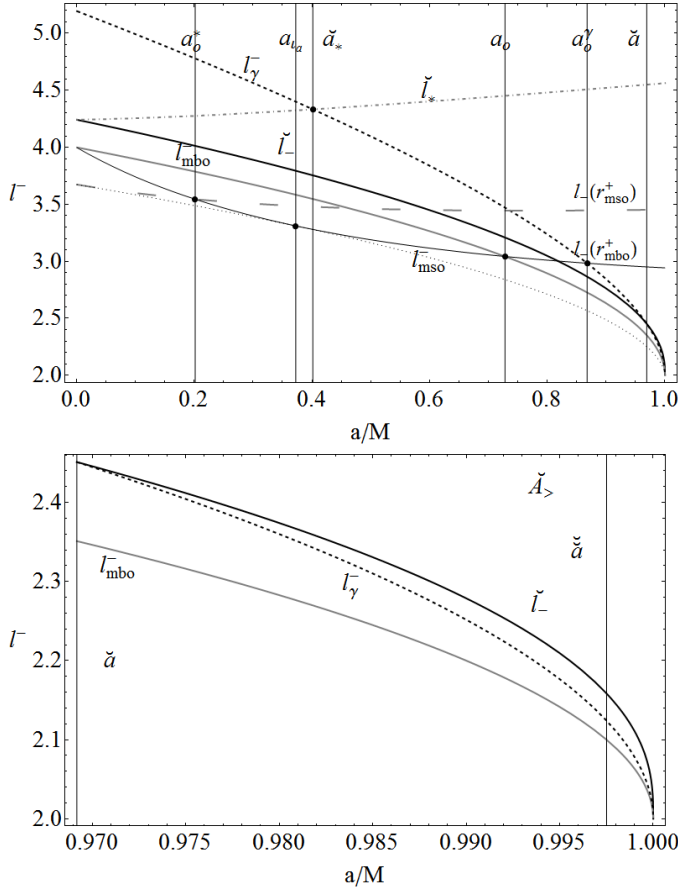


Figure A.10: Corotating fluids: specific angular momentum $\ell_{mbo}^- \equiv \ell^-(r_{mbo}^-)$, r_{mbo}^- , is for the marginally bounded orbit, $\ell_{mso}^- \equiv \ell^-(r_{mso}^-)$ where r_{mso}^- is the marginally stable orbit, $\ell_\gamma^- \equiv \ell^-(r_\gamma^-)$ and r_γ^- is the marginally circular orbit (photon orbit). The angular momentum $\ell^-(r_{mso}^+)$ and $\ell^-(r_{mbo}^+)$, $\check{\ell}_-(a/M)$: $V_{eff}(\check{\ell}_-, r_{mso}^-) = 1$ and $\check{\ell}_* : V_{eff}(\check{\ell}_*, r_{mso}^+) = 1$ are also plotted–see also Fig. A.11. The spins $\{a_o^*, a_{la}, \check{a}_*, a_o, a_o^\gamma, \check{a}, \check{a}\}$ are plotted with black vertical lines, where $\check{a} = 0.997508M$ –see Eq. (A.22). Upper panel shows the range of spin $a \in [0, M]$. Bottom panel shows details of the class of attractors $\check{A}_>$, as defined in Eq. (A.9).

I, in an evolutive scheme where there is a possible time evolution of the disk morphology and topology, the increase of the K_- parameter, with specific angular momentum in $\mathbf{L2}^-$, does not necessarily correspond to a final stage of P-W instability with O_x^{2-} topology, but it will pass through the O_{in}^{2-} phase and then a situation similar to the case with specific angular momentum in $\mathbf{L3}^-$ occurs. Although, increasing K_- , the disk will

finally reach the O_x topology, passing through r_{mso} in O_{in} . In fact, increasing K_2^- for $\ell_2^- \in]\check{\ell}_-, \ell_\gamma^-[$, the sequence of configurations on Σ_K will be $\mathcal{B}_{\ell_2^-}^{2-}|_{\mathbf{II}} = \{C_2^-, O_{in}^{2-}, O_x^{2-}\}$ see Fig. A.11-Upper. We note that the only way to make r_{mso} a P-W point, inducing therefore a gravo-hydrostatic instability in the disk, is to reach $\ell = \ell_{mso}$ where r_{mso} is a cusp point (Pugliese&Montani, 2015). Consider now the lower values of specific angular momentum:

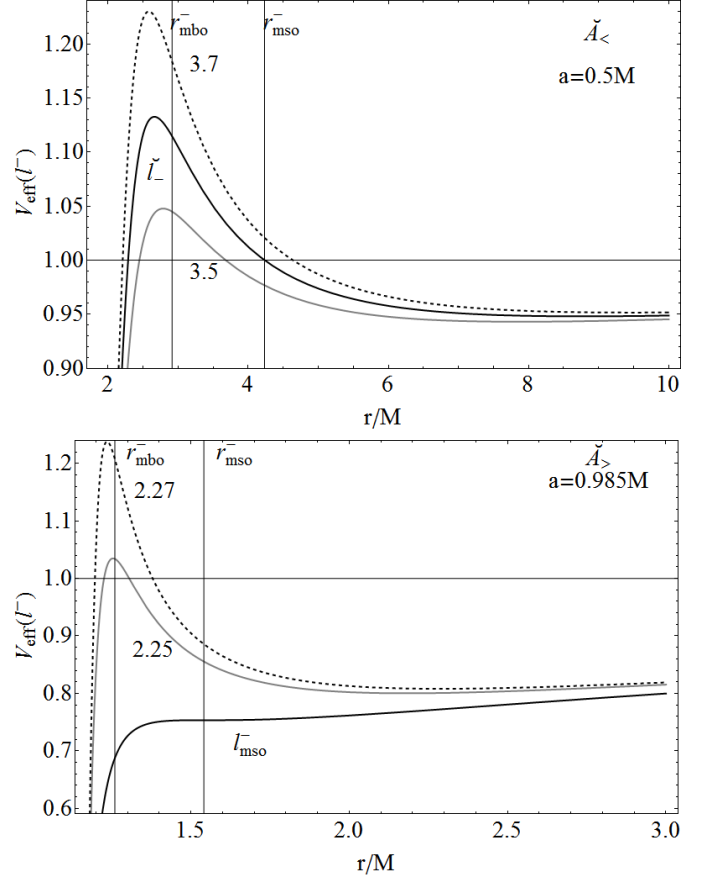


Figure A.11: Corotating fluids C_2^- . Upper panel: For spacetime spin $a = 0.5M \in \check{A}_<$, the outer horizon is $r_+ = 1.86603M$ and $\check{\ell}_- = 3.61088$ and $\ell_\gamma^- = 3.41421$ with $\ell_{mbo}^- = 4.09627$. Bottom panel: For spacetime spin $a = 0.985M \in \check{A}_>$, the outer horizon is $r_+ = 2.16614M$, $\check{\ell}_- = 2.33082$ and $\ell_{mbo}^- = 2.24495$ with $\ell_\gamma^- = 2.3102$.

$\ell_2^- \in]\ell_{mbo}^-, \check{\ell}_-]$. In order to reach an instability of the disk, if it does not include r_{mso} for its density, it is not sufficient to provide a proper elongation, and it has to pass through the point r_{mso} maintaining its equilibrium topology. Then it will include in any case a stage where it acquires an open, not cusped O_{in}^{2-} topology, as discussed for the case of the marginally bounded orbit in Appendix A.1.1.

There is indeed $r_{Max}^{2-} < r_{mbo}^- < r_{mso}^-$, therefore, the sequence of configurations on different Σ_K will be $\mathcal{B}_{\ell_2^-}^{2-}|_{\mathbf{II}} = \mathcal{B}_{\ell_2^-}^{2-}|_{\mathbf{I}} = \{C_2^-, O_{in}^{2-}, O_x^{2-}\}$. Thus, the configuration O_x^{2-} cannot emerge as “direct” consequence of the accretion in an evolutionary model (by increasing K). The correlation in $\mathbf{L2}^-$ can occur only from C_2^- and O_x^{2-} , and the matter cannot pass through a continuum evolution in $\mathbf{L2}^-$. We specify better this statement in the follow-

ing, making reference to the sequence of the effective potentials in Fig. A.11.

First, with $\ell_2^- = \text{constant}$ in $\mathbf{L2}^-|_{\mathbf{I}}$ or $\mathbf{L2}^-|_{\mathbf{II}}$, the disk starting from a regular topology C_2^- cannot reach the P-W point configuration O_x^2 , so far as it passes through O_{in}^2 . Therefore, in order to get a transition (through the surfaces Σ_i) from C_2^- to O_x^2 , it is necessary to change $\ell_2^- \in \mathbf{L2}^-$ only, or also change the K_- parameter. But it is immediate to see that, starting from a closed topology, it is not possible to reach such a transition, and, on the other side, an initial phase of O_{in}^2 has no meaning here. Therefore, the specific angular momentum $\ell_2^- \in \mathbf{L2}^-$ has to be changed together with K_- shift from $\mathbf{K0}$ to $\mathbf{K1}$. However, such a transition, with $\ell^- \in \mathbf{L2}^-$ and $K : \mathbf{K0}^- \rightarrow \mathbf{K1}^-$, has to be continuous and the only possible solution is the one where the final state is $\ell_2^- = \inf \mathbf{L2}^- = \ell_{mbo}^2$, $K = 1$ and $r_{Max}^2 = r_{mbo}^-$.

The only possible evolution in this scheme, starting from a configuration in equilibrium with $\ell \in \mathbf{L2}^-$, is the one leading, for a decrease of the specific angular momentum and the concomitant increase of K_- , to the final configuration with cusp in r_{mbo}^- . Finally, concerning the correlation between the two configurations, O_x^2 and C_2^- , the considerations outlined in Sec. (3) for the (C-J) ℓ corotating systems apply and in particular Eq. (17).

We close this discussion noting that for $\ell^- = \check{\ell}_-$ we have $V_{eff}(\check{\ell}_-, r_{mso}^-) = 1$. For $K_- = V_{eff}(\check{\ell}_-, r_{mso}^-)$, this cannot give rise to a P-W point, but it should correspond to an O_{in}^- surface, see Fig. A.11-bottom.

Then for fast attractors, i.e.,

$$\check{\mathbf{A}}_> \quad \text{at } a/M \in]\check{a}, 1], \quad (\text{A.9})$$

which include the extreme Kerr spacetime ($a = M$), the situation is different with respect to the geometries of $\check{\mathbf{A}}_<$, defined in Eq. (A.7), as $\check{\ell}_- > \ell_\gamma^-$ —Fig. A.10. Then $V_{eff}(\check{\ell}_-, r_{mso}^-) < 1$, providing a situation analogous to the case of slower attractors $\check{\mathbf{A}}_<$, with slow specific angular momentum $\ell_2^- \in]\ell_{mbo}^-, \check{\ell}_-]$.

We summarize the situation as follows:

$$\text{for } a \in \check{\mathbf{A}}_< \equiv [0, \check{a}[\quad \text{at } \mathbf{I} \quad \ell_2^- \in]\check{\ell}_-, \ell_\gamma^-[\quad (\text{A.10})$$

$$\text{when } r_{in}^2 > r_{mso}^- \quad r_{mso}^- \notin C_2^- \quad r_{mso}^- \in]O_x^2- \quad (\text{A.11})$$

$$\text{at } \mathbf{II} \quad \ell_2^- \in]\ell_{mbo}^-, \check{\ell}_- [\quad r_{mso}^- \in C_2^- \quad r_{mso}^- \in]O_x^2- \quad (\text{A.12})$$

$$\text{for } a \in \check{\mathbf{A}}_> \equiv]\check{a}, M], \quad r_{mso}^- \in C_2^- \quad r_{mso}^- \in]O_x^2-. \quad (\text{A.12})$$

(2) The counterrotating disk C_2^+

Figure A.12 sketches the situation for the counterrotating fluids:

$$C_2^+ : \quad \text{for any attractors } -\check{\ell}_+ \in] -\ell_{mbo}^+, -\ell_\gamma^+[, \quad (\text{A.13})$$

therefore:

$$C_2^+ : \quad r_{mso}^+ \in]O_x^2+; \quad \text{and } r_{mso}^+ \in C_2^+ \quad \text{for } -\ell_2^+ \in] -\ell_{mbo}^+, -\check{\ell}_+[, \quad (\text{A.14})$$

$$r_{mso}^+ \notin C_2^+ \quad \text{for } -\ell_2^+ \in] -\check{\ell}_+, -\ell_\gamma^+ [. \quad (\text{A.15})$$

The situation is similar to the corotating fluids orbiting $\check{\mathbf{A}}_<$ attractors—Fig. A.10-Upper.

For specific angular momentum sufficiently low in magnitude, there always exists a region, where the equilibrium disks C_2^+ contain the marginally stable circular orbit r_{mso}^+ . While for higher specific angular momentum, i.e. $-\ell_2^+ > -\check{\ell}_+ \in \mathbf{L2}^+$, the disk cannot include the radius r_{mso}^+ ; see also discussion in Sec. (3.4) and in particular Eq. (17).

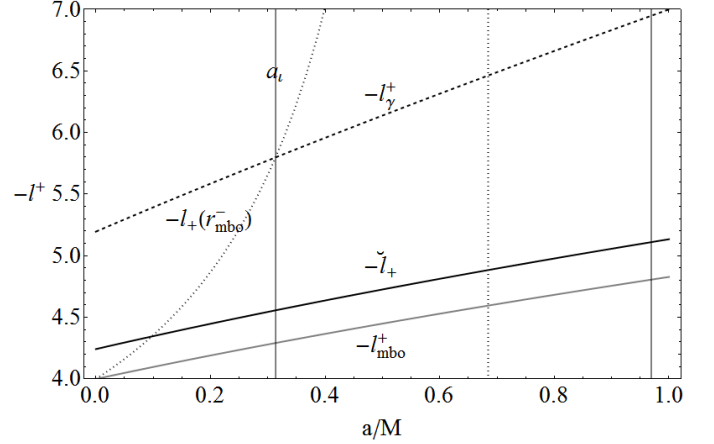


Figure A.12: Counterrotating fluids: the specific angular momentum ℓ_γ^+ and ℓ_{mbo}^+ , boundaries of $\mathbf{L2}^+$, as function of the dimensionless spin a/M . The specific angular momentum $\check{\ell}_+ : V_{eff}(\check{\ell}_+, r_{mso}^+) = 1$. The spin $a_i = 0.3137M$ is also signed where $r_{mbo}^- = r_\gamma^+$ and then $\ell_\gamma^+ = \ell^+(r_{mbo}^-)$.

(3) Comments on the C_2^\pm disks

We can compare the cases of corotating C_2^- disks and counterrotating C_2^+ disks through Figs A.10, A.12.

For the analysis of the corotating disks we refer to Figs A.10 and A.11. First, while the situation for the counterrotating disks is uniform for attractors $a \in [0, M]$ —Fig. A.12, for the corotating disks it was necessary to distinguish between the two classes of attractors $\check{\mathbf{A}}_\leq$.

For the inclusion $r_{mso}^- \in C_2^-$ to be satisfied, the ratio ℓ^-/a has to be sufficiently low. In fact, at high spin, $a \in \check{\mathbf{A}}_>$, the situation is similar to $\mathbf{L1}^-$, and the equilibrium disks C_2^- can always contain r_{mso}^- .

In order to simplify the presentation of the results, we denote here by \mathbf{Q}_\in any quantity \mathbf{Q} which satisfies the inclusion relation, and, respectively, by \mathbf{Q}_\notin any quantity where the inclusion relation is not satisfied; $\Delta\mathbf{Q}$ is the measure of the maximum range of variation for the quantity \mathbf{Q} , thus:

$$C_2^- : \quad \ell_\notin^2 > \ell_\in^2, \quad \Delta\ell_\notin^2 > \Delta\ell_\in^2 \quad \text{for } a \lesssim 0.8M, \\ \Delta\ell_\notin^2 = 0 \quad \text{for } a = \check{a}, \quad \nexists \Delta\ell_\notin^2 \quad \text{for } a \in \check{\mathbf{A}}_> \quad \partial_a \mathbf{Q}_2^- < 0, \\ \text{for } \mathbf{Q}_2^- \in \{\ell_\in^2, \ell_\notin^2, \Delta\ell_\in^2, \Delta\ell_\notin^2, (\Delta\ell_\in^2 - \Delta\ell_\notin^2)\}, \quad (\text{A.16})$$

—see Fig. A.10. For the counterrotating disk C_2^+ , the situation is just reversed:

$$C_2^+ : \quad \ell_\notin^2 > \ell_\in^2, \quad \Delta\ell_\notin^2 > \Delta\ell_\in^2, \quad \partial_a \mathbf{Q}_2^+ > 0, \\ \text{for } \mathbf{Q}_2^+ \in \{\ell_\in^2, \ell_\notin^2, \Delta\ell_\in^2, \Delta\ell_\notin^2, (\Delta\ell_\in^2 - \Delta\ell_\notin^2)\}, \quad (\text{A.17})$$

see Fig. A.12.

However we can still say, that a high value of the ratio $|\ell_+^2|/a$ acts to disadvantage the cases where r_{mso} is included in the equilibrium disks (see also Pugliese&Montani (2015) for the analysis of the disk equilibrium in terms of the rationalized momentum).

Reminding the relation between the specific angular momentum and the position of the pressure maximum points, we may say in general that disks $C_{\epsilon^\pm}^{2\pm}$, including r_{mso}^\pm , are localized in a narrow region of the specific angular momentum values and orbital range. The disks $C_{\epsilon^-}^{2-}$ approach the attractor by increasing the spin of the black hole, while $C_{\epsilon^+}^{2+}$ moves away for increasing a/M .

There are several differences in the ℓ counterrotating couples of equilibrium disks $C_{\epsilon^\pm}^{2\pm}$. The counterrotating disk $C_{\epsilon^-}^{2-}$ demonstrates behavior, related to the spin, that is very similar to $C_{\epsilon^+}^{2+}$. However, the elongation of the disks $C_{\epsilon^+}^{2+}$ can be lower in general than those of $C_{\epsilon^-}^{2-}$, as the configuration density is characterized by lower specific angular momentum available, and specific angular range—see Fig. A.12. The corotating case $C_{\epsilon^-}^{2-}$ presents an articulated morphological characteristic, different for different classes of attractors. For attractors $\check{A}_{<}$, the trend with the spin-mass ratio is similar to $C_{\epsilon^-}^{2-}$. However, for $a < 0.8M$, the extension and the spacing (or conversely the configuration density) of the $C_{\epsilon^-}^{2-}$ disks is greater than of the $C_{\epsilon^+}^{2+}$ disks.

The situation is reversed for higher spin, until at $a \in \check{A}_{>}$ the formation of a $C_{\epsilon^-}^{2-}$ disk is impossible (it is not possible to find $K_2^\pm : r_{mso}^\pm \in C_{\epsilon^\pm}^{2\pm}$). In fact, if it is always possible to find a set of parameters $K_2^\pm : r_{mso}^\pm \in C_{\epsilon^\pm}^{2\pm}$, and indeed the equilibrium disks $C_{\epsilon^\pm}^{2\pm}$ must contain r_{mso}^\pm , as they extend towards the maximum elongation at instability λ_x . On the other side, the extension of the regions $\Delta\ell_{\epsilon^\pm}^{2\pm}$ increases or decreases with the spin more slowly than $\Delta\ell_{\epsilon^\pm}^{2\pm}$. Thus one could say that the morphological characteristics of the $C_{\epsilon^\pm}^{2\pm}$ case are less affected by a change of the spin than those of the $C_{\epsilon^\pm}^{2\pm}$ case.

Appendix A.1.2.3. Configurations $C_3^\pm : \ell_3 \in \mathbf{L3}$.

For the investigation of this case, we will refer to equations (A.7,A.9) and Figs A.10,A.12. There are no critical configurations for fluids at specific angular momentum $\ell_3 \in \mathbf{L3}$. Following arguments similar to those discussed in the previous cases, one can see that for the corotating case, there are no solutions of the problem $\check{\ell}(a/M) \in \mathbf{L3}^- : V_{eff}(\check{\ell}, r_{mso}) = 1$.

Firstly, Figs A.10,A.12 confirm the results for $\ell_1^\pm \in \mathbf{L1}^\pm$.

As proved earlier, it is always possible to find a proper K_1^\pm for the closed configurations in equilibrium C_1^\pm , containing respectively r_{mso}^\pm . In other words, the disk with a specific angular momentum in $\ell_1 \in \mathbf{L1}$, containing the marginally stable orbit, must be in equilibrium, and in order to accrete into the black hole, it must extend far beyond the marginally stable orbit.

Similarly, Figs A.10,A.12 provide an immediate description of the situation for the equilibrium disks C_3^\pm with $\ell_3^\pm \in \mathbf{L3}^\pm$. We detail the results as follows:

(1) The corotating disk C_3^-

Analogously to the fluid configurations with specific angular momentum $\ell_2 \in \mathbf{L2}$, it will be convenient to consider first the corotating case, as illustrated in Fig. A.10.

Equations (A.7, A.7,A.9) hold. Therefore we still need to distinguish the situation for the two classes of attractors \check{A}_{\leq} .

For slow attractors, $\check{A}_{<} : a \in [0, \check{a}]$, we have $\check{\ell}_- \in]\ell_{mso}^-, \ell_\gamma^-]$, this implies:

$$\text{for } a \in \check{A}_{<} \text{ there is } V_{eff}(\ell_3^-, r_{mso}^-) \not\leq 1 \quad (\text{A.18})$$

$$\text{and } r_{mso}^- \notin C_3^-.$$

However, concerning the first inequality of Eq. (A.18), we should consider that the function $V_{eff}(\ell_3^-, r)$ may not be well defined in r_{mso}^- . As mentioned at the beginning of this section, if the potential function is not defined in a point \bar{r} , this constitutes here evidence of the fact that the disk cannot exist at \bar{r} , and therefore Eq. (A.18) is then sufficient to prove that if the effective potential is well defined in r_{mso}^- , then it is not contained in the equilibrium disk³⁰.

The situation is different for the geometries of faster attractors, $\check{A}_{>} \in]\check{a}, M]$, where

$$\text{for } a \in \check{A}_{>} \text{ there is } r_{mso}^- > r_\gamma^-, \quad (\text{A.19})$$

$$\exists K_3^- < V_{eff}(\check{\ell}_3^-, r_{mso}^-) = 1 : r_{mso}^- \in C_3^-$$

and K_3^- will be clearly bounded from below by $V_{eff}(\ell_\gamma^-, \bar{r})$, where $\bar{r} > r_{mso}^-$, corresponding to the condition $\ell_3^- \in \mathbf{L3}^-$. The similarities with the $\mathbf{L2}$ case are evidently in the differentiation between the two classes of attractors \check{A}_{\leq} , but the situation is very different with respect to the role of the specific angular momentum. The case of very fast attractors, seen in Fig. A.11, is particularly interesting. We will analyze deeply the morphology of these regions for the case of the $\check{A}_{>}$ attractors later, comparing them with the counterrotating case.

(2) The counterrotating disk C_3^+

The situation for the counterrotating disks at $\ell_3^+ \in \mathbf{L3}^+$ is illustrated in Fig. A.12.

As Eq. (A.13) holds, then

$$r_{mso}^+ \notin C_3^+. \quad (\text{A.20})$$

Therefore the equilibrium counterrotating disks C_3^+ cannot contain the marginally stable circular orbit, and the disks are entirely contained in an outer orbital region $r > r_{mso}^+$. This situation is indeed similar to the corotating disks orbiting the slower attractors $\check{A}_{<}$.

(3) Comments on the C_3^\pm disks

In conclusion, for specific angular momentum $\ell_3 \in \mathbf{L3}$ only a special class of rotating equilibrium disks, namely C_3^- , orbiting very fast attractors, may contain the marginally stable orbit. The morphology of the range of specific angular momenta for these fluids, is very special. The more relevant aspect probably is that the $\Delta\ell_{\epsilon^-}^{3-}$ region is vanishing at its extremes, i.e., the region $\Delta\ell_{\epsilon^-}^{3-}$ of specific angular momentum ℓ_3^- , whose measure is the distance $(\ell_\gamma^- - \check{\ell}_-)$, has a minimum, with vanishing extension,

³⁰The conditions for which the function $V_\ell(\ell_3, r)$ is not well-defined could be easily provided.

for the two special geometries $a = \check{a}$ and $a = M$ – Figs A.13. The absolute maximum of this region occurs for the geometry associated with spin $\check{a} = 0.997508M$.

Analogously to Eqs (A.16,A.17), we can summarize the situation for the C_3^\pm cases as follows:

$$C_3^- : \quad \begin{aligned} & \text{for } \check{\mathbf{A}}_< \quad r_{mso}^- \notin C_3^-, \\ & \text{for } \check{\mathbf{A}}_> \quad r_{mso}^- \in C_3^-; \quad \inf \Delta \ell_\epsilon^{3-} = 0 \\ & \text{for } a = \{\check{a}, M\}, \end{aligned} \quad (\text{A.21})$$

$$\begin{aligned} \max \Delta \ell_\epsilon^{3-} = 0 & \quad \text{for } a = \check{a} \in]\check{a}, M[. \\ \partial_a \ell_\epsilon^{3-} < 0, \partial_a \Delta \ell_\epsilon^{3-} \geq 0 & \quad \text{for } a \leq \check{a}, \end{aligned} \quad (\text{A.22})$$

$$C_3^+ : \quad r_{mso}^+ \notin C_3^+. \quad (\text{A.23})$$

Possibly the region of specific angular momentum $\Delta \ell_\epsilon^{3-}$, and

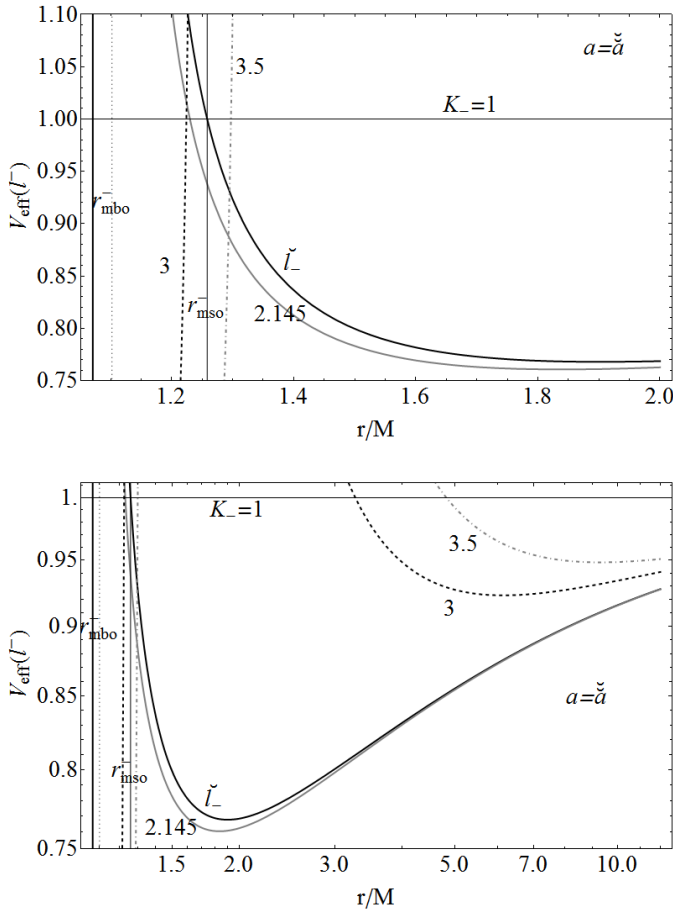


Figure A.13: Corotating fluids C_3^- in a geometry with spin-mass ratio $\check{a} = 0.997508M \in \check{\mathbf{A}}_<$, the outer horizon is $r_+ = 1.07055M$, $\check{\ell}_- = 2.15829$ and $\ell_\gamma^- = 2.12395$ with $r_{mbo}^- = 2.09984$, see also Fig. A.12. The plots show the effective potential $V_{eff}(\ell^-)$ versus r/M , at different specific angular momenta, signed on the curves: the black thick curve is for $\ell^- = \check{\ell}_-$. Upper panel: orbital range $r \in [r_+, r_\epsilon^+]$ where $r_\epsilon^+ = 2M$ is the static limit on the equatorial plane. Bottom panel: orbital range $r > r_\epsilon^+$. Curves $\ln V_{eff}$ against $\ln r/M$, but the labels on the axes indicate the original values of V_{eff} and r/M .

the corresponding orbital region, is infinite extending up to the regions where the Newtonian limit can be considered.

Appendix A.2. Location of the notable radii $r_N^\pm \in ()_\mp$

In this section we examine the location of the radii $r_N^\pm \in ()_\mp$ with respect to the *closed* (cusped or regular) sub-configurations $()_\mp$ respectively. This issue is relevant for example for the analysis of the mixed ℓ counterrotating sub-sequences of a decomposition. As a consequence of this analysis we will distinguish different classes of attractors, deriving conditions on the parameters of the macro-configuration. First, we provide several orbital constraints which locate more precisely the inner and the outer edge of the ring of a decomposition. Then we clarify the possible interaction between two ℓ counterrotating sub-configurations through the geometrical correlation.

In the following discussion, we use the arguments and results of Appendix A.1 and we proceed in analogy to the investigation of the $r_N^\pm \in ()_\pm$ problem.

In Appendix A.2.1 we consider the counterrotating configurations, studying the problem $r_N^- \in ()_+$, while Appendix A.2.2 focuses on the corotating disks, investigating the problem $r_N^+ \in ()_-$. The location of photon circular orbits r_γ^\pm is investigated in Appendix A.3.

Appendix A.2.1. Counterrotating disks: $r_N^- \in ()_+$

Appendix A.2.1.1. Marginally bounded orbit $r_{mbo}^- \in ()_+$

In general, the following propriety holds: as $r_{mbo}^- < r_{mbo}^+$ in any geometry, then, if $r_{mbo}^+ \notin ()_+$, it follows that $r_{mbo}^- \notin ()_+$.

Therefore, as Eq. (A.1) stands, we have

$$r_{mbo}^- \notin C_3^+. \quad (\text{A.24})$$

We remind then that the C_3 configurations do not allow critical topologies with $\ell \in \mathbf{L3}$.

Similarly, for an accretion configuration in $\mathbf{L2}^+$, Eq. (A.2) holds. It follows $r_{mbo}^- \notin C_2^+$. Regarding the location of r_{mbo}^- with respect to the open counterrotating configuration O_x^+ , we should consider two different classes of attractors. In fact, the general considerations introduced at the beginning of this section apply strictly only for a closed (cusped or regular) topology while for the open topologies O_x , we need to consider the geometries where $r_{mbo}^- \in \Delta r_J^+$, i.e. $a \in \mathbf{A}_l^< \equiv [0, a_l[$, and the geometries with $a \in \mathbf{A}_l^> \equiv]a_l, M]$, where $r_{mbo}^- < r_J^+$.

Then we could summarize the results as follows:

$$\begin{aligned} r_{mbo}^- \notin C_2^+, \quad \text{and we have } r_{mbo}^- \in O_x^{2+} (r_{mbo}^- > r_J^{2+}) \\ \text{only if } a < a_l \quad \text{for } -\ell^+(r_{mbo}^-) \in [-\ell_{mbo}^+, -\ell^+(r_{mbo}^-)]. \end{aligned} \quad (\text{A.25})$$

We specify that for the slower attractors, $a \in [0, a_l[$, also the configurations with $r_{mbo}^- \in O_x^{2+}$ are possible, while such a situation is forbidden in the spacetimes of the faster attractors. Accordingly, the notation \in (not $\in!$) has been used in Eq. (A.25). This is because for $a < a_l$, there is $r_{mbo}^- > r_J^+$, and the open surfaces can include the marginally bounded orbit r_{mbo}^- , i.e. $r_J^+ < r_{mbo}^-$, or not include r_{mbo}^- , i.e. $r_J^+ > r_{mbo}^-$. This distinction clearly depends on the specific angular momentum, and one should analyze the condition for which $-\ell_2^+ \in$

$[-\ell^+(r_{mbo}^-), -\ell_\gamma^+]$ where, for $\ell = -\ell^+(r_{mbo}^-)$, the launch point³¹ is exactly $r_J^{2+} = r_{mbo}^-$, as pictured in Fig. A.12, which also confirms that $-\ell^+(r_{mbo}^-) \in [-\ell_{mbo}^+, -\ell^+(r_{mbo}^-)]$ for $a < a_t$.

In the geometry with $a = a_t$, introduced in Sec. (3), there is $r_\gamma^+ = r_{mbo}^-$, and then it follows that this case represents a limit, defining the γ -surface O_x^+ , that can be never reachable also for the C_2^+ configurations (alternatively one can see this fact also as a consequence of the first inequality in Eq. (A.2)).

The situation for C_1^+ can be described using Eq. (A.3), and we obtain

$$r_{mbo}^- \notin C_1^+ \quad \text{and} \quad r_{mbo}^- \notin C_x^{1+}. \quad (\text{A.26})$$

Appendix A.2.1.2. Marginally stable orbit $r_{mso}^- \in (0)_+$.

We focus now on the location of the marginally stable orbit: $r_{mso}^- \in (0)_+$.

Using arguments similar to those used to locate the marginally bounded orbit, we note that since $r_{mso}^+ > r_{mso}^-$ in any Kerr geometry, it follows that $r_{mso}^- \notin (0)^+$, if $r_{mso}^+ \notin (0)^+$ (in this case $r_{in}^+ > r_{mso}^+$). Therefore, we first concentrate our analysis on the cases where $r_{mso}^+ \in (0)^+$.

In fact, the critical topologies $(0)_x^+$ are good candidates for counterrotating configurations including the orbit r_{mso}^- , as these rings always contain the marginally stable orbit r_{mso}^+ —see Eq. (A.4).

However, we point out that the inclusion $r_{mso}^+ \in (0)^+$ is a necessary but not sufficient condition for the inclusion of r_{mso}^- in the disks $(0)^+$, as the investigation of $r_{mso}^+ \notin (0)^+$ provides a condition to rule out a series of situation where r_{mso}^- is certainly not included in $(0)^+$.

Appendix A.2.1.3. On the configurations C_1^+ and C_x^{1+} .

Consider first the configurations $(0)_1^+$. Then, as Eq. (A.6) holds (which is necessary condition for $r_{mso}^- \in (0)_1^+$), one has to distinguish the following two classes of geometries:

$$\begin{aligned} \mathbf{A}_{a_t}^> : a > a_{t_a} \quad (r_{mso}^- < r_{mbo}^+), \quad \text{and} \quad (\text{A.27}) \\ \mathbf{A}_{a_t}^< : a < a_{t_a} \quad (r_{mso}^- > r_{mbo}^+), \quad \text{where} \\ a_{t_a} \equiv 0.372583M. \end{aligned}$$

In fact, we consider only configurations where $r_{mso}^+ \in (0)_1^+$, ensured by Eq. (A.6).

Because of Eq. (A.3), the inner edge of the C_x^{1+} disk is $r_{in}^{1+} \in \Delta r_x^+ \equiv]r_{mbo}^+, r_{mso}^+[$ (we exclude the case where $r_{in}^{1+} = r_{mso}^+$). Then, from Eq. (A.26), for the disk C_1^+ , there is $r_{in}^{1+} \in \Delta r_x^+ \cap [r_{mso}^+, r_{min}^{1+}[$.

If $r_{mso}^- < r_{mbo}^+$, this implies $r_{mso}^- \notin C_1^+$ and $r_{mso}^- \notin C_x^{1+}$, and this occurs for sufficiently fast attractors $\mathbf{A}_{a_t}^>$ —Eq. (A.27). Therefore, we will consider only these lower attractors $\mathbf{A}_{a_t}^<$.

Note that these attractor spins also include the spin a_t : in these geometries, where $r_{mso}^- \in \Delta r_x^+$, one can always find a $K_1^+ : r_{mso}^- \in C_x^{1+}$, or also $K_1^+ : r_{mso}^- \in C_1^+$, for sufficiently

high magnitude of the specific angular momentum (we recall that $\lambda_x^\pm = \sup \lambda^\pm$ and $\Lambda_x^\pm \supset \Lambda^\pm$).

It can be important in some circumstances to fix the topology of the counterrotating (outer) configuration $(0)_1^+$ of a couple, especially if one assumes that a possible gravo-hydrostatic instability may lead to destabilization on the inner (corotating) configuration, as considered for example in Secs (3,4).

The situation where $r_{mso}^- \in C_x^+$ is ensured by the condition on the specific angular momentum $-\ell_1^+ \in [-\ell_1^+(r_{mso}^-), \ell_{mbo}^+ [\subset \mathbf{L1}^+$. In fact, if $\ell_1^+ = \ell_1^+(r_{mso}^-)$, then $r_{Max}^{1+} = r_{mso}^-$. The limiting values $\ell_1^+(r_{mso}^-) \in \mathbf{L1}^+$ vary with the spin, see Figs 5,4.

For $K_1^+ = K_{Max}^{1+}$, there is $r_{in}^{1+} = r_{Max}^{1+} = r_{mso}^- = r_x^+$, thus with increasing $|\ell_1^+|$ the maximum point r_{Max}^{1+} decreases³² and there is $r_{Max}^{1+} < r_{mso}^-$.

In conclusion:

$$\mathbf{A}_{a_t}^> : a > a_{t_a} : r_{mso}^- \notin C_1^+ \quad \text{and} \quad r_{mso}^- \notin C_x^{1+}, \quad (\text{A.28})$$

$$\mathbf{A}_{a_t}^< : a < a_{t_a} : -\ell_1^+ \in]-\ell_{mso}^+, -\ell_1^+(r_{mso}^-)[,$$

$$r_{mso}^- \notin C_x^{1+}, \quad r_{mso}^- \notin C_1^+, \quad (\text{A.29})$$

$$\ell_1^+ = \ell_1^+(r_{mso}^-), \quad r_{in}^{1+} = r_{Max}^{1+} = r_{mso}^- = r_x^+, \quad (\text{A.30})$$

$$r_{mso}^- \in C_x^{1+}, \quad r_{mso}^- \notin C_1^+, \quad (\text{A.31})$$

$$-\ell_1^+ \in [-\ell_1^+(r_{mso}^-), -\ell_{mbo}^+[, \quad r_{mso}^- \in !C_x^{1+}, \quad r_{mso}^- \in C_1^+.$$

(1) On the configurations $r_{mso}^- \in (0)_2^+$

We consider now the configuration $(0)_2^+$. The necessary condition for $r_{mso}^- \in (0)_2^+$ in Eq. (A.14) (see also Eq. (A.17)) showed the presence of a specific angular momentum threshold $\check{\ell}_2^+$ (we recall that $\check{\ell}(a/M) : V_{eff}(\check{\ell}, r_{mso}) = 1$, solution of a quadratic equation for the variable ℓ —see also Figs A.10, A.12, introduced in Appendix A.1.2; here we pointed out the belonging of the specific angular momentum in $\mathbf{L2}$ with the subscript). Following this analysis, we can state that for any Kerr attractor there is

$$r_{mso}^- \notin C_2^+ \quad \text{if} \quad -\ell_2^+ \in]-\check{\ell}_2^+, -\ell_\gamma^+[. \quad (\text{A.32})$$

Thus, for the closed (and regular) configurations C_2^+ , we shall focus on the range of specific angular momenta $-\ell_2^+ \in]-\ell_{mbo}^+, -\check{\ell}_2^+[$ where $r_{mso}^- \in C_2^+$.

The photon circular orbit r_γ is the upper boundary of the orbital range associated with the momentum range $\mathbf{L2}$, and the lower boundary is r_{mbo} .

Equation (A.25) holds, which means, for a closed regular topology of a C_2^+ disk, that $r_{mbo}^- < r_{in}^{2+}$ for $a < a_t$ but, as $r_{mbo}^- < r_{mso}^-$. This is not sufficient to rule out the condition $r_{mso}^- \in C_2^+$ in these geometries.

However, for the critical configuration O_x^{2+} , one could say that as $r_{mbo}^- \in O_x^{2+}$ only for $a < a_t$ then, as $r_{mbo}^- < r_{mso}^-$, for proper values of the specific angular momentum, r_{mso}^- must be included in O_x^{2+} .

We could see, from Fig. 4-Upper that at $a < a_{t_a}$, where $a_{t_a} :$

³¹In fact this follows from the general behavior of the curves $\mp \ell_\pm$ as function of r/M demonstrated in Fig. 2 and trends of the criticality indices as described in Eq. (9).

³²Since for $a \in]0, a_{t_a}[$ we have $r_{mso}^- \in \Delta r_x^+$, where the function $-\ell_1^+$ is monotonically decreasing, then there is always $\ell_1^+(r_{mso}^-) \in \mathbf{L1}^+$.

$r_{mso}^- = r_{mbo}^+$, we have $r_{mso}^- > r_{mbo}^+$, and in conclusion

$$r_{mso}^- \in \text{O}_x^{2+} \quad \text{for} \quad \mathbf{A}_{a_t}^<, \quad -\ell_2^+ \in \mathbf{L}2^+, \quad (\text{A.33})$$

see Fig. A.12 and also Figs 5.4. We note that in the relation (A.33), there is the intensifier $\in!$, meaning that *all* the configurations O_x^{2+} , in the spacetimes where $a < a_t$, *must* contain r_{mso}^- i.e. $r_J^{2+} < r_{mso}^-$, because in those spacetimes there is $r_{mso}^- > r_b^+$.

Conversely, this does not imply $r_{mso}^- \notin \text{O}_x^{2+}$ for $a \in \mathbf{A}_{a_t}^>$ (here we used the intensifier (!) to emphasize that the non-inclusion relation does need to be always verified).

As $r_J^{2+} \in]r_{mbo}^+, r_\gamma^+[$, it follows that the radius $r_{mso}^- < r_\gamma^+$ is not included even in the open topology, or

$$\begin{aligned} \text{for} \quad a > a_{\gamma_+}^- \equiv 0.638285M > a_{t_0} : r_\gamma^+ = r_{mso}^-, \\ \text{there is} \quad r_{mso}^- \notin \text{O}_x^{2+}, \quad r_{mso}^- \notin \mathbf{C}_2^+, \end{aligned} \quad (\text{A.34})$$

$$\text{for} \quad a \in]a_{t_0}, a_{\gamma_+}^-[\quad \text{there is} \quad r_{mso}^- \in \text{O}_x^{2+}. \quad (\text{A.35})$$

We stress that in Eq. (A.35) there is \in and not $\in!$, on the other hand, for this relation to be satisfied, it has to be $-\ell_2^+ \in [-\ell_2^+(r_{mso}^-), -\ell_\gamma^+]$ (one can see the general behavior of the curves $\mp \ell_\pm$ versus r/M in Fig. 2), see also Fig. 5.

Thus one can specify Eq. (A.35) as follows:

$$\begin{aligned} r_{mso}^- \in \text{O}_x^{2+} \quad \text{for} \quad a \in]a_{t_0}, a_{\gamma_+}^-[\quad \text{and} \\ -\ell_2^+ \in [-\ell_2^+(r_{mso}^-), -\ell_\gamma^+]. \end{aligned} \quad (\text{A.36})$$

The situation is more structured for the closed \mathbf{C}_2^+ configurations—see Fig. 4-bottom.

In order to establish the location of the r_{mso}^- in the counterrotating disks \mathbf{C}_2^+ , we can consider the following three cases:³³

$$r_{mso}^- \in]r_{mbo}^+, r_{mso}^+[\quad \text{for} \quad a \in]0, a_{t_0}[\quad (\text{A.37})$$

$$\begin{aligned} a_{t_0} \equiv 0.372583M : r_{mso}^- = r_{mbo}^+, \\ r_{mso}^- \in]r_\gamma^+, r_{mbo}^+[\quad \text{for} \quad a \in]a_{t_0}, a_{\gamma_+}^-[\end{aligned} \quad (\text{A.38})$$

$$\begin{aligned} a_{\gamma_+}^- = 0.638285M : r_{mso}^- = r_\gamma^+, \\ r_{mso}^- < r_\gamma^+ \quad \text{for} \quad a > a_{\gamma_+}^-. \end{aligned} \quad (\text{A.39})$$

The case (A.39) was ruled out by Eq. (A.34). Therefore we will investigate the situation for slower attractors, i.e. $a < a_{\gamma_+}^-$, considering Eq. (A.32).

From Eq. (A.38) we have $r_{mso}^- < r_{mbo}^+$, but we find also $r_{mbo}^+ \notin \mathbf{C}_2^+$ from Eq. (A.2). Therefore, it follows that³⁴

$$r_{mso}^- \notin \mathbf{C}_2^+ \quad \text{for} \quad a > a_{t_0} \quad (\mathbf{A}_{a_t}^>), \quad (\text{A.40})$$

³³We note that in dealing with multiple surfaces formed by ℓ counterrotating fluids, the static limit represents an important limitation. On the equatorial plane, this is placed on the orbit $r_\epsilon^+ = 2M$, which is invariant with respect to the change of the attractor spin. The static limit and the inner region $\Sigma_\epsilon^+ \equiv]r_+, r_\epsilon^+[$ (ergoregion), have very peculiar characteristics; the static limit, for any spacetime $a \neq 0$, acts in some way as a *semipermeable membrane*, separating materials in counterrotating orbits confined in the outer region, from matter corotating with the source. Corotating fluids can penetrate and possibly also to exit from the static limit. In the processes of energy extraction from the black hole, for example the Penrose process, matter can go outside Σ_ϵ^+ , crossing r_ϵ^+ with greater initial momentum and energy (Pugliese&Quevedo, 2015). Note that the efficiency of the energy extraction by the Penrose process in the field of Kerr black holes (Abramowicz&Fragile, 2013) is significantly lower than in the field of Kerr naked singularities (Stuchlík&Schee, 2013; Stuchlík, 1980)

³⁴We address here some general considerations on the arguments that we use

in accord with Eq. (A.34).

However we need to discuss the location of the counterrotating proto-jet point r_J^+ . Indeed, due to Eq. (A.2), we find $r_{mbo}^+ \in \text{O}_x^{2+}$. This task has been completed in Eq. (A.34) and Eq. (A.36).

We focus then on the toroidal fluids orbiting with proper specific angular momentum $-\ell_2^+ \in]-\ell_{mbo}^+, -\check{\ell}_2^+[$, around attractors with $a < a_{t_0}$, considered in Eq. (A.37), where there is $r_{mso}^- \in]r_{mbo}^+, r_{mso}^+[$.

The effective potential function decreases monotonically in this orbital range, but it does not reach the maximum (as the range of specific angular momentum is $\mathbf{L}2$). Thus, we consider a “starting” configuration “embedded” in an effective potential $V_{eff}(\ell_2^+, r_{mso}^-) < 1$, where $-\ell_2^+ \in]-\ell_{mbo}^+, -\check{\ell}_2^+[$, for Eq. (A.14) (that is not in contradiction with Eq. (A.32)).

However, we have $r_{mbo}^+ \notin \mathbf{C}_2^+$ for Eq. (A.2), which means $V_{eff}(\ell_2^+, r_{mbo}^+) > 1$. It follows then that a radius $\bar{r} \in]r_{mbo}^+, r_{mso}^+[$: $V_{eff}(\ell_2^+, \bar{r}) = 1$ exists. Following arguments similar to the ones developed in Appendix A.1.2, in order to evaluate if there are actually solutions of this problem under the condition $-\ell_2^+ \in]-\ell_{mbo}^+, -\check{\ell}_2^+[$ on the specific angular momentum, we have to know the situation for $V_{eff}(\ell_2^+, r_{mso}^-)$. Therefore we look for the solutions of the problem $\exists \check{\ell}_{2_+}^- : V_{eff}(\ell_2^+, r_{mso}^-) = 1$ in $-\ell_2^+ \in]-\ell_{mbo}^+, -\check{\ell}_2^+[$.

Fig. 4 is a restriction of Fig. A.12 and shows the situation for $-\ell_2^+ \in]-\check{\ell}_2^+, -\ell_{mbo}^+[$ where, according to Eq. (A.32), configurations \mathbf{C}_2^+ including r_{mso}^- are possible. We expect therefore that there will be an orbital region included in Δr_x^{2+} , and a range of specific angular momentum for the counterrotating matter in $\mathbf{L}2^+$ satisfying this condition. The figure shows the function $\check{\ell}_{2_+}^-$, as evaluated in r_{mso}^- .

In general, one finds that for $-\ell_2^+ \in]-\ell_{mbo}^+, -\check{\ell}_{2_+}^-]$, there is $V_{eff}(\ell_2^+, r_{mso}^-) < 1$. Therefore, there can be $r_{mso}^- \in \mathbf{C}_2^+$, while for $-\ell_2^+ \in]-\check{\ell}_{2_+}^-, -\check{\ell}_2^+[$ we find $r_{mso}^- \notin \mathbf{C}_2^+$.

Concluding this paragraph we note that to establish an analogue inclusion relation with respect to the open surfaces O_x^{2+} , we can compare the two analysis.

(2) Concluding remarks on the problem $r_{mso}^- \in \text{O}_x^{2+}$

We have shown that the solution of this problem is different for different classes of attractors. This property, as all other

in this section, clarifying particularly certain aspects behind the results given in Eq. (A.40). The main issue is to locate the inner edge of the disk, in this specific case a \mathbf{C}_2^+ disk, in particular with respect to r_{mso}^- . Equation (A.40) indicates that the \mathbf{C}_2^+ disk cannot include r_{mso}^- for a very large class of fast attractors, say $a \gtrsim 0.37M$. In fact, the inner edge is $r_{in}^{2+} > r_{mso}^- < r_{mbo}^+$. This relation is trivial when relation $r_{mso}^- < r_\gamma^+$ is satisfied, occurring in the geometries $a > a_{\gamma_+}^- \gtrsim 0.638M$. For the geometries with $a \in]a_{t_0}, a_{\gamma_+}^-]$, we have $r_{mbo}^+ > r_{mso}^-$ —see also Fig. A.14-bottom; but the necessary condition for the inclusion of r_{mso}^- into a \mathbf{C}_2^+ configuration is that there would be $r_{mbo}^+ \in \mathbf{C}_2^+$. However previous results in Eq. (A.2) had proved that this condition is *never* satisfied, and the reason for this is that the effective potential for the disk with specific angular momentum $\mathbf{L}2^+$ is too “large” (i.e. $K_2^+(r_{mbo}^+) > 1$) as shown in Fig. A.14-bottom. This obviously creates a barrier, essentially due to the centrifugal component of the effective potential, due to which the disk cannot include, while remaining in equilibrium, the orbit r_{mbo}^+ and, therefore, a fortiori the orbit r_{mso}^- . In fact this result is not in contradiction with the results reflected in Fig. 4-bottom.

cases in which different classes of attractors were pointed out, turns to be a possible useful tool for the identification of features possibly distinguishing between different gravitational sources.

More specifically, here the class of attractors with spin in $]0, a_{\gamma_+}^-[$ is then decomposed in the following sub-classes $]0, a_{\gamma_+}^- [=]0, a_{i_a} [\cup] a_{i_a}^* [\cup] a_{i_a}^* [, a_{\gamma_+}^- [,$ where:

$$a_{i_a}^* = 0.61834M \in]a_{\mathbb{N}_1}, a_{\gamma_+}^-[: \quad \check{\ell}_+ = \check{\ell}_{2_+}^-, \quad (\text{A.41})$$

and $a_{\gamma_+}^-$ was introduced in Eq. (A.34).

However, these considerations are only necessary to ensure the condition $r_{mso}^- \in C_2^+$, but not sufficient. Indeed, considerations (A.40) rule out the geometries $\mathbf{A}_{i_a}^>$, although in those spacetimes the condition $V_{eff}(\ell_2^+, r_{mso}^-) < 1$ holds.

Essentially, the (centrifugal) barrier, provided at r_{mbo}^+ , does not allow the inclusion of r_{mbo}^+ in the disk and we recall that the upper boundary of the range of specific angular momentum is intrinsically related to r_{mso}^+ —see Fig. A.14-bottom. In fact, for $a < a_{i_a}$ see Fig. A.14-upper, there is $r_{mso}^- \in]r_{mbo}^+, r_{mso}^+ [\equiv \Delta r_x^+$ and, if the specific angular momentum is low enough, i.e., $-\ell_2^+ \in]-\ell_{mbo}^+, -\check{\ell}_{2_+}^- [,$ then the inner edge r_{in}^{2+} can be chosen, if the disk is sufficiently dense or equivalently, if the hydrostatic pressure is sufficiently large (i.e., the difference between the pressure at its maximum and the pressure at its minimum located at the disk boundary), so that the counterrotating disk can incorporate r_{mso}^- .

As we have already noted, in many of these issues, the component of the potential that further changes the behavior of the disk is its centrifugal part: for the specific angular momentum too low (in magnitude), no disk will form. By increasing the specific angular momentum a disk with low density and very small size arises. At larger angular momenta, the minimum density of the disk, given as a function of K , increases and the disk, in order to counterbalance this effect, will move the point of maximum pressure away from the central attractor, while its inner edge will move towards the gravitational attractor, increasing thus its extension until arriving to an unstable phase.

Further increasing of the specific angular momentum leads to destruction of the closed topology, the outer edge being a P-W instability point.

Thus, in conclusion for the $\mathbf{A}_{i_a}^<$ spacetimes, we have $r_{mso}^- \in C_2^+$ only for $-\ell_2^+ \in]-\ell_{mbo}^+, -\check{\ell}_{2_+}^- [,$ this situation is reflected very clearly by Fig A.14.

With reference to Fig. 4-bottom, this region of the specific angular momentum decreases with the spin in $]0, a_{i_a} [$ up to a_{i_a} : $r_{mso}^- = r_{mbo}^+$, where it vanishes and no such configurations are possible, see also Eq. (A.37)³⁵. We can summarize this analysis

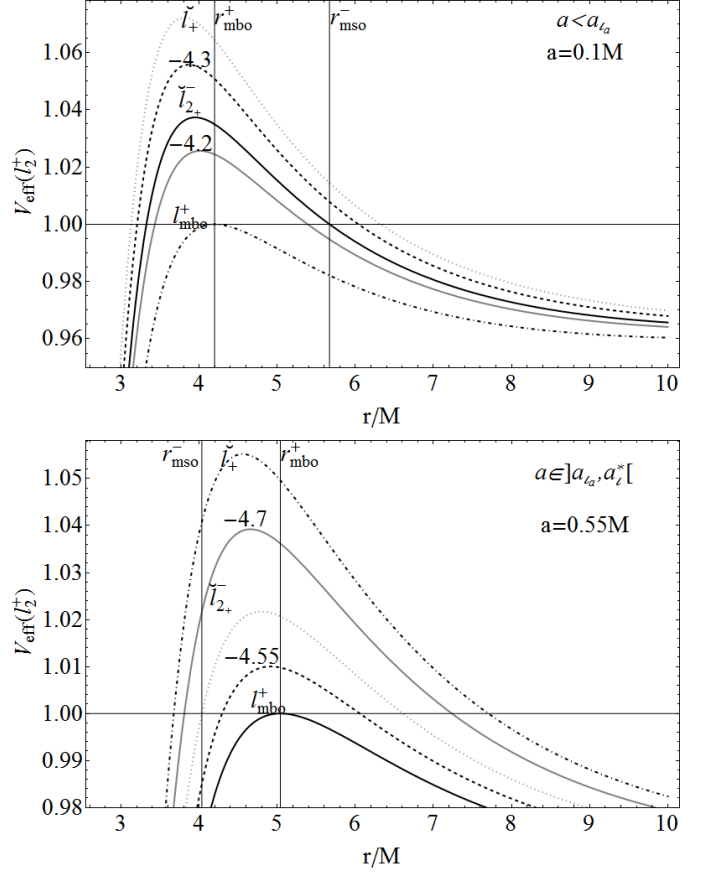


Figure A.14: Counterrotating fluids: disks C_2^+ . Upper panel: spacetime with spin $a = 0.1M < a_{i_a}$, potentials given for different specific angular momenta. At $-\ell_2^+ \in]-\ell_{mbo}^+, -\check{\ell}_{2_+}^- [,$ with $r_{mso}^- \in C_2^+$. The outer horizon $r_+ = 1.99499M$ and $\check{\ell}_{2_+}^- = -4.24107$, $\ell_{mbo}^+ = -4.09762$, $\check{\ell}_+ = -4.3478$. Bottom panel: spacetime with spin $a = 0.55M \in]a_{i_a}, a_{i_a}^* [,$ there are no disk with $r_{mso}^- \in C_2^+$. In this spacetime $r_+ = 1.83516M$, $\check{\ell}_{2_+}^- = -4.61392$, $\ell_{mbo}^+ = -4.48998$, $\check{\ell}_+ = -4.77024$.

by saying that:

$$r_{mso}^- \notin C_2^+ \quad \text{if} \quad -\ell_2^+ \in]-\check{\ell}_{2_+}^-, -\ell_{\gamma_+}^+ [\in \mathbf{L2}^+, \quad (\text{A.42})$$

$$r_{mso}^- \notin C_2^+, \quad r_{mso}^- \notin \mathbf{O}_x^{2+}, \quad \text{for} \quad a > a_{\gamma_+}^- > a_{i_a}, \quad (\text{A.43})$$

$$r_{mso}^- \notin C_2^+ \quad \text{for} \quad a > a_{i_a}, \quad (\text{A.44})$$

$$r_{mso}^- \in \mathbf{!O}_x^{2+} \quad \text{for} \quad a \in]a_{i_a}, a_{\gamma_+}^- [\quad \text{and} \quad (\text{A.45})$$

$$-\ell_2^+ \in]-\ell_2^+(r_{mso}^-), -\ell_{\gamma_+}^+ [, \quad (\text{A.46})$$

$$r_{mso}^- \in \mathbf{!O}_x^{2+} \quad a < a_{i_a}, \quad -\ell_2^+ \in \mathbf{L2}^+, \quad (\text{A.46})$$

$$r_{mso}^- \in C_2^+ \quad \text{for} \quad a < a_{i_a} \quad \text{and} \quad -\ell_2^+ \in]-\ell_{mbo}^+, -\check{\ell}_{2_+}^- [. \quad (\text{A.47})$$

(3) On the configurations $r_{mso}^- \in \mathbf{O}_3^+$

We can now focus on a C_3^+ disk, considering the marginally stable orbit r_{mso}^- . Equation (A.20) holds. As $r_{mso}^- < r_{mso}^+$, this proves that:

$$r_{mso}^- \notin C_3^+. \quad (\text{A.48})$$

³⁵Similarly, regular C_2^+ disks, satisfying this property, will be constrained in terms of the possible orbital range. The situation is different for attractors with spin in $]a_{i_a}, a_{i_a}^* [,$ where the orbital range increases again with the spin up to the upper boundary of the second class, $a_{i_a}^*$ —see also Eq. (A.41), where maximum extension of the orbital region occurs, and in the third, very restricted class $]a_{i_a}^*, a_{\gamma_+}^- [$.

Appendix A.2.2. Corotating disks: $r_{\mathcal{N}}^+ \in ()_-$

Appendix A.2.2.1. Marginally stable orbit $r_{mso}^+ \in ()_-$.

It is convenient to consider first the location of the marginally stable orbits. We can compare r_{mso}^+ with the radius $r_{mso}^- < r_{mso}^+$. Clearly it is always possible to select the specific angular momentum $\ell^-(r_{mso}^+)$ such that the disk can be centered on r_{mso}^+ , see Fig. 5. This disk can be stable, in regular topology C^- , or in accretion for the cusped topology C_x^- , depending on the specific angular momentum $\ell^-(r_{mso}^+) \in \mathbf{Li}$, see Fig. 5.

We obtain

$$\begin{aligned} \ell^-(r_{mso}^+) \in \mathbf{L1}^- \text{ for } a < \check{a}_{\mathcal{N}} \approx 0.4618544M \in]a_{\mathcal{N}0}, a_{\mathcal{N}}[\\ \check{a}_{\mathcal{N}} : \ell^-(r_{mso}^+) = \ell_{mbo}^-, r_{mso}^+ = r_{cent}^- \in \{C_1^-, C_x^-\}, \end{aligned} \quad (\text{A.49})$$

$$\ell^-(r_{mso}^+) \in \mathbf{L2}^- \text{ for } a \in]\check{a}_{\mathcal{N}}, \check{a}_{\mathcal{N}}[\quad (\text{A.50})$$

$$\check{a}_{\mathcal{N}} = 0.73688M : \ell^-(r_{mso}^+) = \ell_{\gamma}^- \quad (\text{A.51})$$

$$\begin{aligned} r_{mso}^+ = r_{cent}^- \in \{C_2^-, O_x^-\}, \\ \ell^-(r_{mso}^+) \in \mathbf{L3}^- \text{ for } a > \check{a}_{\mathcal{N}} \quad r_{mso}^+ = r_{cent}^- \in C_3^-, \end{aligned} \quad (\text{A.52})$$

We now enquire on the situation where the disk is not exactly centered in r_{mso}^+ . This analysis is specially relevant in the investigation of a possible interaction between rings orbiting with specific angular momenta in different ranges \mathbf{Li} .

Equations (A.50,A.51,A.53) show that the relation $r_{mso}^+ \in ()_-$ is invariant for a slight change of specific angular momentum around the value $\ell^-(r_{mso}^+)$. However, the orbit r_{mso}^+ may be non included in a corotating ring with lower specific angular momentum (with $r_{cent}^- < r_{mso}^+$), or larger specific angular momentum (with $r_{cent}^- > r_{mso}^+$): the first case for $r_{out}^- < r_{mso}^+$, the second for $r_{in}^- > r_{mso}^+$.

We should compare the value of the maximum K_{Max}^- , with the value of the potential at r_{mso}^+ . In fact, it is immediate to see that, for $\ell^- < \check{\ell}^- \equiv \ell^-(r_{mso}^+)$, the effective potential $V_{eff}(\ell^-, r_{mso}^+) < 1$, but $r_{Max}^- > \check{r}_{Max}^- \equiv r_{Max}^-(\check{\ell}^-)$.

If $V_{eff}(\ell^-, r_{mso}^+) > K_{Max}^-$, then $r_{out}^- < r_{mso}^+$, where there is an angular momentum $\ell^- < \check{\ell}^-$ such that a maximum r_{Max} exists. In fact, the condition $V_{eff}(\ell^-, r_{mso}^+) > K_{Max}^-$ can be verified, for definition of maximum point, only in the asymptotic region $r > r_{min}^-$, as one assumes $K_{Max}^- < 1$ —see also the analysis in Fig. A.16.

On the other hand, we note that the condition $V_{eff}(\ell^-, r_{mso}^+) < K_{min}^- = V_{eff}(\ell^-, r_{min}^-)$ cannot be fulfilled for the definition of minimum. Then:

$$K_{min}^- < V_{eff}(\ell^-, r_{mso}^+) < K_{Max}^- = V_{eff}(\ell^-, r_{Max}^-), \quad (\text{A.54})$$

if r_{Max}^- exists, and then ℓ^- is in $\mathbf{L1}^-$ or $\mathbf{L2}^-$ (we will analyze later the case $\mathbf{L3}^-$). Thus $r_{mso}^+ \in ()^+$ can be, but we can always verify (sufficient condition) that if $V_{eff}(\ell^-, r_{Max}^-) > 1$, then ℓ^- is in $\mathbf{L2}^-$ and $r_{mso}^+ \in O_x^-$.

The general argument, summarized at the end of this section,

is the following: as we know that $r_{Max}^- < r_{mso}^- < r_{min}^-$ then³⁶

$$\begin{aligned} \text{if } \ell^- < \check{\ell}^- \text{ there is} \\ \check{r}_{Max}^- < r_{Max}^- < r_{mso}^- < r_{min}^- < r_{mso}^+, \\ \text{and thus } r_{mso}^+ \notin C_x^-. \end{aligned} \quad (\text{A.55})$$

So far we have considered $\ell^- \in \mathbf{L1}^-$, therefore it holds for any Kerr attractor according to the Equations (A.50,A.51,A.53), also for fast attractors where there are no \check{r}_{Max} , see Eq. (A.53). Then

$$\begin{aligned} \text{if } \ell^- > \check{\ell}^- \text{ there is} \\ r_{Max}^- < \check{r}_{Max}^- < r_{mso}^- < r_{mso}^+ < r_{min}^- \\ \text{and thus } r_{mso}^+ \in ()_x^-. \end{aligned} \quad (\text{A.56})$$

In terms of the maximum points, conditions in Eq. (A.56) hold where maximum points of the effective potential exist. Precisely, we can always select a K , where $K_{Max}^- < 1$ (which occurs for $\ell^- \in \mathbf{L1}^-$). The situation is different for proper specific angular momentum in the ranges $\mathbf{L2}^-$ and $\mathbf{L3}^-$ where, if $V_{eff}(\ell^-, r_{mso}^+)$ is well defined, it should be $V_{eff}(\ell^-, r_{mso}^+) < 1$, and there would be an upper limit on the specific angular momentum $\ell^- > \check{\ell}^-$ depending on the black hole spin.

Let us consider then Eq. (A.56) for the minimum points: $V_{eff}(\check{\ell}^-, r_{mso}^+) < 1$ for $\check{\ell}^- < \check{\ell}_*$, where $\check{\ell}_* : V_{eff}(\check{\ell}_*, r_{mso}^+) = 1$, see Fig. A.10. We can now trace easily come conclusions:

$$\begin{aligned} r_{mso}^+ \in C^- : \text{ for } a \in [0, \check{a}_*] \quad V_{eff}(\ell^-, r_{mso}^+) < 1 \\ \text{in } \mathbf{L1}^- \cup [\ell_{mbo}^-, \check{\ell}_*] \subset \mathbf{L2}^-, \end{aligned} \quad (\text{A.57})$$

$$\text{for } a \in]\check{a}_*, M] \quad V_{eff}(\ell^-, r_{mso}^+) < 1 \quad (\text{A.58})$$

$$\begin{aligned} \text{in } \mathbf{L1}^- \cup \mathbf{L2}^- \cup]\ell_{\gamma}^-, \check{\ell}_*] \subset \mathbf{L3}^-, \\ \text{where } \check{a}_* \equiv 0.401642M : \check{\ell}_* = \ell_{\gamma}^-. \end{aligned} \quad (\text{A.59})$$

We recall that Eqs (A.57–A.59) are indeed necessary but not sufficient, for it is always possible to find an appropriate $K < 1$ such that r_{mso}^+ is included in the disk, and then in particular $r_{mso}^+ < r_{out}^-$.

It should be ensured that the maximum of the potential, being located at $r_{Max}^- < r_{mso}^+$ while it exists, satisfies the relation $K_{Max}^- \geq V_{eff}(\ell^-, r_{mso}^+)$.

In the case $\mathbf{L2}^- \cup \mathbf{L3}^-$, the conditions in Eqs (A.57–A.59) are also sufficient. While this is not immediate for the disks

³⁶In fact: if $\ell^- < \check{\ell}^-$, then $r_{Max}^- > \check{r}_{Max}^-$. But if $r_{Max}^- > \check{r}_{Max}^-$ then there is $K_{Max}^- < \check{K}_{Max}^-$ —see Fig. 2-bottom. Therefore, we have $\check{r}_{out}^- > r_{out}^-$ (we recall that in the case of critical configurations the outer cross point of the curves $K_{crit} = \text{constant}$ in Fig. 2-bottom is exactly the outer edge of the critical accretion disk). On the other side, we know that $\check{r}_{out}^- > r_{mso}^+$, because $r_{mso}^+ = \check{r}_{min}^-$, from the definition of $\check{\ell}^-$, as this fact implies that $\check{K}_{Max}^- > K_{mso}^-$ —see Fig. 2-bottom. However, it has to be $K_{Max}^- \in]K_{mso}^-, K_{crit}^-(r_{mso}^+)[\cup]K_{crit}^-(r_{mso}^+), \check{K}_{Max}^-[$. We recall that $\ell^- < \check{\ell}^- = \ell^-(r_{mso}^+)$, because there is $r_{mso}^+ = \check{r}_{min}^-$. Now, if $K_{min}^- < K_{Max}^- \in]K_{mso}^-, K_{crit}^-(r_{mso}^+)[$, then $r_{out}^- < r_{mso}^+$, as immediate to see by considering the curves K_- in Fig. 2-bottom, and this finally proves the result in Eq. (A.55). The condition above implies that there is the specific angular momentum $\ell^- \in]\ell_{mso}^-, \check{\ell}_{mso}^+[$, where $\check{\ell}_{mso}^+ > 0 : V_{eff}(\check{r}_{Max}^-, \check{\ell}_{mso}^+) = K_{crit}^-(r_{mso}^+)$. In the second case, Eq. (A.56), where $r_{mso}^+ \in C_x^-$, we know that $r_{min}^- \in]r_{mso}^-, r_{mso}^+[$ for assumption, and then the specific angular momentum $\ell^- \in]\ell_{mso}^-, \check{\ell}^- = \ell^-(r_{mso}^+)[$, and therefore $r_{Max}^- \in]\check{r}_{Max}^-, r_{mso}^+[$. However, $\check{K}_{Max}^- > K_{mso}^+$ if $\check{K}_{Max}^- > K_{Max}^- > K_{mso}^+$, and then we have $\check{r}_{Max}^- < r_{Max}^- < \check{r}_{mso}^+$.

with momentum in $\mathbf{L1}^-$, for which $K_{Max}^1 < 1$. Therefore, we should consider the condition $K_{Max}^1 > V_{eff}(\ell_1^-, r_{mso}^+)$, implying restriction on $\mathbf{L1}^-$, see Fig. 2-bottom.

It is worth to say that the location of the outer edge of the disk, so far ignored in this analysis, becomes relevant in the discussion of the problem of inclusion for the corotating disk. In fact, the position of r_N , with respect to the outer margin, is basically determined by the possibility to find out a proper K .

Appendix A.2.2.2. Marginally bounded orbit $r_{mbo}^+ \in ()_-$.

The issue of the location of the r_{mbo}^+ with the respect to a corotating configuration is extremely significant. The situation is rather complex and here we will provide some general considerations in the analysis of different specific situations.

The corotating configuration could be located either in the region $r > r_{mbo}^+$ or $r < r_{mbo}^+$, as detailed in Sec. (4). The investigation of this case involves the distinction of two classes of attractors and the analysis of the location of r_{mbo}^+ with respect to both the inner and outer edge of the closed configurations. More specifically, we will need to compare the situation for r_{mbo}^+ with that for r_{mso}^- and r_{mbo}^- . As such we distinguish the two classes of attractors: $\mathbf{A}_{a_a}^<$: $a \in [0, a_{a_a}[$, where $r_{mbo}^+ < r_{mso}^-$, and $\mathbf{A}_{a_a}^>$: $a \in]a_{a_a}, M]$, where $r_{mbo}^+ > r_{mso}^-$; at $a = a_{a_a}$ we have $r_{mbo}^+ = r_{mso}^-$, see Fig. 4.

In the second class of geometries, $\mathbf{A}_{a_a}^>$, the radius r_{mbo}^+ can correspond to a center of the disk, or also any point of the configuration, but not a critical point. For $\mathbf{A}_{a_a}^<$ attractors, the r_{mbo}^+ can be any point of the disk in general, but not the center of the closed configuration, it can be however its critical cusped point.

In other words:

$$\begin{aligned} \text{for } \mathbf{A}_{a_a}^< : & \quad a \in [0, a_{a_a}[; \quad r_{mbo}^+ \notin \{r_J^-, r_{cent}^-\}; \\ \text{it could be } & \quad r_{mbo}^+ = r_x^- \quad \text{or} \quad r_{mbo}^+ \in ()_- \Big|_{\Theta(r_{cent} - r_{in})} \end{aligned} \quad (\text{A.60})$$

$$\text{for } \mathbf{A}_{a_a}^> : \quad a \in]a_{a_a}, M]; \quad r_{mbo}^+ \notin \{r_J^-, r_x^-\}; \quad (\text{A.61})$$

$$\text{it could be } \quad r_{mbo}^+ = r_{cent}^- \quad \text{or} \quad r_{mbo}^+ \in ()^-, \quad (\text{A.62})$$

where $()^-$, as usually, does not particularize the topology, $\Theta(r_{cent} - r_{in})$ in Eq. (A.60) is the Heaviside (step) function such that $\Theta(r_{cent} - r_{in}) = 1$ for $r_{cent} > r_{in}$ and $\Theta(r_{cent} - r_{in}) = 0$ for $r_{cent} < r_{in}$. We need now to specify the specific angular momentum ℓ^- and the topology of the corotating configuration. We look at the closed regular corotating topologies because any critical topology must contain the marginally stable orbit, that is $r_{mso}^- \in !()_x^-$. This is because the margins of the critical configurations (both the inner as well as the outer edges of the closed cusped topology) are univocally fixed by the specific angular momentum, see curves $K_{crit} = \text{constant}$ in Fig. 2-bottom. Then we need essentially to find the appropriate specific angular momentum for $\ell_\beta^- : V_{eff}(\ell_\beta^-, r_{mbo}^+) < 1$.

We can provide some immediate constraints for the class of geometries $\mathbf{A}_{a_a}^<$ in Eq. (A.61), by considering the location of $r_{mbo}^+ < r_{mso}^-$. For the configurations where $r_{mso}^- \notin C^-$, it must be $r_{mbo}^+ \notin C^-$. Therefore, from the former analysis, in the conditions provided by Eq. (A.10) for the attractors $\check{\mathbf{A}}_< \supset \mathbf{A}_{a_a}^<$, we

find $r_{mso}^- \notin C_2^-$ (in this case the $r_{in}^{2-} > r_{mso}^- > r_{mbo}^+$) and from Eq. (A.18) for all the $\check{\mathbf{A}}_<$ black holes, there is $r_{mso}^- \notin C_3^-$ (in this case, the inner margin of C_3^- is far beyond r_{mso}^- and r_{mbo}^+). Therefore, one finds:

$$\begin{aligned} \text{for } \mathbf{A}_{a_a}^< \text{ it is } & \quad r_{mbo}^+ \notin C_3^-; \quad \text{and for } \ell_2^- \in]\check{\ell}_-, \ell_\gamma^-[\\ \text{it is } & \quad r_{mbo}^+ \notin C_2^- \text{ as } \quad r_{in}^{2-} > r_{mso}^- > r_{mbo}^+. \end{aligned} \quad (\text{A.63})$$

The results in Eq. (A.63) explain the situation, for the slow attractors completely for the C_3^- configurations and for C_2^- , but not for the C_1^- disks.

Similarly to what has been done in previous cases, we can face this problem introducing the specific angular momentum $\ell_\beta^- : V_{eff}(\ell_\beta^-, r_{mbo}^+) = 1$, as shown in Fig. A.15-left. From the figure it follows that

$$\begin{aligned} \ell_\beta^- \in \mathbf{L2}^- \quad \text{for } & \quad a < a_{\gamma_-}^\beta \supset \mathbf{A}_{a_a}^<, \quad \text{and } \ell_\beta^- \in \mathbf{L3}^- \quad \text{for} \\ & \quad a > a_{\gamma_-}^\beta \subset \mathbf{A}_{a_a}^>, \quad a_{\gamma_-}^\beta > a_{a_a} \quad \text{for } \ell^- < \ell_\beta^-. \end{aligned} \quad (\text{A.64})$$

In $\mathbf{L1}_-$ the effective potential is always less then its asymptotic limit, and it follows that it is possible to locate, with a proper elongation, the disk such that

$$\begin{aligned} r_{mbo}^+ \in ()_1^-; \quad r_{mbo}^+ \in ()_2^- \quad \text{for } & \quad a > a_{\gamma_-}^\beta \quad \text{and for} \\ a < a_{\gamma_-}^\beta \quad \text{at } & \quad \ell^- < \ell_\beta^-, \quad r_{mbo}^+ \notin ()_2^- \end{aligned} \quad (\text{A.65})$$

$$\text{for } \ell^- > \ell_\beta^-, \quad (\text{A.66})$$

$$\begin{aligned} r_{mbo}^+ \notin C_3^- \quad \text{for } & \quad a < a_{\gamma_-}^\beta, \quad \text{and for} \\ a > a_{\gamma_-}^\beta \quad \text{and } & \quad \ell > \ell_{\gamma_-}^\beta; \quad r_{mbo}^+ \in C_3^- \end{aligned} \quad (\text{A.67})$$

$$\text{for } a > a_{\gamma_-}^\beta \quad \text{and } \ell < \ell_{\gamma_-}^\beta; \quad (\text{A.68})$$

these results are in fact verified in Fig. A.15 and they confirm the conclusion of Eq. (A.63). Equations (A.66,A.68) close discussion of the problem of inclusion.

However, in order to fully characterize this situation we can consider the specific angular momentum $\ell^-(r_{mbo}^+)$, plotted as function of a/M in Fig. A.10-upper. In fact, as a general premise we note that for $\ell^- = \ell^-(r_{mbo}^+)$, a critical point must be located in r_{mbo}^+ , according to Eqs (A.60,A.61).

In the $\mathbf{A}_{a_a}^<$ geometries, for fluids with momentum ℓ_{mbo}^+ , the orbit r_{mbo}^+ has to correspond to an unstable point, but it is not r_J because, for possible $\ell^-(r_{mbo}^+) \in \mathbf{L3}^-$, it could happen according to the discussion in Appendix A.1.2 that the potential is not well defined, but in this case, for these attractors, Eq. (A.63) holds.

Once the center r_{min}^- is shifted with respect to r_{mbo}^+ , such that $r_{min}^- \leq r_{mbo}^+$ (for $\ell^- \neq \ell^-(r_{mbo}^+)$), one can always select a K_- so that the elongation of the C^- configuration is small enough to ensure $r_{mbo}^+ \notin C^-$. Besides, a more specific constraint on K_- could be provided in dependence on ℓ^- , according to the analogue analysis suggested in (Pugliese&Stuchlík, 2015), whereas in this section we will provide constraints on the rotation parameters $(a/M, \ell)$ for the location of the center.

We know that the gap $\Delta_{\ell^-}^{mbo} \equiv \check{\ell}_- \pm \ell^-(r_{mbo}^+) > 0$ between the specific angular momenta (the \pm sign is due to the requirement of positive $\Delta_{\ell^-}^{mbo}$ according to the different location of r_{mbo}^+ with respect to r_{cent}) is proportional to the distance between the

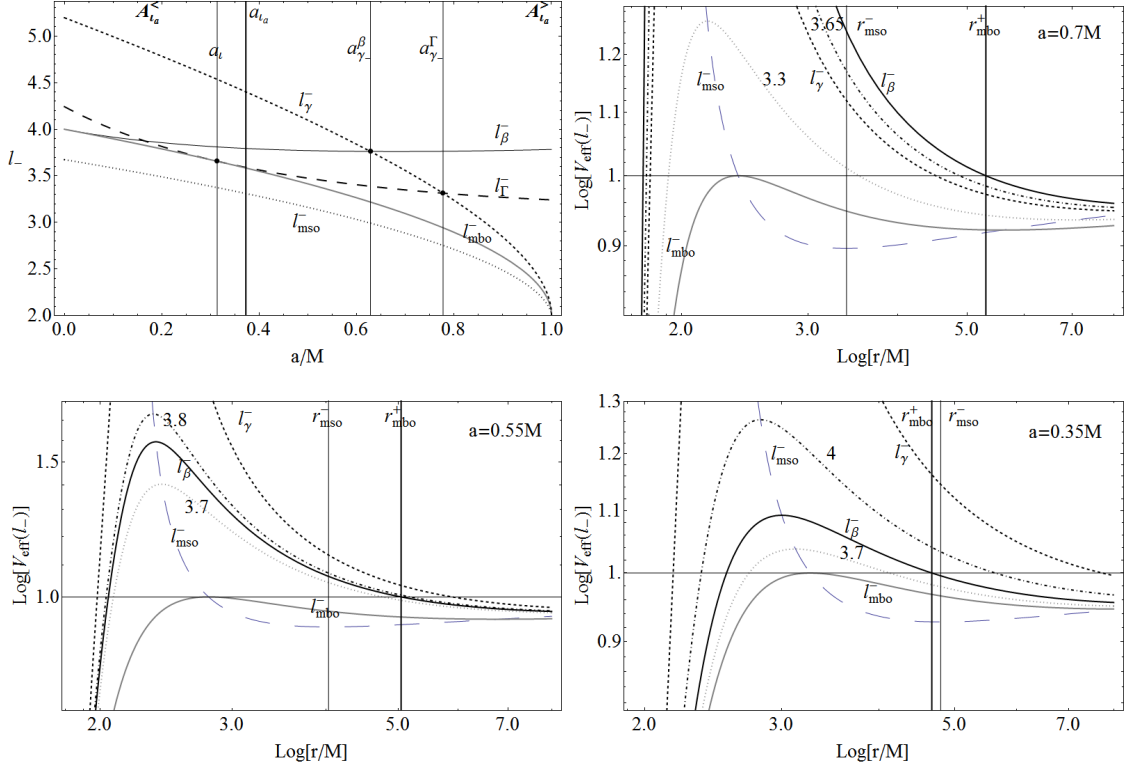


Figure A.15: Corotating disks: $r_N^+ \in ()_-$: Left-upper-panel: specific angular momenta $\ell_{mbo}^- \equiv \ell^-(r_{mbo}^-)$, r_{mbo}^- is the marginally bounded orbit, $\ell_{mso}^- \equiv \ell^-(r_{mso}^-)$, r_{mso}^- is the marginally stable orbit, $\ell_{\gamma}^{\pm} \equiv \ell^-(r_{\gamma}^{\pm})$, r_{γ}^{\pm} is the marginally circular orbit (photon orbit). Notation (\pm) is for counterrotating and corotating fluids respectively. The specific angular momentum $\ell_{\beta}^{\pm} : V_{\text{eff}}(\ell_{\beta}^{\pm}, r_{mbo}^{\pm}) = 1$ and $\ell_{\Gamma}^{\pm} : V_{\text{eff}}(\ell_{\Gamma}^{\pm}, r_{\gamma}^{\pm}) = 1$ are also plotted. The spin a_{ia} defines the two classes of attractors $\mathbf{A}_{ia}^<$ and $\mathbf{A}_{ia}^>$ respectively. $a_{\gamma}^{\beta} \equiv 0.628201M : \ell_{\beta}^{\pm} = \ell_{\gamma}^{\pm}$ and $a_{\gamma}^{\pm} \equiv 0.777271M : \ell_{\Gamma}^{\pm} = \ell_{\gamma}^{\pm}$. Right-upper-panel and bottom panels: effective potentials as functions of r/M , at different a/M and ℓ .

radii, or generally $\partial_{\bar{\Delta}_r^{mbo}}(\bar{\Delta}_r^{mbo}) > 0$, where $\bar{\Delta}_r^{mbo}$ is the (positive) distance between the radii (r_{mbo}^+ , r_{cent}). This must imply the possibility of large specific angular momentum and then a larger K_- , or a larger range of variation for K_- . Because r_{cent} is a minimum of the effective potential with $r_{mbo}^+ > r_{Max}^-$, then it is always $V_{\text{eff}}(r_{mbo}^+) - V_{\text{eff}}(r_{cent}) > 0$, and this grows with increasing specific angular momentum (we note that if it would be $r_{mbo}^+ < r_{Max}^-$, then the problem would be solved immediately as $r_{mbo}^+ \notin C^-$).

Considering the various locations of $\ell^-(r_{mbo}^+) \in \mathbf{LI}^-$, we finally investigate four classes of attractors, defined by the spins $\{a_o^*, a_{ia}, a_o, a_o^{\gamma}\}$ as in Fig. A.10-upper:

I. At $a = a_{ia}$ it is $r_{mso}^- = r_{mbo}^+$ and $\ell^-(r_{mbo}^+) = \ell_{mso}^-$, thus

$$\begin{aligned} \text{at } a \in]a_{ia}, a_o[\subset \mathbf{A}_{ia}^> \text{ it is } \ell^-(r_{mbo}^+) \in]\ell_{mso}^-, \ell_{mbo}^-[= \mathbf{L1}^-, \\ r_{cent}^1 \leq r_{mbo}^+ \text{ for } \ell \leq \ell^-(r_{mbo}^+), \end{aligned} \quad (\text{A.69})$$

and then, for $\ell < \ell^-(r_{mbo}^+)$, the ring density can span in higher values.

II. At $a = a_o$ we have $\ell_{mbo}^- = \ell_-(r_{mbo}^+)$, therefore the configuration \mathbf{O}_x^- has the unstable point $r_J^- = r_{mbo}^-$ and $r_{cent}^- = r_{mbo}^+$.

$$\begin{aligned} \text{For } a \in]a_o, a_o^{\gamma}[\subset \mathbf{A}_{ia}^> \text{ it is } \ell_-(r_{mbo}^+) \in]\ell_{mbo}^-, \ell_{\gamma}^-[= \mathbf{L2}^-, \\ r_{cent}^2 \leq r_{mbo}^+ \text{ for } \ell \leq \ell^-(r_{mbo}^+), \end{aligned} \quad (\text{A.70})$$

and, for $\ell = \ell^-(r_{mbo}^+)$, the center of the disk will be at $r = r_{mbo}^+$. The region of lower specific angular momentum, and the corresponding orbital range, increases with the spin and thus one could conclude that the separated configurations are favored also with relatively high elongation of the corotating equilibrium disk.

III. Finally:

$$\begin{aligned} \text{for } a \in]a_o^{\gamma}, M[\subset \mathbf{A}_{ia}^> \quad \ell^-(r_{mbo}^+) \in \mathbf{L3}^- \\ r_{cent}^3 \leq r_{mbo}^+ \text{ for } \ell \leq \ell^-(r_{mbo}^+). \end{aligned} \quad (\text{A.71})$$

In this case the range of lower specific angular momentum is relatively small and it increases with the spin of the attractor. At $a = a_o^{\gamma}$, the center is located at r_{mbo}^+ for $\ell^- = \ell^-(r_{mbo}^+)$.

IV. For lower spin, in the $\mathbf{A}_{ia}^<$ geometries, there is $r_{mbo}^+ \in]r_{mbo}^-, r_{mso}^-[$. Therefore, for momenta $\ell_-(r_{mbo}^+)$ (for those in $\mathbf{L1}^-$), the orbit r_{mbo}^+ is a critical r_x point. The disk center thus will be located far from r_{mso}^+ , with maximum distance in the static case. For an attractor with $a = a_{ia}$, the center will be located at r_{mso}^- . Therefore, for smaller a/M , at $\ell < \ell^-(r_{mbo}^+) \in \mathbf{L1}^-$, the disk center will be located close enough to the attractor and the disk in its critical (closed) topology will be close to r_{mso}^- .

The specific angular momentum range for a ring centered in $]r_{mbo}^+, r_{mso}^-[$ is higher at smaller a/M and, at $a = a_o^*$, the disk is

centered in r_{mso}^+ with accretion point in r_{mbo}^+ .

We note that $r_{mbo}^- < r_{mbo}^+$, and for $a < a_{ta}$ we have $r_{mso}^- > r_{mbo}^+$. Therefore no C^- disk can be centered in r_{mbo}^+ . It is necessary then to discuss the location of r_{mbo}^+ with respect to the inner edge of the disk. For the larger spin, we find $r_b^+ \in]r_\gamma^-, r_{mso}^+[$ and a C^- disk can be centered in r_{mbo}^+ . Then we could say that for sufficiently high spin, and with high specific angular momentum for low spin, it can be $r_{mbo}^+ \in C^-$, and for $a < a_{ta}$, it has to be $r_{mbo}^+ \in](0)_x^-$. For fast attractors, one has to consider also the outer margin of the disk and the location of the marginally stable orbit as addressed in the previous point –see also the analysis in Fig. A.16.

Appendix A.3. On the location of the photon orbits and general consideration on the methods

We complete our study by considering the location of the ring with respect to the photon orbits r_γ^\pm . The results of this investigations contribute to possibility to localize more accurately a corotating configuration, with respect to the counterrotating geodesic structure of the Kerr geometry– Fig. 4.

It is clear that the inclusion relations $r_\gamma^\pm \notin (0)_\pm$ as well as $r_\gamma^- \notin (0)^+$, due to $r_\gamma^- < r_\gamma^+$, can be derived by immediate considerations of the geodesics structure of the Kerr spacetime. It is now necessary to discuss the relation $r_\gamma^+ \in (0)^-$. This analysis, together with the considerations drawn on the inclusion relation $r_{mbo}^+ \in (0)^-$ at the end of Appendix A.2.2, complete the discussion on the ℓ counterrotating couple $(0)_\pm$ and their possible correlation.

We find:

$$\begin{aligned} \text{for } a \in \mathbf{A}_l^< \equiv [0, a_l] \quad & \text{it is } r_\gamma^+ \in]r_\gamma^-, r_{mbo}^-] \equiv \Delta r_j^-; \\ \text{for } a \in]a_l, a_{\gamma_+}^-] \quad & \text{it is } r_\gamma^+ \in]r_{mbo}^-, r_{mso}^-] \equiv \Delta r_{x^-}, \\ \text{for } a > a_{\gamma_+} \quad & \text{it is } r_\gamma^+ > r_{mso}^-. \end{aligned} \quad (\text{A.72})$$

From these relations, and considering also the results of Appendix A.1.1 and particularly Eqs (A.1,A.2.A.3), we infer that

$$\begin{aligned} \text{for } a \in [0, a_l] \quad & \text{it is } r_\gamma^+ \notin (C^-, C_x^{1-}), \\ a \in]a_l, a_{\gamma_+}^-] \quad & \text{it is } r_\gamma^+ \notin C_3^-; r_\gamma^+ \notin C_2^- \\ \text{for } \ell_2^- \in]\check{\ell}_-, \ell_\gamma^-] \quad & \end{aligned} \quad (\text{A.73})$$

Concerning the disks in the geometries with $a \in]a_l, a_{\gamma_+}^-]$, certainly $r_\gamma^+ \notin (0)^-$ when $r_{mso}^- \notin (0)^-$, for example in the different conditions laid down in Appendix A.1.2, and particularly in Eqs (A.10,A.14,A.18).

However, to be more precise, we need to refer to the specific angular momenta as in Figs A.15-left. Then we can introduce the angular momentum $\ell_\Gamma^- : V_{eff}(\ell_\Gamma^-, r_\gamma^+) = 1$ such that $\ell_\Gamma^- \in \mathbf{L2}^-$ for $a < a_{\gamma_-}^-$, while there is $\ell_\Gamma^- \in \mathbf{L3}^-$ when $a > a_{\gamma_-}^-$. We have:

$$\begin{aligned} a_l < a_{\gamma_+}^- < a_{\gamma_-}^- < \check{a}, \quad a_l \equiv 0.3137M, \quad a_{\gamma_+}^- \equiv 0.638285M, \\ a_{\gamma_-}^- \equiv 0.777271M, \quad \check{a} \equiv 0.969174M. \end{aligned} \quad (\text{A.74})$$

It follows that:

$$\begin{aligned} \text{for } a \in [0, a_{\gamma_-}^-] \quad & \\ \text{it is } r_\gamma^+ \in (0)_1^-, \quad r_\gamma^+ \in (0)_2^- \quad & \text{for } \ell^- < \ell_\Gamma^-, \\ r_\gamma^+ \notin (0)_2^- \quad & \text{for } \ell^- > \ell_\Gamma^- \in \mathbf{L2}^-; \quad r_\gamma^+ \notin C_3^-, \\ \text{for } a \in]a_{\gamma_-}^-, M]^* \quad & \text{it is } r_\gamma^+ \in (0)_1^- \quad r_\gamma^+ \in (0)_2^-, \quad (\text{A.75}) \\ r_\gamma^+ \in (0)_3^- \quad & \text{for } \ell^- < \ell_\Gamma^- \in \mathbf{L3}^- \\ r_\gamma^+ \notin (0)_3^- \quad & \text{for } \ell^- > \ell_\Gamma^- \in \mathbf{L3}^-. \end{aligned} \quad (\text{A.76})$$

We conclude that this kind of configuration is favored for corotating matter, when both rotation parameters, $(a/M, \ell^-)$, have sufficiently low values (in accordance with the balance of centrifugal and gravitational component of the effective potential to which the configuration is subject). In case of the closed configurations, this property helps for setting the inner and outer edge of the disk.

We note that the relations in Eqs (A.75,A.76) are *not* in contradiction with the result of Eq. (A.73). In fact these two results should be considered together, and ensure that in this case the potential is lower than its asymptotical limit, but the point, in this case the orbit r_γ^+ , is located in a right range of the maximum point, where the function is increasing with the radius (in the case of momenta in $\mathbf{L3}^-$ there is no minimum of the hydrostatic pressure).

These results are confirmed by Fig. A.17, moreover we note that also Eqs (A.66,A.68), confirmed by the analysis in Figs A.15, are not in contradiction with the constraints provided by the geodesic structure. This is because for the orbit r_* it follows: $V_{eff}^2(\ell_3, r_*) > 0$ and $K_{Max}^i \equiv V_{eff}(\ell_i, r_{Max}) \geq V_{eff}(\ell_i, r_*)$ for $\ell_i \in \{\mathbf{L1}, \mathbf{L2}\}$, where $r_{Max} < r_*$. This is always true for $\ell \in \mathbf{L2}$; then for the closed topologies it is necessary to choose a proper elongation and density such that $K_2 < K_{Max}^2$. The situation for the momenta in $\ell_i \in \mathbf{L1}$, where the maximum of the centrifugal barrier has $K_{Max}^1 < 1$, is more articulated. The constraint $K_{crit} \leq K_{crit}(r_*)$ provides a relation $r = r(a)$. This analysis is shown in Fig. A.16, which also explains the asterisk (*) in Eq. (A.76). On the other hand, this is evident from the shape of the curve ℓ_Γ^- in Fig. A.15.

Acknowledgments

D. P. acknowledges support from the Junior GACR grant of the Czech Science Foundation No:16-03564Y. Z. S. acknowledges the Albert Einstein Centre for Gravitation and Astrophysics supported by grant No. 14-37086G. The authors thank the anonymous reviewer for the constructive suggestions which helped us to improve the manuscript.

References

- Abramowicz, M. A. 1971, Acta. Astron., 21, 81
- Abramowicz, M. A. 1985, Astronomical Society of Japan, 37, 4, 727-734
- Abramowicz, M. A. 2004, doi:10.1007/11403913-49 astro-ph/0411185. Lectures given at Conference: C04-06-21 Proceedings
- Abramowicz, M. A. 2008, arXiv:astro-ph/0812.3924
- Abramowicz, M. A., Calvani, M. & Nobili, L. 1983, Nature302, 597-599

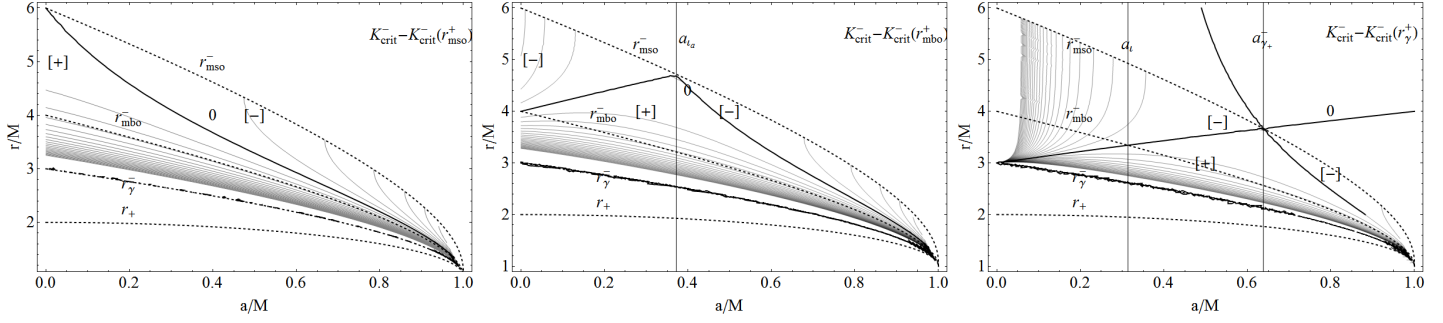


Figure A.16: Location of the notable radii $r_N^\pm \in ()_\mp$. Curves $K_{crit}^-(r) - K_{crit}^-(r_N^\pm) = \text{constant}$ in the plane $r/M - a/M$. The zero, $K_{crit}^-(r) = K_{crit}^-(r_N^\pm)$, is the black thick curve. The region of positive (negative) value of the constant $K_{crit}^-(r) - K_{crit}^-(r_N^\pm)$ is indicated with [+] ([−]). Radii r_{mso} (corotating marginally stable orbit), r_{mbo} (corotating marginally bounded orbit) and r_γ (corotating photon orbit) are also plotted, r_+ is the Kerr outer horizon. At $a = a_{\gamma^+}$ there is $r_{mso}^- = r_\gamma^+$, see also Figs 5,4.

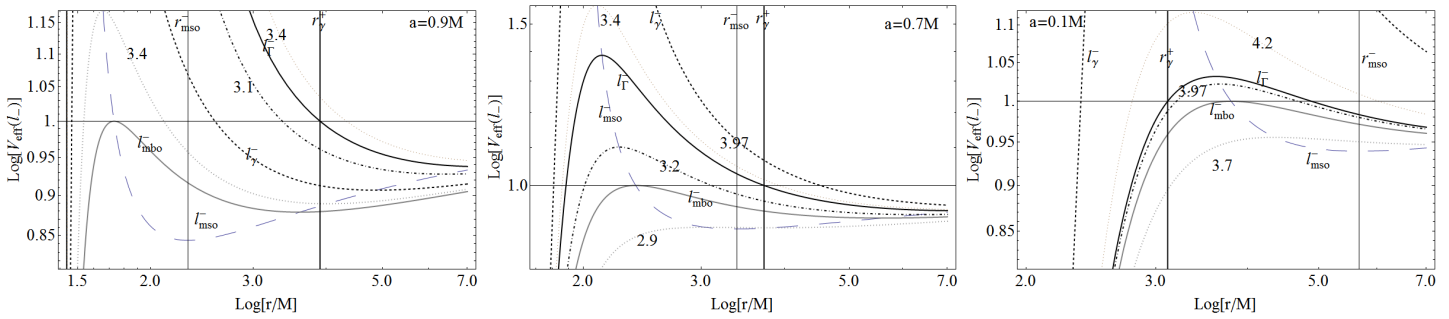


Figure A.17: Location of the photon orbit $r_\gamma^+ \in ()^+$: Effective potential for corotating fluids versus r/M , for different spin-mass ratios of the black hole. For fixed attractor, the effective potential is evaluated at the specific angular momentum ℓ_{mbo}^- of the marginally bounded orbit r_{mbo}^- , the specific angular momentum ℓ_{mso}^- of the marginally stable orbit r_{mso}^- , at ℓ_γ^- for the corotating photon orbit r_γ^- and for $\ell_\gamma^+ \equiv \ell^-(r_\gamma^+)$ where r_γ^+ is counterrotating photon orbit. Numbers close to the curves are further values of the specific angular momentum. Radii r_{mso} and r_γ^+ are also plotted.

Abramowicz, M. A. & Fragile, P.C. 2013, Living Rev. Relativity, 16, 1
Abramowicz M.A., Lanza A., Percival M.J. 1996, ApJ, 479, 179
Abramowicz, M.A., Jaroszynski, M., Kato, S., et al. 2010, A&A, 521, A15
Abramowicz, M.A., Jaroszynski, M. & Sikora, M. 1978, A&A, 63, 221
Abramowicz, M. A. & Straub O. 2014, Scholarpedia, 9(8), 2408
Abramowicz, M.A., & Sharp, N.A. 1983, ApJS, 96, 431
Agol, E. & Krolik, J. 2000, ApJ, 528, 161
Alig, C., Schartmann, M., Burkert, A., Dolag, K. 2013, ApJ, 771, 2, 119
Allen, S. W., Dunn, R.J.H., Fabian, A.C., et al 2006, MNRAS, 1, 372, 21
Aly, H., Dehnen, W., Nixon, C. & King, A. 2015, MNRAS, 449, 1, 65
Bonnerot C., Rossi E. M., Lodato G. & Price D. J. 2016, MNRAS, 455, 2, 2253
Boyer, R.H. 1965, Proc. Camb. Phil. Soc., 61, 527
Bromley, B. C., Miller, W. A. & Pariev, V. I. 1998, Nature, 391, 54, 756
Carmona-Loaiza, J.M., Colpi, M., Dotti, M. & Valdarini R. 2015, MNRAS, 453, 1608
Chakrabarti, S. K. 1990, MNRAS, 245, 747
Chakrabarti, S. K. 1991, MNRAS, 250, 7
Chen, Y., Zhang, X., Zhang, H. et al 2015, apss, 357, 2, 100
Coughlin, E. R. & Begelman, M. C. 2014, ApJ, 781, 82
DeGraf, C., Dekel, A., Gabor, J. and Bournaud, F. 2017, MNRAS, 466, 1462
De Villiers, J-P. & Hawley, J. F. 2002, ApJ, 577, 866
Dogan, S., Nixon, C., King, A., & Price, D. J. 2015 MNRAS, 449, 2, 1251
Dyda, S., Lovelace, R.V.E., Ustyugova, G.V., Romanova, M.M. & Koldoba, A. V. 2015, MNRAS, 446, 613
Ferreira, J. & Casse, F. 2004, ApJ, 601, L139
Font, J. A. & Daigne, F. 2002b, ApJ, 581, L23–L26
Fragile, P. C., Blaes, O. M., Annino, P., Salmonson, J. D. 2007, ApJ, 668, 417–429
Fragile, P.C., Wilson, J. & Rodriguez, M. 2012, MNRAS, 424, 524

Frank, J., King, A., Raine, D., *Accretion Power in Astrophysics*, Cambridge University Press-2002
Gafton, E., Tejada, E., Guillochon, J., Korobkin, O. & Rosswog, S. 2015, MNRAS, 449, 1, 771
Gilli, R., Comastri, A. and Hasinger, G. 2007, A&A, 463, 79
Ghisellini, G., Tavecchio, F., Maraschi, L., et al. 2014 Nature, 515, 376
Igumenshchev, I. V. & Abramowicz, M. A. 2000, ApJS, 130, 463
Jaroszynski, M., Abramowicz, M. A., Paczynski, B. 1980, Acta Astronomica, 30, 1, 1-34
Karas, V. & Sochora, V., 2010, ApJ, 725, 2, 1507–1515
Kawakatu, N., Ohsuga, K. 2011, MNRAS, 417, 4, 2562–2570
Kovar, J., Slany, P., Cremaschini, C., Stuchlik, Z., Karas, V. and Trova, S. A. (2016), Phys. Rev. D. 93, 12, 124055
Kozłowski, M., Jaroszynski, M. & Abramowicz, M. A. 1978, A&A 63, 1–2, 209–220.
Krolik, J.H. & Hawley, J.F. 2002, ApJ, 573, 754
Lasota, J.-P., Vieira, R.S.S., Sadowski, A., Narayan, R. & Abramowicz M. A. 2016, A&A., 587, A13
Lei, Q., Abramowicz, M. A., Fragile, P. C., Horak, J., Machida, M. & Straub O. 2008, A&A., 498, 471
Li, L. X. 2012, MNRAS, 424, 1461
Lovelace, R. V. E. & Chou, T. 1996, ApJ, 468, L25
Lovelace, R. V.E., Romanova, M. M., Lii, P. & Dyda, S. 2014, Computational Astrophysics and Cosmology, 1-3
Lyutikov, M. 2009, MNRAS, 396, 3, 1545–1552
Madau, P. 1988, ApJ, 1, 327, 116–127
Maitra, D., Markoff, S., Brocksopp C., et al. 2009, MNRAS, 398, 4, 1638–1650
Maraschi, L. & Tavecchio, F. 2003, ApJ, 593, 667
Marchesi, S. et al. 2016, ApJ, 830, 100, 20

Marchesi, S., Ajello, M., Comastri, A., Cusumano, G., Parola, V. L., Segreto, A. 2017, *ApJ*, 836, 1, 116

Marscher, A. P., Jorstad, S. G., Gomez, J. L., et al 2002, *Nature*, 417, 625–627

Masini, A. *et al.* 2016, *A&A*, 589, A59

McKinney, J.C., Tchekhovskoy, A., & Blandford, R.D. 2013, *Science*, 339, 49

Miller, J.M., Pooley, G.G., Fabian, A.C., et al. 2012, *ApJ*, 757, 11

Nixon, C., King, A. & Price, D. 2013, *MNRAS*, 434, 1946

Oka, T., Tsujimoto, S., Iwata, Y., Nomura, M. & Takekawa, S. 2017, *Nature Astronomy-Letter*, doi:10.1038/s41550-017-0224

Okuda T., Teresi, V., Toscano E. & Molteni, D. 2005, *MNRAS*, 357, 295

Paczyński, B. 1980, *Acta Astron.*, 30, 4

Paczyński, B. 2000, *astro-ph/0004129*.

Porth O., Olivares H., Mizuno Y., Younsi Z., Rezzolla L., Moscibrodzka M., Falcke H. Kramer M. 2016, arXiv:1611.09720 [gr-qc].

Pugliese, D. & Kroon, J.A.V. 2012, *Gen. Rel. Grav.*, 44, 2785

Pugliese, D. & Montani, G. 2015, *Phys. Rev. D*, 91, 083011

Pugliese, D., Montani, G., & Bernardini, M. G. 2012, *MNRAS*, 428, 952

Pugliese, D. & Quevedo, H. 2015, *Eur. Phys. J. C.* 75, 5, 234

Pugliese, D., Quevedo, H. & Ruffini, R. 2011, *Phys. Rev. D*, 84, 044030

Pugliese, D., Quevedo, H. & Ruffini, R. 2013, *Phys. Rev. D*, 88, 2, 024042

Pugliese, D. & Stuchlík, Z. 2015, *ApJS*, 221, 2, 25

Pugliese, D. & Stuchlík, Z. 2016, *ApJS*, 223, 2, 27

Pugliese, D. & Stuchlík, Z., *submitted*

Pugliese, D. & Stuchlík, Z. 2017a, *ApJS*, 229, 2, 40

Pugliese, D. & Stuchlík, Z. 2017c, *to be submitted*.

Regan, J., Visbal, E., Wise, J. H., Haiman, Z., Johansson, P. H. and Bryan, G. L. 2017, *Nature Astronomy*, 1, 0075

Sbarrato, T., Padovani, P. & Ghisellini, G. 2014, *MNRAS*, 445, 1, 81.

Sadowski, A., Lasota, J.P., Abramowicz, M.A. & Narayan, R. 2016, *MNRAS*, 456, 4, 3915

Sadowski, A. & Narayan, R. 2005,

Schee, J. & Stuchlík, Z. 2009, *Gen. Rel. Grav.*, 41, 1795

Schee, J. & Stuchlík, Z. 2013, *JCAP*, 2013

Shafee, R., McKinney, J. C., Narayan, R. et al. *ApJ*, 687, L25

Sikora, M. 1981, *MNRAS*, 196, 257

Slány, P. & Stuchlík, Z. 2005 *Class. Quantum Gravity*, 22, 3623

Sochora, V., Karas, V., Svoboda, J. & Dovciak, M. 2011, *MNRAS*, 418, 276–283

Storchi-Bergmann, T., Schimoia, J. S., Peterson, B. M., Elvis, M., Denney, K. D., Eracleous, M., and Nemmen, R. S. 2017, *ApJ*, 835, 2

Stuchlík, Z. 1980, *Astronomical Institutes of Czechoslovakia, Bulletin*, 31, 3, 129-144

Stuchlík, Z., Hledík, S. & Novotny, J. 2016, *Phys. Rev. D* 94, 10, 103513

Stuchlík, Z., Kotrlova, A. and Torok G. 2013, *Astron. Astrophys.* 552, A10

Stuchlík, Z. & Schee J. 2013, *Class. Quant. Grav.*, 30, 7, 075012

Stuchlík, Z., Schee, J., Toshmatov B., Hladík J. and Novotný J. 2017, *JCAP*, 1706, 06, 056

Stuchlík, Z., Slany, P., Hledik, S. 2000, *A&A*, 363, 425-439

Stuchlík, Z., Slany, P. and Kovar, J. 2009, *Class. Quant. Grav.* 26, 215013

Stuchlík, Z., Slany P., Torok G. and Abramowicz M. A. 2005, *Phys. Rev. D* 71, 024037

Tadhunter, C., Spence, R., Rose, M., Mullaney, J. and Crowther, P. 2017, arXiv:1702.02573 [astro-ph.GA].

Zanotti O. & Pugliese D. 2015, *Gen. Rel. Grav.*, 47, 4, 44

Zhang J., Xue Z.W., He J.J., Liang E.W. & Zhang S.N. 2015, *ApJ*, 807, 1, 51

Yu, X., Zhang, X., Zhang, H., Xiong, D., et al. 2015, *Ap&SS*, 357, 14

Volonteri, M., 2007, *ApJ*, 663, L5

Volonteri, M., 2010, *A&AR*, 18, 279

Volonteri, M., Sikora, M., Lasota, J.-P., 2007, *ApJ*, 667, 704